CHEMICAL ENGINEERING SCIENCE
GENIE CHIMIQUE

VOL. 9 1958 Nos. 2/3

The influence of surface phenomena on the performance of distillation columns*

F. J. ZUIDERWEG and A. HARMENS

Koninklijke/Shell Laboratorium, Amsterdam (N.V. De Bataafsche Petroleum Maatschappij)

(*Received* 4 *March* 1958 ; *in revised form* 27 *March* 1958)

Abstract—A study has been made on the influence of changes in surface tension on the formation of interfacial area in different types of distillation equipment. It has been found that liquid films are stabilized when the surface tension of the reflux increases down the column, whereas with decreasing surface tension liquid films break up into narrow rivulets or droplets. Interfacial area in sprays, however, is not much influenced by changes in surface tension.

For a given liquid mixture, break-up or stabilization of films can be demonstrated by reversing the direction of mass transfer ; the magnitude of the effects depends distinctly on the magnitude of the surface tension gradient developing in the reflux.

In apparatus where the interfacial area is mainly of the film type, mass transfer rates for mixtures causing the surface tension of the reflux to increase may be twice as high (or more) as those in systems in which the surface tension of the reflux decreases. In the case of technical equipment with interfacial area mainly in the form of droplet sprays, this influence of the system on mass transfer is but small.

Résumé—Les auteurs ont étudié l'effet de changements dans la tension superficielle sur la formation de l'interface dans différents types de colonnes de distillation. Ils ont trouvé que les films de liquide sonte stabilisés quand la tension superficielle du liquide de reflux augmente, tandis qu'une diminution de la tension superficielle cause la rupture de ces films en formant de petits ruisseaux ou gouttes. Cependant, dans des systèmes de gouttes l'interface n'est pas influencée beaucoup par des changements dans la tension superficielle.

Pour un mélange de liquides donné, on peut démontrer la rupture ou la stabilisation des films en changeant la direction du transfert de masse ; la grandeur des effets dépend nettement de la valeur du gradient de la tension superficielle qui se forme dans le liquide en reflux.

Dans les colonnes où l'interface a principalement la forme d'un film, les vitesses du transfert de masse, pour le cas de mélanges qui provoquent une augmentation de la tension superficielle du liquide de reflux, peuvent être deux fois (ou plus) plus élevées que celles qui se présentent lorsque la tension superficielle du liquide de reflux diminue. Dans le cas d'installations industrielles comportant des interfaces principalement en forme de gouttes, cette influence du système sur le transfert de masse n'est que faible.

Zusammenfassung—Eine Untersuchung über den Einfluss von Änderungen der Oberflächenspannung auf die Grenzflächenbildung in Destillationskolonnen verschiedener Art hat ergeben, dass Flüssigkeitsfilme stabilisiert werden, wenn die Oberflächenspannung des Rückflusses zunimmt, während bei abnehmender Oberflächenspannung solche Filme zu schmalen Strömen oder Tropfen zerrissen werden. Jedoch wird die Grenzfläche in Tropfensystemen von Änderungen der Oberflächenspannung nicht stark beeinflusst.

*The contents of this paper were read at an " Interne Arbeitssitzung des Fachausschusses Destillation, Rektifikation und Extraktion der V.D.I. Fachgruppe Verfahrenstechnik," 24 April, 1956, Bingen-on-Rhine (Germany) [13].

Für ein bestimmtes Flüssigkeitsgemisch lässt sich das Zerreissen oder Stabilisieren der Filme nachweisen, indem die Richtung des Stoffaustausches umgekehrt wird; die Effekte werden deutlich von der Grösse des sich im Rückfluss entwickelnden Oberflächenspannungsgefälles bedingt.

In Apparaturen, wo die Grenzfläche hauptsächlich in Form eines Films auftritt, kann bei Gemischen, die die Oberflächenspannung des Rückflusses steigern der Stoffaustausch zweimal so schnell (oder schneller) sein als der bei Systemen, wo die Oberflächenspannung des Rückflusses abnimmt. Bei technischen Apparaturen mit einer Grenzfläche hauptsächlich in Form eines Sprudelbetts ist dieser Einfluss des Systems auf den Stoffaustausch nur gering.

1. Introduction

In operations of mass transfer between a gas or vapour and a liquid the transfer rates obtained depend on the rates of diffusion in the two phases and the magnitude of the contact area between the phases. These quantities are influenced by the type of equipment in which the operation is carried out, the physical properties of the phases and the operating conditions applied. Frequently the effect of these factors is mutually dependent and cannot clearly be separated. As an example, the change in operating conditions may affect the mass transfer rates on a bubble cap tray quite differently from those in a packed column. This is particularly true in connexion with the subject of the present study, which discusses the influence of surface forces on vapour–liquid interfacial area and the resulting mass transfer rates.

In general, little attention has been paid in the past to the formation of interfacial area in actual vapour–liquid mass transfer operations. Most of the work done concerns the study of bubble sizes emerging from submerged orifices, the degree of wetting of packing units in a packed column or the characteristics of liquid sprays. The formation of interfacial area under conditions of mass and/or heat transfer is not covered by these previous studies. It is found that the interfacial area depends primarily on the flow conditions of the phases and mass forces. Surface forces influence the interfacial area to a minor degree, the general effect being a smaller area with increasing surface tension.

This situation, however, may change considerably if the formation of interfacial area takes place under mass and/or heat transfer, particularly if owing to these phenomena surface tension gradients develop along the vapour–liquid interface. It has long been known that surface tension gradients cause rapid movements in the surface and may lead to a spreading or a contraction of the surface [7]. Such contraction phenomena have indeed been observed under certain conditions in the absorption of ethyl alcohol vapour [8], and ammonia [1] into water films. It is readily understandable that the contraction of the liquid surface into small rivulets will have a profound effect on the overall mass transfer rates. Presumably many hitherto unexplained anomalies in mass transfer rates reported in literature [3, 10] have to be ascribed to this type of surface effects.

It is noteworthy that the relation between mass transfer and interfacial area has recently received attention in the case of liquid–liquid contacting [9]. The stability of dispersed droplets has been shown to depend on changes of surface tension caused by the transfer of a solute through the interface.

Complex surface phenomena as quoted above are in general very difficult to analyse theoretically. The accumulation of a general insight into these problems is a first objective that is best obtainable by carrying out adequate experiments. It has been found that in the case of vapour–liquid contacting (distillation) the latter can be realized relatively easily. The first purpose of this paper is to describe such experiments, and to give a discussion and possible explanation of the results.

2. Surface Tension Changes in Distillation

The surface tension or interfacial tension of the reflux is subject to changes during the downward flow of the liquid in the fractionating column. This is caused by the changes in composition and the increasing temperature. It is possible that

temperature and composition effects reinforce or neutralize each other in this respect. Since in vapour–liquid systems temperature and composition are closely interrelated, the possible variations in surface tension can easily be calculated from the equilibrium compositions and temperatures and the surface tension of the pure components at the same temperatures.

It is then found that for systems composed of compounds of homologous series, the possible changes in surface tension are about 2–3 dyn/cm. For mixtures of compounds of a less related nature much larger variations in surface tensions are, however, possible. Mixtures of hydrocarbons and alcohols, for instance, may show surface tension ranges of about 5 dyn/cm at their boiling points. Pure hydrocarbon systems can also show large surface tension gradients, if they are composed of paraffins and aromatics. For instance, the surface tensions in the system benzene–*n*-heptane range between 21 and 12 dyn/cm, those of the mixture *n*-heptane–toluene between 12 and 18·5 dyn/cm. From these data it is seen that in a normal distillation the reflux running down in a fractionating column decreases in surface tension in the first case, whereas with the second mixture an increase occurs. It will be clear however, that these changes in surface tension only develop if the operation of the column is such that a gradient in concentration and temperature occurs along the column. In the case of operation close to minimum reflux the changes in composition, and therefore also the gradient in surface tension in the reflux stream are small, even if there is a wide gap between the surface tensions of the pure components of the system. This applies in a more general sense to all mixtures where relative volatility is small. In that case, even at total reflux, the concentration gradient in the reflux may be negligible. An example of such a system is the widely used test mixture *n*-heptane–methyl*cyclo*hexane. Though the surface tensions of the components (12 and 15 dyn/cm) differ considerably, the low α value (1·07) does not allow of the building up of noticeable surface tension gradients in the reflux under normal conditions of distillation.

From the above description it is seen that three types of systems can be distinguished with respect to the changes in surface tension developing in the reflux flow. For convenience these types will be denoted as negative, positive and neutral respectively. In *negative* systems, the reflux decreases in surface tension; in *positive* systems it increases. In both cases the relative volatilities in the system have to be large enough to allow the development of appreciable gradients. The term *neutral* is given to those systems in which either the components do not show a difference in surface tension or in which the relative volatility is very low and the gradients in surface tension are consequently always small.

The mixtures employed in the present study are listed in Table 1.

Table 1. *Survey of binary systems used*

System	*Boiling point* (°C)	*Surface tension at boiling point* (*dyn/cm*)
n-heptane–	98·4	12
methyl*cyclo*hexane	101·8	15
n-heptane–	98·4	12
toluene	110·7	18·5
benzene–	80·2	21
n-heptane	98·4	12
benzene–	80·2	21
toluene	110·7	18·5
benzene–	80·2	21
*cyclo*hexane	80·8	17·5
(azeotrope)	77·5	20
ethanol–	78·3	18
2.2.4–trimethylpentane	99·1	11·5
(azeotrope)	71	16

Most of the experiments were done with the negative benzene–*n*-heptane, the positive *n*-heptane–toluene and *n*-heptane–methyl*cyclo*hexane mixtures. Because of the low α value, the latter mixture will, however, be taken as a representative of a neutral system.

Two systems are of particular interest—viz. the mixtures ethanol–2.2.4–trimethylpentane and benzene–*cyclo*hexane. These mixtures both show an azeotrope at about equimolar compositions. As a result the changes in surface tension are different in sign, according to whether the mixture

distilled has a low or a high content of the low-boiling constituent.

3. Equipment Used

The formation of interfacial area differs according to the type of equipment used. Roughly, two groups can be distinguished. In the first, interfacial area is obtained by spreading the liquid in thin films over area already present in the equipment. In this case therefore, one can speak of supported interfacial area. A prototype of this group is the wetted wall column. Packed columns and modified wetted wall columns such as Vigreux columns also belong to this group.

In the second type of equipment, the interfacial area is obtained by mixing the liquid and vapour phases. As a result, the formation of vapour bubbles and droplets occurs; the interfacial area in this case is not directly supported by the equipment. Examples are all types of tray columns which may operate either with predominantly liquid film interfacial area (foam and bubble systems) or droplet interfacial area. Pure droplet interfacial area is obtained in spray columns in which the liquid is dispersed by a mechanical atomizing device.

It is found that, with respect to the effect of changes in surface tension, supported interfacial area behaves quite differently from unsupported interfacial area. Therefore, representative types of equipment of both groups defined above were used in the present study. Particulars about the equipment are listed in Table 2.

Table 2. Survey of equipment used

(1) *Concentric tube column*
Length 200 mm, internal diameter 6 mm, width of annular space 0·60 mm. Only the outer wall wetted, inner wall dry.

(2) *Vigreux columns*
Varying length, diameter 25 mm, distance between similar indentations 40 mm.

Packed column

(3) Length 250 mm, diameter 40 mm. Packing: porcelain Raschig rings, 6 mm diameter.

(4) *Packed column*
Length 100 mm, diameter 25 mm. Packing: metal Fenske helices, 3 mm, or Dixon gauze rings, 3 mm.

(5) *Spray column*
18 rotating discs, 40 mm diameter, spaced 30 mm apart on axis. Column diameter 100 mm.

(6) *Oldershaw sieve plate column* [2]
Diameter 25 mm, plate spacing modified to 100 mm, 2 or 5 plates.

(7) *Perforated plate column*
Diameter 450 mm, 16 per cent open area plate, 10 mm hole size. Plate spacing 400 mm.

4. Surface Tension Effects with Supported Interfacial Area

(1) *Wetted wall type columns*

A most striking example of the influence of surface phenomena on the performance of distillation equipment is obtained when operating a wetted wall column. HETP data measured for the small concentric tube column at total reflux are given in Fig. 1. In the case of the *n*-heptane–methyl*cyclo*hexane system, the liquid phase showed complete wetting of the column wall and the separating power observed agreed very well with the theoretically predicted values [12].

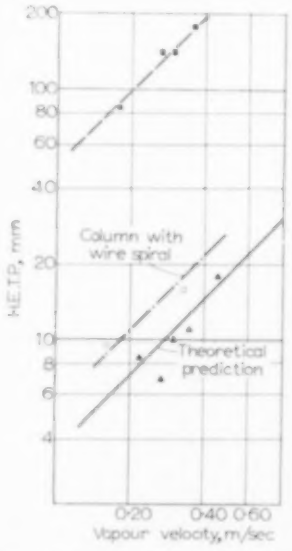

Fig. 1. Separating power of concentric tube column with different test mixtures.
▲ *n*-heptane–methyl*cyclo*hexane
■, □ benzene–*n*-heptane

However, with the negative benzene–*n*-heptane system very bad separation was obtained, the HETP being about ten times the theoretical value. It was observed that in this case the column wall was poorly wetted ; the liquid flowed down in narrow rivulets. Improvement could be obtained by fixing a wire coil of low pitch (about 2 mm) along the column wall. Because of capillary forces, the liquid was now retained and spread out on the wall and nearly the same HETP was observed for the benzene–*n*-heptane mixture as for *n*-heptane–methyl*cyclo*hexane (Fig. 1).

A similar difference in separating power caused by a different degree in wetting is observed with the Vigreux columns. Total reflux data were obtained for a variety of systems under a wide range of load conditions. In the range of vapour velocities of about 0·4 to 0·6 m/sec the separating power was approximately constant. The average HETP values observed in this range are plotted in Fig. 2 against average mixture composition. As shown, the HETP data for the negative mixture are nearly twice

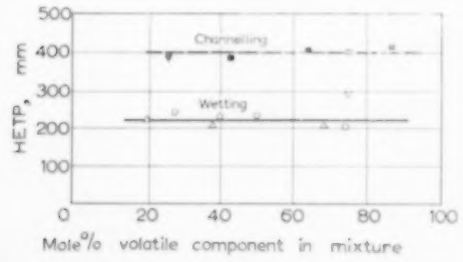

Fig. 2. Separating power of 25 mm Vigreux column with various test mixtures. Vapour velocity 0·4–0·6 m/sec.

■ benzene–*n*-heptane
▼ ▽ } benzene–*cyclo*hexane
○ *n*-heptane–toluene
△ *n*-heptane–methyl*cyclo*hexane

those observed for the *n*-heptane–methyl*cyclo*-hexane and the *n*-heptane–toluene systems. The wetting of the column wall observed visually was in accordance with these results : in the case of benzene–*n*-heptane partial wetting and the formation of rivulets, as illustrated in Fig. 3, occurred, whereas the other two mixtures showed almost complete wetting. The similar behaviour of the latter two explains the almost identical HETP values for these mixtures.

The observation that particularly the benzene–*n*-heptane mixture gave poor wetting only seems explicable by surface effects. Since there is no major difference in the " static " surface tensions of the different systems employed, it was believed that the sign of the changes in the reflux surface tension might perhaps be responsible. In order to test this supposition, some more experiments were done with the Vigreux column. First, total reflux distillations were carried out with the mixture benzene–*cyclo*hexane. At high benzene concentrations, this constituent is the less volatile because of the azeotrope in the system. Therefore, reflux surface tension increases downwards in the column (" positive " mixture). Complete wetting was observed in this case. With a low benzene content of the mixture, *cyclo*hexane is the less volatile component and the surface tension of the reflux decreases (" negative " system). As with benzene–*n*-heptane channelling of the reflux was now observed. The separating power measured for the two mixture compositions was in accordance with the wetting characteristics found (see Fig. 2).

In a second series of experiments it was attempted to measure mass transfer rates with the normally " positive " systems *n*-heptane–toluene and *n*-heptane–methyl*cyclo*hexane under " negative " conditions. This cannot be realized in normal distillation ; however, by countercurrent absorption of vapour rich in volatile component into a liquid rich in the heavy component the direction of mass transfer may be reversed and thus also the sign of the surface tension changes in the downflowing liquid. Moreover, by changing the length of the Vigreux column or by adjusting the compositions of entering liquid and vapour, the surface tension gradient in the liquid can easily be varied and its influence determined.

Data on the absorption experiments with Vigreux columns of various lengths are collected in Table 3. Besides top and bottom flow rates and composition, the average driving force, i.e. the average difference between the operating

line and equilibrium line is given (in terms of liquid composition). The latter is representative for the average changes in concentration (and hence for changes in surface tension) in the reflux over one theoretical tray. At a high driving force, mass transfer is rapid and a large gradient in the reflux surface tension results. At low driving forces, the reverse is true.

As expected, under all conditions where reflux surface tension decreased in the absorption experiments, channelling of the reflux occurred. This became more severe the higher the driving force applied. Consequently, the HETP also increased with the driving force. This is clearly illustrated in Fig. 4, in which the HETP data are plotted. It is seen that for both systems the data fall on one single line. Furthermore, the HETP value obtained in normal distillation with the "channelling" benzene–*n*-heptane mixture correlates well with this line if plotted at the average driving force applied in the distillation experiments.

Fig. 4 also shows the data obtained under fully wetting conditions with various mixtures. The value for the *n*-heptane–methyl*cyclo*hexane system at high driving force was obtained by the absorption of methyl*cyclo*hexane into *n*-heptane (see Table 3). It is seen that under conditions of positive changes in surface tension there is no influence of the driving force on the HETP, presumably because the wetting is almost complete. Further, it may be concluded from Fig. 4 that at low driving forces, the HETP of negative systems seems to approach that of the positive mixtures, i.e. wetting becomes complete and channelling disappears.

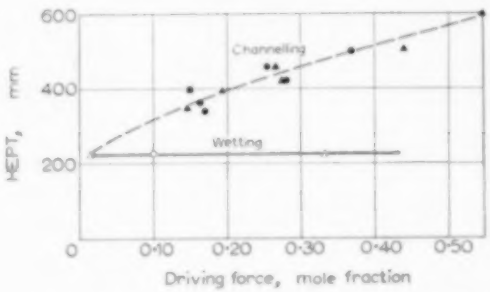

Fig. 4. Effect of driving force on separating power of Vigreux column, tested with various test mixtures. Vapour velocity 0·3–0·4 m/sec.
■ benzene–*n*-heptane
△▲ *n*-heptane–methyl*cyclo*hexane
○● *n*-heptane–toluene

Table 3. Absorption experiments in Vigreux columns. Average vapour velocities 0·3 m/sec. Concentrations in mole per cent n-heptane

System	*Column length (m)*	*Feed rates (mole/hr)*		*Product rates (mole/hr)*		*Compositions, (mole per cent) Feeds*		*Products*		*Average driving force (mole %)*	*Theoretical plates*	*HETP (mm)*
		top	*bottom*	*top*	*bottom*	*top*	*bottom*	*top*	*bottom*			
n-heptane–toluene	1·78	16·8	16·0	10·0	22·8	0	100	14	64	16·5	4·9	360
,,	1·48	17·8	15·5	10·1	23·2	0	100	14·5	60·5	17	4·3	340
,,	1·06	17·6	16·6	11·9	22·3	0	100	30	58	25·5	2·3	460
,,	0·88	16·6	16·7	12·8	20·5	0	100	34·5	60	28	2·1	420
,,	0·65	18·1	17·4	14·7	20·8	0	100	44	52·5	37	1·3	500
n-heptane–methyl*cyclo*hexane	1·78	21·9	15·5	11·8	25·6	0	100	3·0	59	14·5	5·1	350
,,	1·48	20·9	16·6	12·1	25·4	0	100	8·5	61	19	3·8	390
,,	1·06	16·5	15·1	11·6	20·0	0	100	23·5	61	26·5	2·3	460
,,	0·88	21·1	16·9	14·6	23·4	0	100	23	57·5	27·5	2·1	420
,,	0·65	15·9	15·7	13·0	18·6	0	100	43	54	44	1·3	500
,,	0·48	16·3	16·3	14·1	18·5	0	100	55	46	55	0·8	600
,,	0·48	19·7	18·1	16·2	21·6	100	0	71	38	33	2·0	240

FIG. 3. Photograph of channelling phenomenon in Vigreux column when distilling benzene–*n*-heptane.

There is one remarkable feature in the correlation of the HETP data in Fig. 4 which should be mentioned. The difference in surface tension between *n*-heptane and methyl*cyclo*hexane is less than half the difference in surface tension between *n*-heptane and toluene or benzene. This means that since for all mixtures the range of liquid concentration under channelling conditions is about the same, the surface tension gradient in the reflux during the *n*-heptane–aromatics tests was about double the gradient in the *n*-heptane–methyl*cyclo*hexane experiments. In spite of this fact the intensity of channelling in the formation of interfacial area seems to be the same.

The observations of channelling liquid phases reported in literature are also to be interpreted on the basis of decreasing surface tensions. Molstad and Parsly [8] found that the contraction of water films in grid type tower packings occurred when ethanol vapour was absorbed. In this case surface tensions of the liquid film decrease because of the increasing ethanol concentration.

Bond and Donald [1] observed the break-up of water films when hydrogen chloride or ammonia was absorbed in a rippling film in a wetted wall column. Owing to the heat of absorption, a decrease in surface tension also develops in these cases. It is interesting that the break-up did not occur when rippling of the liquid film was prevented.

(2) *Packed columns*

In packed columns the interfacial area is supported by randomly distributed packing elements. In view of the results obtained with the wetted wall columns, the effect of the direction of surface tension changes on the HETP was also determined for this type of columns. Two types of packing were investigated in relatively small columns : 6 mm porcelain Raschig rings (in a 40 mm diameter column) and two fine metal packings (in a 25 mm diameter column). In the case of the Raschig rings, efficiency varied but little with the boil-up rate at vapour velocities of 0·2 to 0·3 m/sec. HETP data measured under these conditions are plotted in Fig. 5. It is seen that just as with Vigreux columns, the HETP for the *n*-heptane–methyl*cyclo*hexane and *n*-heptane–toluene mixtures are about the same, whereas for the negative benzene–*n*-heptane mixture about the double HETP values are recorded.

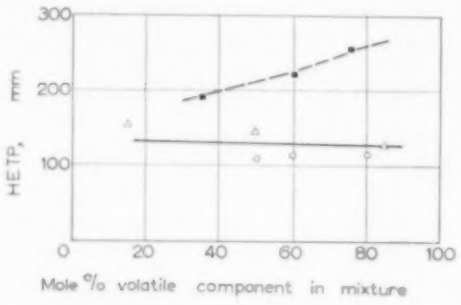

Fig. 5. Separating power of 6 mm Raschig rings, with various test mixtures. Vapour velocity 0·2–0·3 m/sec.
■ benzene–*n*-heptane
△ *n*-heptane–toluene
○ *n*-heptane–methyl*cyclo*hexane

A similar difference between HETP values observed with positive and negative systems was found for the fine metal packings such as Fenske helices and Dixon gauze rings. Table 4 shows the data obtained :

Table 4. HETP data for fine metal packings. Average liquid composition 65 mole per cent volatile component

Packing	*System*	*Vapour velocity (m/sec)*	*HETP (mm)*
Fenske helices	*n*-heptane–toluene	0·06	15
	benzene–*n*-heptane	0·06	30
Dixon rings	*n*-heptane–toluene	0·12	20
	benzene–*n*-heptane	0·15	35

Though in the cases of the packed columns the actual flow of liquid over the packing elements was difficult to observe, it may be safely assumed that the differences in separating power with the different systems must again be ascribed entirely to a different degree in wetting.

5. Surface Tension Effects with Unsupported Interfacial Area

(1) *Spray columns*

In order to study the effect of changes in surface tension when interfacial area is formed by dispersed drops, use was made of a spray column in which the droplets were generated by rotating discs. The column, diameter 100 mm, was provided with a central rotating axis on which discs of 40 mm diameter were mounted. The reflux was guided onto the top disc, which sprayed it to the wall. From the wall, the liquid was collected in a peripheral gutter, from which it was fed back to the next rotating disc. In total the column contained eighteen discs and peripheral gutters. The separating power of this column at 1000 r.p.m. of the discs was determined with *n*-heptane–toluene and benzene–*n*-heptane. The data obtained are shown in Fig. 6. Hardly any

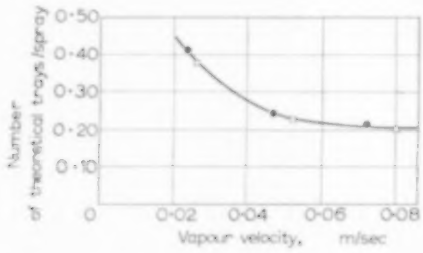

Fig. 6. Separating power of spray column with various test mixtures.
- ● *n*-heptane–toluene
- □ benzene–*n*-heptane

difference in mass transfer rate between the two systems is observed. This result is not entirely unexpected, since in this particular type of apparatus droplet formation occurs by external forces; moreover, once they are formed there seems little possibility for interaction and coalescence between the droplets because of the short residence time. Furthermore, the droplets formed are of such small size that they can scarcely be expected to disintegrate still further by the action of decreasing surface tension. Since only such disintegration or coalescence can alter the magnitude of interfacial area, the absence of effects of changes in surface tension on separating power for this particular type of equipment seems sufficiently explained.

(2) *Perforated plate columns*

In perforated plate columns where the plates have a low percentage of open area and small perforations, the dispersion of the vapour into the liquid frequently leads to the formation of bubbles or foam. A specimen of equipment of this type is the Oldershaw perforated plate [2] laboratory column. Plate efficiencies for this column were determined with a variety of systems. Data obtained are recorded in Table 5, part of which is plotted in Fig. 7.

It is now seen that approximately the same plate efficiency (about 50–55 per cent) is observed for " neutral " or " negative " mixtures, whereas

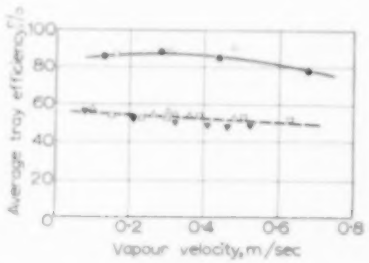

Fig. 7. Separating power of Oldershaw sieve plates with various test mixtures.

		Average mole % of volatile component
▼	benzene–toluene	50 %
□	benzene–*n*-heptane	40 %
△	*n*-heptane–methyl*cyclo*hexane	50 %
●	*n*-heptane–toluene	15 %
○	*n*-heptane–toluene	75 %

for the positive *n*-heptane–toluene system nearly the double efficiency of 90 per cent is reached. This result is obvious when the behaviour of the liquid on the trays is observed: with the *n*-heptane–toluene system severe foaming develops, whilst the other systems, in contrast, show a moderately high spray bed. This is clearly demonstrated by the photographs in Fig. 8.

As with the Vigreux column the relation of the observed phenomena with the direction of changes in surface tension was investigated more closely by the distillation of an azeotropic mixture and

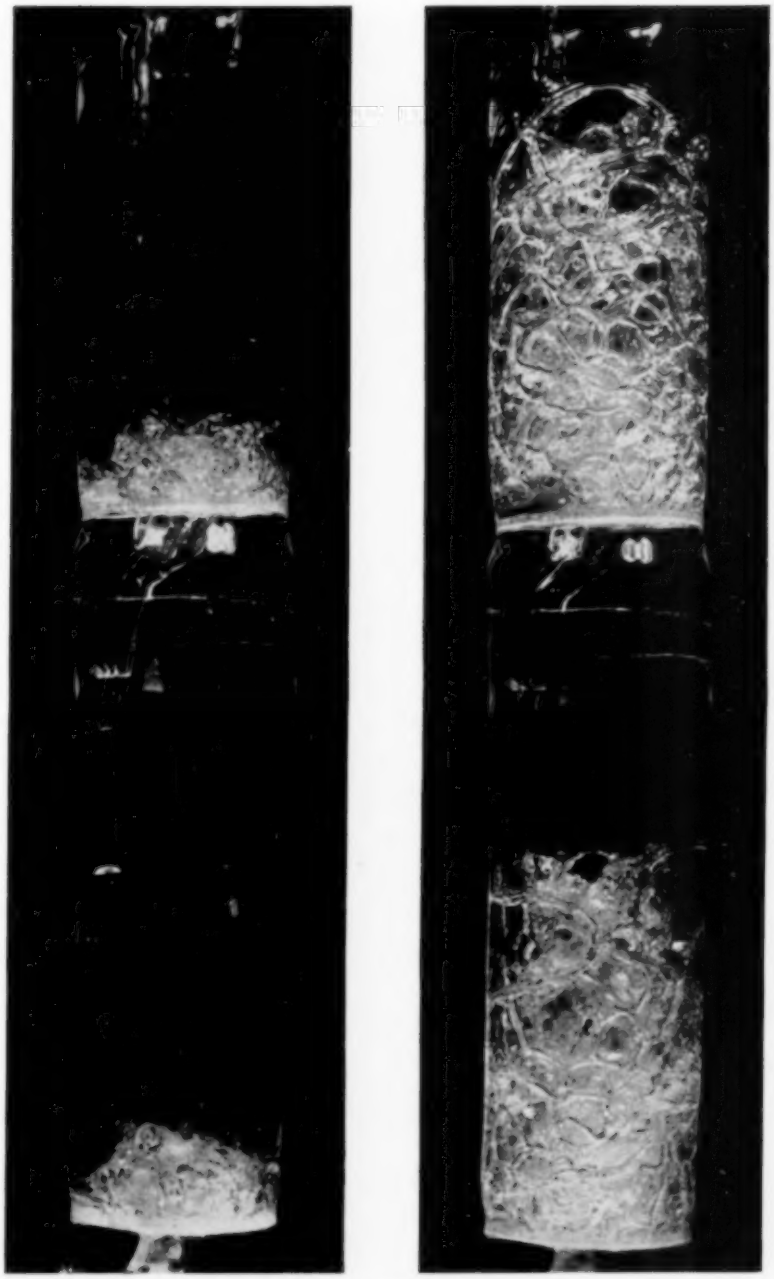

FIG. 8. Tray action on Oldershaw sieve plates with benzene–*n*-heptane (left) and *n*-heptane–toluene system (right) respectively. Vapour velocity about 0·3 m/sec.

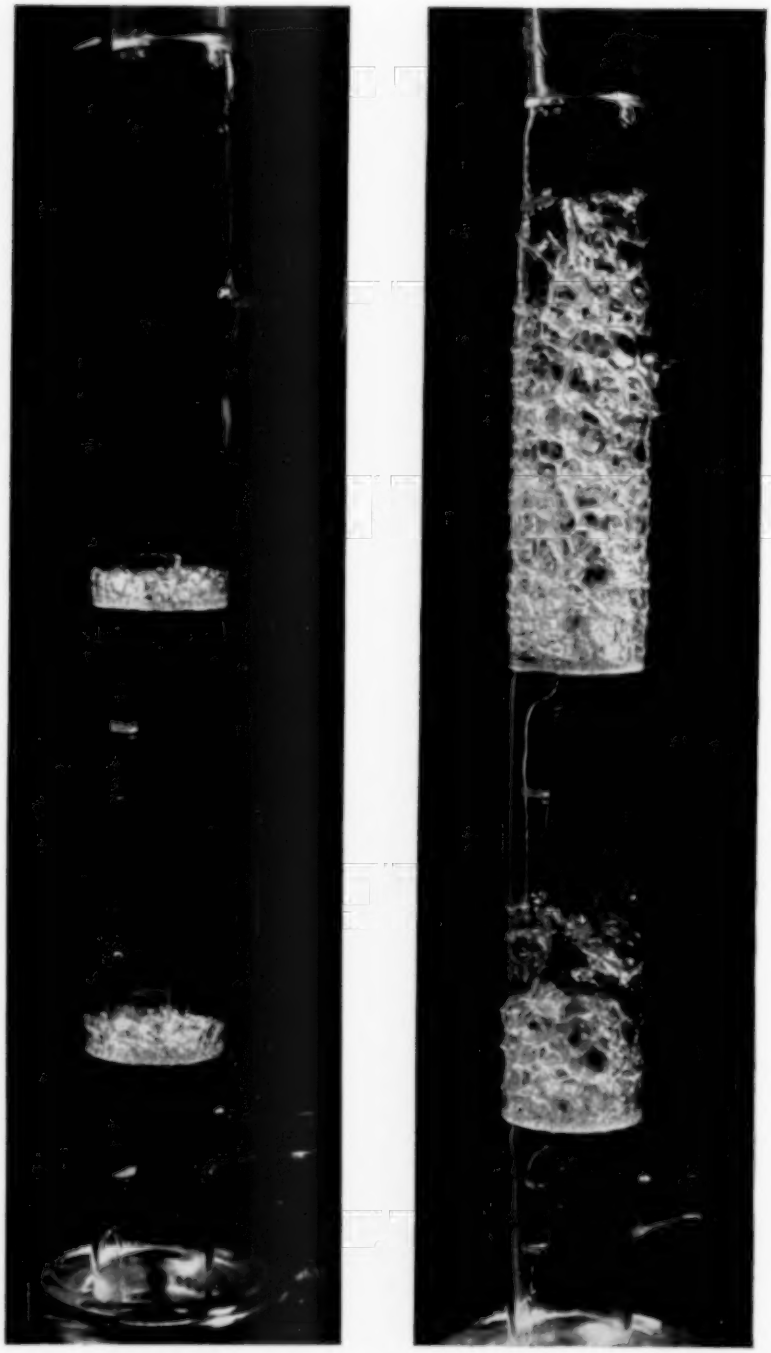

FIG. 9. Tray action on Oldershaw sieve plates with ethanol–2,2,4–trimethylpentane mixtures. Left 7% ethanol, tray efficiency 30–40 per cent. Right 75% ethanol, tray efficiency about 70 per cent.

Table 5. Efficiency of Oldershaw sieve plates

System	*Average mole % volatile comp.*	*Vapour velocity (m/sec)*	*Tray efficiency (%)*	*Foam Height (mm)*
n-heptane–methylcyclohexane	50	0·10	57	
		0·26	54	10
		0·30	56	
		0·32	54	
		0·36	54	20
		0·48	52	
benzene–toluene	50	0·08	56	
		0·21	53	10
		0·32	51	
		0·40	49	
		0·46	48	20
		0.52	49	
benzene–*n*-heptane	85	0·30	50	
		0·38	50	10
		0·47	43	
		0·55	46	20
		0·68	44	
	40	0·14	55	
		0·23	53	10
		0·30	55	
		0·38	55	
		0·50	53	20
		0·62	52	
n-heptane–toluene	15	0·13	83	
		0·28	88	40
		0·44	85	
		0·67	78	
	40	0·13	97	
		0·21	100	
		0·29	100	60
	75	0·15	88	
		0·30	90	40
		0·48	91	
	87	0·13	73	
		0·30	80	20
		0·47	75	
	92	0·15	65	
		0·29	63	
		0·30	68	15
		0·48	64	
ethanol–2.2.4–trimethylpentane	7	0·20	30–40	5–10
	75	0·25	70	50–100

by carrying out absorption experiments. The azeotropic mixture ethanol–2.2.4–trimethylpentane was used. At ethanol concentrations below 53 mole per cent, this component is the most volatile. Since the surface tension of 2.2.4–trimethylpentane is lowest, the system behaves "negatively" in this region of concentration. At ethanol concentrations above 53 mole per cent, the octane is the most volatile component and the mixture shows "positive" properties. This conclusion is confirmed in a spectacular manner by the distillation tests. Fig. 9 shows photographs

of the liquid–vapour behaviour for low and high ethanol concentrations at about the same vapour velocities. The tray efficiencies (30–40 per cent and about 70 per cent respectively) are in accordance with the formation of interfacial area observed.

Absorption experiments with the Oldershaw sieve plates were carried out with *n*-heptane–methyl*cyclo*hexane and *n*-heptane–toluene mixtures under conditions of increasing surface tension changes in the reflux flow. Table 6 gives the collected data. Tray efficiencies and visually observed foam heights of the absorption and total reflux distillation experiments are plotted against liquid driving force in Figs. 10 and 11, which are hence similar to the HETP graph given in Fig. 4 for the Vigreux column.

A distinct similarity is noted between the dependence of tray efficiency and foam heights on the average driving forces applied. The degree of foaming and increase in tray efficiency with the two mixtures, however, is clearly different and in line with the surface tension differences in both systems. This is in contrast to the Vigreux column, in which—with decreasing surface tensions and using a channelling mixture—no such influences of the system could be detected.

Figs. 10 and 11 show that at low driving force, the foaming effect seems to disappear and the 50–55 per cent tray efficiency is approached. In normal distillation practice these low driving forces are obtained at low or high concentrations or under "pinched" conditions. In these circumstances, a loss in tray efficiency is therefore

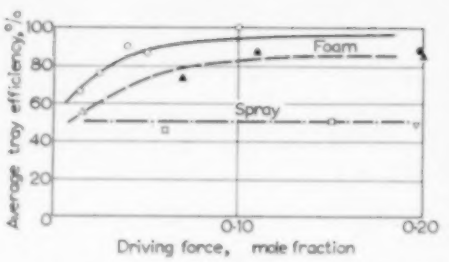

Fig. 10. Influence of driving force on tray efficiency of Oldershaw sieve plates for various test mixtures. Vapour velocity about 0·3 m/sec.

□ benzene–*n*-heptane
▽ benzene–toluene
○ ● *n*-heptane–toluene
△ ▲ *n*-heptane–methyl*cyclo*hexane
Open points : normal distillation
Closed points : absorption experiments

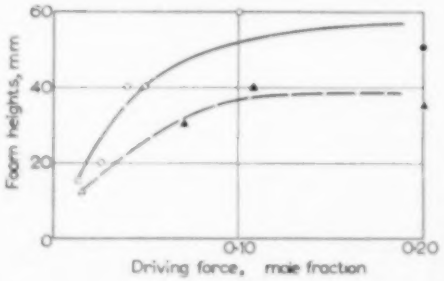

Fig. 11. Influence of driving force on foam height on Oldershaw sieve plates with increasing surface tensions of reflux.

○ ● *n*-heptane–toluene
△ ▲ *n*-heptane–methyl*cyclo*hexane
Open points : normal distillation
Closed points : absorption experiments

Table 6. Absorption experiments with Oldershaw sieve tray column. Column with 5 plates, average vapour velocity 0·3 m/sec. Concentrations in mole per cent n-heptane

System	*Feed rates (mole/hr)*		*Product rates (mole/hr)*		*Compositions, (mole per cent)* *Feeds*		*Products*		*Average driving force (mole %)*	*Theoretical plates*	*Plate efficiency (%)*	*Foam height (mm)*
	top	*bottom*	*top*	*bottom*	*top*	*bottom*	*top*	*bottom*				
n-heptane–methyl*cyclo*hexane	13·8	17·8	14·1	17·5	100	0	78·5	15·5	20	4·2	84	35
,,	14·9	18·2	15·6	17·5	78·5	20	67·0	28·0	11	4·4	88	40
,,	15·4	18·1	16·1	17·5	58	26	51·5	31·0	7	3·7	74	30
n-heptane–toluene	18·8	18·1	15·8	21·1	100	0	91·0	21·0	20	4·3	86	50

to be expected when a positive mixture is distilled. For total reflux distillation this is shown explicitly in Fig. 12.

The concentration effect on plate efficiency as demonstrated in Fig. 12 has also been reported in the literature; in all cases in which noticeable

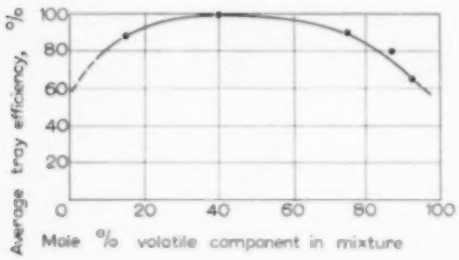

Fig. 12. Effect of concentration on tray efficiency of Oldershaw sieve plates in distillation with *n*-heptane–toluene. Average vapour velocity 0·3 m/sec.

effects were recorded the binary system used can be identified as positive. Fig. 13 shows data of Thijssen [10, 11] for the distillation of methyl*cyclo*hexane–toluene and *n*-heptane–methyl*cyclo*hexane in a small perforated plate column (38 mm

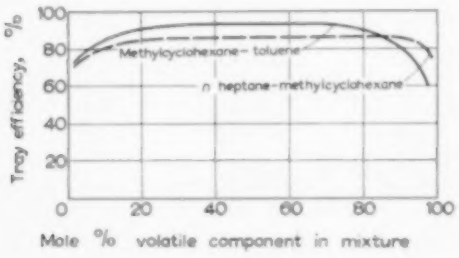

Fig. 13. Concentration effect on tray efficiency of perforated plates observed by Thijssen. Average vapour velocity about 0·2 m/sec.

diameter). The behaviour of the first system was to be expected because of its high driving forces and large difference in surface tension (3·5 dyn/cm). It is of interest to note that also the *n*-heptane–methyl*cyclo*hexane mixture, in spite of its low relative volatility, shows the concentration effects under extreme compositions. This mixture should therefore be considered as slightly positive instead of neutral.

Tray efficiency maxima at mid-concentrations as found by Thijssen and by the present authors for hydrocarbon systems have also been observed for ethanol–water mixtures [4, 5]. Because of the low surface tension and high volatility of ethanol this system should also be identified as positive.

Further, some interesting cases are reported for the distillation of nitrogen–oxygen mixtures. Nitrogen is the most volatile component and has a low surface tension at the boiling point (about 9 dyn/cm), whereas the heavy component oxygen has a high surface tension of about 13·5 dyn/cm. Accordingly, Grassmann and Frank [3] found that when transferring oxygen from vapour bubbles into oxygen–nitrogen liquid mixtures, higher transfer rates were observed than for the opposite case in which nitrogen vapour was transferred to the liquid. From the surface tensions of the pure compounds it is clear that in the first case positive surface tension changes develop in the liquid, which changes stabilize the bubble formation and hence favour mass transfer rates.

The positive characteristics of the nitrogen–oxygen system can also be derived from the distillation experiments with perforated plates carried out by Linde [6]. In the middle concentration range foaming was observed, whereas at extreme mixture compositions only a low spray bed developed. The same was found for the system nitrogen–argon, but foaming was absent with the mixture argon–oxygen. These results are in accordance with the surface tensions and relative volatilities in the respective systems (Nitrogen–argon : boiling point difference 10°C, surface tensions 9 and 12·5 dyn/cm respectively; argon–oxygen : boiling point difference about 1°C, surface tensions 12·5 and 13·5 dyn/cm respectively).

The effects reported above with perforated plate columns in general pertain to plates with very small open area and small perforations, conditions which are favourable for foam formation. In technical columns, however, a higher free area and large perforations are used. Therefore, and also because of higher vapour velocities, a relatively larger amount of spray is formed and foaming diminishes. The results obtained with the spray column give rise to the expectation that

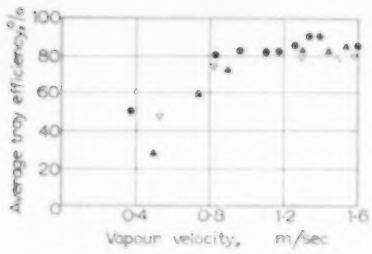

Fig. 14. Tray efficiency of a perforated tray, 16 per cent open area, 10 mm holes.
● *n*-heptane–toluene, about 50%
▲ *n*-heptane–methyl*cyclo*hexane, about 50%
▽ benzene–toluene, about 50%

there would therefore be less difference between positive and negative mixtures with respect to tray efficiency. This is indeed the case and can be seen from Fig. 14 in which tray efficiencies observed for a perforated plate with 16 per cent open area, 10 mm hole size, (diameter 0·45 m) are plotted for three different systems.

6. Discussion

The experiments reported in the preceding paragraphs have shown that, depending on the type of equipment used, decreasing or increasing surface tensions of the reflux may influence interfacial area and separating power quite markedly. A survey of the main trends observed is given in Table 7. For convenience, the properties pertaining to systems in which no surface tension changes occur (neutral systems) have been denoted in this table as "unity".

In order to give an explanation of these phenomena, it should be recalled that liquid surfaces of high interfacial tension contract when contacted with a surface of lower surface tension. This is known as the "Maragnoni effect". Maragnoni [7], however, did not consider the influence of vapour–liquid interaction in his studies.

A very well-known phenomenon in which liquid film contraction occurs as a result of mass transfer effects is the so-called "wine-glass effect". Wine creeps up the wall of the glass because of its wetting tendency. When a film has been formed, alcohol preferentially evaporates, leaving a residue of higher water content and therefore higher surface tension. When fresh wine creeps up the wall, and comes into contact with the aqueous film, the latter contracts into small rivulets.

A similar explanation can be given for the channelling phenomenon taking place when distilling a negative mixture in a wetted wall type of column. Liquid films descending in such a column are never of uniform thickness, and hence, locally, thin places will become more rapidly saturated with heavy component than the remainder of the film. Since the heavy component has the lowest surface tension, areas of lower surface tension develop locally; the remaining parts with higher surface tensions therefore contract and the liquid film breaks up into rivulets.*

*Essentially the same explanation has been given by Bond and Donald [1] for their observations of the breakdown of water films in the case of ammonia absorption.

Table 7. Survey of surface phenomena in distillation equipment

Surface tension changes	*Supported interfacial area*			*Unsupported interfacial area*		
	Wetting	*Separating power**	*Effect of driving force*	*Type of interfacial area*	*Separating power**	*Effect of driving force*
no changes (neutral)	complete	1	none	spray	1	none
increasing (positive)	complete	~ 1	none	foam	> 1	severe
decreasing (negative)	partial	< 1	severe	spray	~ 1	none

*Separating power denoted unity for "no change."

Once the rivulets are formed, the edges, because of their smaller volume, will always be more saturated with the heavy component. Surface tension is thus lower at the edges and this stabilizes the contraction of the liquid (see sketch in Fig. 15).

It is easily understood that the differences of concentration in the liquid surfaces will become higher and contraction will become more severe if the mass transfer per unit area is higher. The latter is produced either by an increased

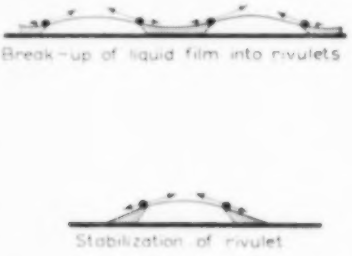

FIG. 15. Schematic illustration of break-up of a liquid film in a "negative" system. Shaded areas denote liquid of lower surface tension.

driving force or because of higher mass transfer coefficients (i.e. smaller HETP values). For the Vigreux column, the driving force effect has already been illustrated in Fig. 4. The influence of the HETP on the severity of the channelling phenomenon is recognized when comparing the results from the small concentric tube column (Fig. 1) and the Vigreux column (Fig. 2). Fig. 16

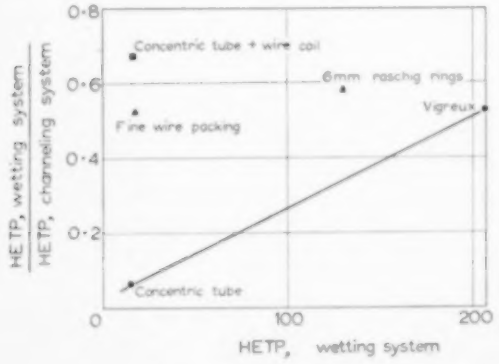

FIG. 16. Relation between loss in separating power and HETP when distilling benzene–*n*-heptane in various types of equipment.

gives a graphical representation of the relation between the ratio of HETP's with channelling and complete wetting and the HETP of the columns with complete wetting. Furthermore, the same HETP ratios observed for the packed columns are plotted in this graph.

It is thus seen that at the same HETP, the packed columns suffer a smaller loss in efficiency than the wetted wall type of columns. This is easily explained by the fact that in the packed columns liquid is retained by capillary forces in interstices between the packing elements. The contraction of the liquid surface in this case will be less effective and the loss in interfacial area will therefore be smaller. Reduction of the channelling effect in this sense has also been found when providing the concentric tube column with a thin wire spiral.

The distillation of "positive" mixtures in the Vigreux column and the Raschig rings column did not reveal any significant differences with respect to the distillation of a "neutral" mixture in the same equipment. Considering for this case again the non-uniformities in the liquid films, it is now seen that thin and weak spots become preferentially saturated with the component with the highest surface tension. The weak spots are thus reinforced, and as a result the film tends to become of more uniform thickness and break-up will be prevented (see the sketch in Fig. 17). Wetting of the supporting solid surface with a film of the positive mixture will therefore be approximately the same as with

FIG. 17. Schematic illustration of the stabilization of a liquid film in a "positive" system. Shaded areas denote liquid of lower surface tension.

mixtures in which surface tension gradients are absent.

The latter conclusion, however, only holds good for supported interfacial area. In a system where the vapour is dispersed into a liquid, the lifetime of the bubbles formed may increase considerably because of the reinforcement of

weak spots. These weak spots occur between adjacent bubbles (see Fig. 18); the preferential saturation of these spots with heavy component

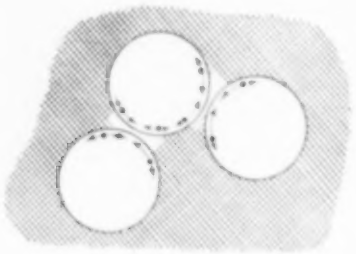

Fig. 18. Schematic illustration of the stabilization of vapour bubbles in a "positive" system. Shaded areas denote liquid of lower surface tension.

causes the surface tension to rise locally. Therefore, liquid is drawn in between the bubbles and coalescence of the adjacent bubbles is prevented. If the changes in surface tension are large enough, even a foam may develop in this manner.

Since the degree of bubble stabilization will depend on the change in surface tension of the liquid on the trays, the relation of foam height and tray efficiency to driving force as shown in Figs. 10 and 11 seems quite logical.

Finally, the behaviour of neutral systems and negative mixtures in a perforated plate column will be briefly considered. For hydrocarbon mixtures in which no appreciable changes in surface tension occur, the stabilizing factor tending to produce prolonged bubble life is absent. Accordingly, bubbling is poor with such systems and spray formation occurs preferentially. From what has been said about the instability of liquid films when distilling a negative mixture, it will be clear that in this case the bubble stabilizing factor is also absent. Approximately, the same interfacial area can therefore be expected for the two types of systems; accordingly about equal tray efficiencies are observed for the "neutral" and negative systems.

7. Conclusions

The experimental facts observed and the qualitative interpretation provided give rise to some definite conclusions regarding the formation of interfacial area in vapour–liquid contacting equipment.

The main conclusion is that changes in surface tension occurring in the liquid phase can have a spectacular effect on the interfacial area. Break-up of liquid films results from decreasing surface tensions and is of particular importance for wetted wall columns and packed columns. Stabilization of liquid films occurs when the interfacial tension increases; even foaming may develop in this case. The latter effect is of particular interest for the operation of plate columns. Since mass transfer rates are directly proportional to interfacial area, the surface tension effects are reflected in the HETP values of the various types of equipment.

The above phenomena become especially noticeable when the differences in surface tension between the components of the mixtures at the boiling point are higher than about 2 dyn/cm and at driving forces above 5 mole per cent.

A further conclusion is that equipment with high mass transfer efficiencies is relatively more sensitive to the surface effects than less efficient apparatus. From a practical point of view this means that the effects are of particular importance for laboratory apparatus, whilst technical equipment will be much less sensitive to the surface phenomena described.

Finally, it is of interest to note that the influence of the changes in surface tension on mass transfer in general is quite severe and appreciably more pronounced than the effect of variations in the static properties of the liquid phase, such as density, viscosity and diffusivity. Thijssen [10, 11], also Molstad [8] *et al.*, have in fact argued that variations in these properties could not account for their observations. In this connexion it may be pointed out that when studies are made in which the static properties of the phases are the main subject, (e.g. when the contribution of the vapour and liquid phases to the resistance against mass transfer is assessed) care must be taken to select experimental conditions such that the surface effects do not affect the observations. From the results of the present study it may be concluded that such conditions cannot easily be realized.

References

[1] Bond J. and Donald M. B. *Chem. Engng. Sci.* 1957 **6** 237.

[2] Collins F. C. and Lantz V. *Industr. Engng. Chem.* (*Anal.*) 1936 **18** 673.

[3] Grassmann P. and Frank A. *Interne Arbeitssitzung des Fachausschusses Destillation, Rektifikation und Extraktion der V.D.I. Fachgruppe Verfahrenstechnik*, Göttingen 1957.

[4] Keyes D. B. and Byman L. *Univ. Ill. Engng. Exp. Sta. Bull.* Ser. 328 1941.

[5] Kirschbaum E. *Chem.-Ing. Tech.* 1951 **23** 213.

[6] Linde G. *Chem.-Ing. Tech.* 1955 **27** 661.

[7] Maragnoni C. *Ann. Phys. Lpz.* 1871 **143** 337.

[8] Molstad M. C. and Parsly L. F. *Chem. Engng. Progr.* 1950 **46** 20.

[9] Sigward K. Z. *Ver. Dtsch. Ing.* 1956 **98** 453.

[10] Thijssen H. A. C. *Effect of Liquid Composition on Plate Efficiency in the Rectification of Binary Mixtures.* Versl. Landbouwk. Onderzoek, The Hague No. 61.12. 1955.

[11] Wijk W. R. van and Thijssen H. A. C. *Chem. Engng. Sci.* 1954 **3** 153.

[12] Willingham C. B., Sedlak V. A., Rossini F. D. and Westhaver J. *Industr. Engng. Chem.* 1947 **39** 706.

[13] Zuiderweg F. J. *Chem.-Ing. Tech.* 1956 **28** 587.

Chemical Engineering Science, 1958, Vol. 9, pp. 104 to 118. Pergamon Press Ltd.

The final stage in the removal of the lighter component of a binary mixture by batch rectification

J. Buiten

Central Laboratory, Staatsmijnen in Limburg, Geleen, Netherlands

(*Received* 12 *November* 1957)

Abstract—This article gives a mathematical treatment of the batch rectification of a binary mixture in the range of low concentrations of the lighter component in the distillate, both for the case in which the amount of holdup in the column may be neglected (Part I) and for the case in which this holdup has to be taken into consideration (Part II). It is assumed that at phase equilibrium the concentration of this component in the vapour is directly proportional to the concentration in the liquid.

The relations derived in Part I show the importance of choosing a high reflux ratio in the process of removing the lighter component. A graph is given which facilitates the finding of suitable values of the reflux ratio and of a suitable number of "transfer units" or theoretical plates for the column. A comparison is made between removal of the lighter component by batch and by continuous rectification. It is found that, economically, batch rectification is inferior to continuous rectification if a high degree of purity of the heavier component is to be reached.

The amount of holdup is taken into consideration by assuming that the column is continuously in a state characterized by constant concentration ratios at a constant ratio between the amount of holdup and the amount of material contained in the still. This state is termed the stationary state of the second order. The influence of the holdup is illustrated in a number of graphs, which bring to light several particularities. Finally, a discussion is given of some effects connected with the holdup, which are termed the accumulation, accommodation, pinch and dead space effects (the first two correspond respectively to the depletion and flywheel effects of Pigford *et. al.* An example is given of a numerical computation.

Résumé—On donne un traitement mathématique de la rectification discontinue d' un melange binaire dans le domaine de basses concentrations du composant le plus volatil dans le distillat, aussi bien dans le cas où la quantité de la retenue de la colonne est négligeable (Première Partie) que dans le cas où il n'en est pas ainsi (Deuxième Partie). On admet qu'en cas d'équilibre des phases, la concentration de ce composant dans la vapeur est directement proportionnelle à la concentration dans le liquide.

Il s'avère des relations dérivées dans la Premiere Partie que pour l'enlèvement du composant le plus volatil, on a intérêt à choisir un taux de reflux élevé. Un graphique est donné en vue de faciliter la recherche de valeurs convenables pour le taux de reflux et du nombre de " transfer units " ou du nombre de plateaux théoriques de la colonne. L'enlèvement du composant le plus volatil par rectification discontinue est comparé à celui réalisé par rectification continue. Cette comparaison montre qu'au point de vue économique, la rectification discontinue le cèdeà la rectification continue, s'il s'agit d'obtenir une pureté élevée de la composante la moin s volatile.

Pour porter en calcul la quantité de la retenue on admet que la colonne est continuellement dans un état qui est, le rapport entre la quantité de la retenue et le continu de la chaudière étant constant, caractérisé par des rapports de concentration constants et qui est nommé état stationnaire du deuxième ordre. L'influence de la retenue est illustrée par quelques graphiques, où se révèlent différentes particularités. On traite enfin quelques effets qui se rattachent à la retenue, effets dits d'accumulation, d'accommodation (ceux-ci correspondent respectivement à l'effet d'épuisement et à l'effet-volant de Pigford et collaborateurs), de " pinch " et d'espace mort. On donne l'exemple d'un calcul numérique.

Zusammenfassung—Der Aufsatz gibt eine mathematische Behandlung der absatzweisen-Rektifikation einer binären Mischung im Bereich kleiner Konzentrationen der leichteren Komponente im Destillat, und zwar sowohl für den Fall, dass die Grösse des Betriebsinhalts (holdup) vernachlässigt werden kann (Teil I), als auch für den Fall, dass dieser Betriebsinhalt berücksichtigt werden muss. Es wird angenommen, dass beim Phasengleichgewicht die Konzentration dieser Komponente im Dampf direkt proportional der Konzentration in der Flüssigkeit ist.

Die in Teil I abgeleiteten Beziehungen zeigen die Wichtigkeit der Wahl eines hohen Rückflussverhältnisses, um die leichteren Komponente zu entfernen. Ein mitgeteiltes Diagramm erleichtert das Auffinden geeigneter Werte des Rückflussverhältnisses und einer geeigneten Zahl von " Transferunits " Einheiten oder theoretischer Böden für die Kolonne. Die Entfernung der leichteren Komponente bei der absatzweisen-Rektifikation wird mit der bei kontinuierlichem Betrieb verglichen. Esz eigt sich, dass wirtschaftlich gesehen die absatzweisen-Rektifikation derkont inuierlichen Rektifikation unterlegen ist, wenn ein hoher Reinheitsgrad der schwereren Komponente erreicht werden soll.

Der Betrag des Betriebsinhalts wird durch die Annahme berücksichtigt, dass die Kolonne ständig in einem Zustand ist, der durch konstante Konzentrationsverhältnisse und ein konstantes Verhältnis zwischen dem Betriebsinhalt und dem Blaseninhalt gekennzeichnet ist. Dieser Zustand wird stationärer Zustand zweiter Art genannt. Der Einfluss des Betriebsinhalts wird durch Diagramme erläutert, in denen sich verschiedene Einzelheite erkennen lassen. Schliesslich werden einige Wirkungen diskutiert, die mit dem Betriebsinhalt in Zusammenhang stehen, nämlich die der Akkumulation, der Akkomodation, des " pinch " und des toten Raums (die ersten beiden stimmen überein unterschiedlich mit dem Erschöpfungseffekt und dem Schwungradeffekt nach Pigford u.a.). Eine zahlenmässige Berechnung wird als Beispiel gegeben.

Introduction

As a consequence of the non-stationary character of batch rectification computation of the process is rather difficult even if the amount of the holdup may be neglected and, consequently, the concentrations existing at a given moment may be equalized to those existing in a stationary state [12]. To account for the amount of holdup the aid of big computing machines [10, 13, 14] has had to be called in. The finding of a solution in the form of ordinary algebraic expressions seems to be fraught with unsurmountable mathematical difficulties [10]. Zuiderweg [15], however, did succeed in finding along semi-empirical lines an expression for the so-called pole height, a measure of the slope of the rectification curve at $x_D = 0{\cdot}5$, introduced by Bowman and Cichelli [2]. This equation is of great importance in the choice of the right conditions [6]. Zuiderweg further gave a relation between the pole height and the amount of the intermediate fraction between two symmetrical values of x_D (e.g. 0·95 and 0·05). This relation by itself is of no avail if one wants to know the amount of the lighter component which is left in still and column after the take-off of the intermediate fraction has been stopped, and which contaminates the product obtained by simply emptying still and column or by distillation.

One cause of the mathematical difficulties is the non-linear character of the equilibrium equation. We have therefore restricted our considerations to the range of low concentrations of the lighter component in the distillate (e.g. $x_D < 0{\cdot}1$), so that is becomes permissible at phase equilibrium to assume the concentration of this component in the vapour to be directly proportional to its concentration in the liquid:

$$y^* = \alpha x \qquad (1)$$

This renders possible a certain assumption, to be named in Part II, by means of which a set of ordinary algebraic equations can be found, describing batch rectification in the range of low concentrations of the lighter component when the holdup cannot be neglected. Although in this way no direct contribution is made to the solution of the general problem, we see the following advantages:

(a) Calculation of the ratio between x_D and x_S (the mole fraction of the lighter component in the still) or x_D and $\bar{x}$ (the mean mole fraction in still and column). This may be used as an addition to the results

obtained by Zuiderweg. The method is further useful for the calculation of x_S or $\bar{x}$, if x_D is known (e.g. from a measurement).

(b) Computation of the batch rectification process in the range of low x_D values. This computation is important in those cases where the lighter component has to be thoroughly removed or where the available column has a low separating power.

(c) Getting an insight into the influence of the amount of holdup.

In order to get a general understanding and to provide a background for Part II, in Part I calculations and considerations will be given in which the amount of holdup is neglected. In Part II allowance will be made for the amount of holdup.

Before proceeding to the derivation of equations something should be said about the measure that will be used for expressing the separating power of a column.

The separating power of a column can be expressed in a number of theoretical plates (N) or in a number of transfer units (A). The number of theoretical plates of a plate column can easily be determined if the " Murphree plate efficiency " is known [8]. If a column is used in which vapour and liquid are not contacted stage-wise, but continuously, e.g. by the use of a packing or the wall of a tube, the number of transfer units is the obvious measure to be used for the separating power [3].

For N and A Colburn [4] has derived equations which apply if the column is in a stationary state, the line of equilibrium satisfies equation (1) and the operating line is straight. In these equations N and A are related to α, V/L, and the change in concentration. By dividing one equation by the other Colburn finds*

$$\frac{A}{N} = \frac{\ln \alpha R}{\alpha R - 1} \qquad (2)$$

This equation renders it possible to assign a number of transfer units to a column of which the number of theoretical plates is known, and vice versa.

It is likely that a plate column and a packed column having the same amount of holdup (evenly distributed) and having the same separating power in the stationary state, will not behave very differently in batch rectifications. This implies that, by means of equation (2), results of calculations for a packed column may be applied to a plate column and vice versa. For this reason our calculations have been carried out for that type of column which seemed to involve the least mathematical difficulty, namely the type in which vapour and liquid are not contacted stage-wise and for which the number of transfer units is characteristic of the separating power.

Part I

Rectification in a Column with Negligible Holdup

Derivation of equations

Before proceeding to the derivation of equations, the following assumptions must be mentioned:

(a) The mixture to be rectified is a binary mixture. The lighter component constitutes only a small percentage of the distillate, so that equation (1) may be used to express the equilibrium relation.

(b) The vapour leaving the still is in equilibrium with the liquid in the still.

(c) The reflux has the same composition as the distillate.

(d) The flows of vapour and liquid are the same in any cross-section.

(e) Vapour and liquid are not contacted stage-wise. The rate of mass transfer is described by the expression given by Chilton and Colburn [3] (right-hand member of equation (4)).

(f) Neither in the vapour nor in the liquid is there any diffusion or mixing in the direction of flow.

* Equation (2) can easily be derived (also for an equilibrium line of the type $y^* = ax + b$) by calculating the number of transfer units corresponding to the concentration change over one theoretical plate.

(g) The number of transfer units of the column does not change with time.

(h) The reflux ratio does not change with time.

If the amount of holdup may be left out of consideration, the material balance for batch rectification is:

$$d(x_S W) + x_D dD = 0$$
$$W + D = W_0$$

from which can be derived:

$$\frac{d \ln x_S}{d \ln W} = \frac{1 - X_S}{X_S} \qquad (3)$$

in which equation X_S has been written for $\frac{x_S}{x_D}$, the ratio of the mole fractions of the lighter component in still and distillate. The quantity X_S must now be related to the relative volatility (α), the reflux ratio (r), and the number of transfer units (A). For the reader's convenience this will be discussed in some detail.

Drawing up a material balance for an imaginary disk of a column provides the equation:

$$V \frac{dy}{dl} = K O (y^* - y) \qquad (4)$$

The right-hand member is the expression for the rate of mass transfer given by CHILTON and COLBURN [3]. After introduction of the dimensionless quantity λ, defined by:

$$\frac{d\lambda}{dl} = \frac{KO}{V} \quad *$$

and termed the number of transfer units (after CHILTON and COLBURN), the equation changes to:

$$\frac{dy}{d\lambda} = y^* - y$$

or, in the form of an integral,

$$A = \int_{y_S}^{y_D} \frac{dy}{y^* - y}$$

A material balance for the part of a column above an arbitrary horizontal cross-section is given by the following well-known equation applying to stationary states:

$$y = \frac{r}{r+1} x + \frac{y_D}{r+1} \qquad (5)$$

Using equations (1) and (5) the integral may be worked out, which results in:

$$A = \frac{1}{\alpha R - 1} \ln \frac{(\alpha - 1)/\alpha}{(\alpha R - 1) X_S - 1/r}$$

This equation results also from a conversion of an equation derived by COLBURN [4].

The equation given above may also be written as:

$$X_S = \frac{\{(\alpha - 1)/\alpha\} \exp[-(\alpha R - 1) A] + 1/r}{\alpha R - 1} \qquad (6)$$

From equation (6) it is seen that X_S is a constant, i.e. it is independent of x_S or x_D. We remark that this conclusion could already have been drawn after replacing x and y by the ratios X and Y in the equations from which equation (6) has been derived (this replacement is possible because of the homogeneous form of the equations). Equation (3) may now be changed to:

$$\ln \frac{x_S}{x_{S0}} = \ln \frac{x_D}{x_{D0}} = \frac{1 - X_S}{X_S} \ln \frac{W}{W_0} \qquad (7)$$

An analogous relation between x_S and W has already been derived for simple distillation from a still by RAYLEIGH [11].

For $A \to \infty$, $X_S \to X_{S\infty} = \frac{1}{(\alpha - 1)(r + 1) + 1}$.

Insertion of this expression for X_S in equation (7) results in:

$$\ln \frac{x_S}{x_{S0}} = \ln \frac{x_D}{x_{D0}} = (\alpha - 1)(r + 1) \ln \frac{W}{W_0} \qquad (8)$$

This equation has already been derived, in a different form, by COLBURN and STEARNS [5].

It appears that equation (8) is already a good approximation when A has a relatively small value. Because equation (8) represents a removal of the more volatile component which is as rapid as possible at a given reflux ratio, it is in practice desirable to give A a value which is

* Purposely this is not expressed as $\frac{\lambda}{l} = KO/V$, so as to leave open the possibility that KO/V is a function of l.

sufficiently great to get a near approximation of equation (8). To survey quickly the requirements as to A we have drawn up a diagram (Fig. 1) which relates to each other A, α, r, and a quantity ϵ which represents the relative deviation of X_S from $X_{S\infty}$:

$$\epsilon = \frac{X_S}{X_{S\infty}} - 1$$

This diagram is based on the following equation:

$$\epsilon = (z - 1) \exp\left[-zm/(z - 1)\right] \qquad (6a)$$

which is another form of equation (6) and in which m and z are defined as

$$m = (\alpha - 1)\, A \quad z = \frac{1}{\alpha X_{S\infty}} = \frac{(\alpha - 1)(r + 1) + 1}{\alpha}$$

Other variables could have been chosen instead of m and z. But the latter have the advantage that, if α is left out of consideration, the one (m) is a function of A only, the other (z) of r only.

The diagram may also be used in the calculation

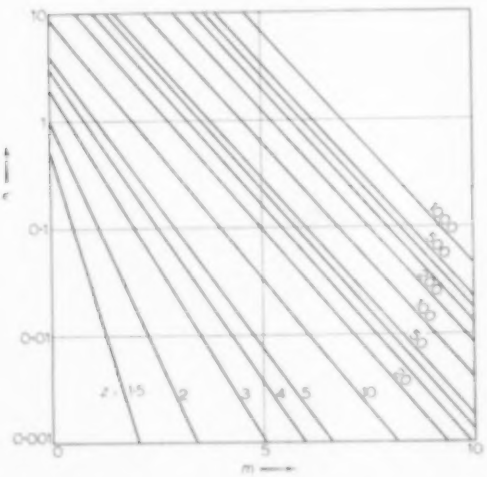

FIG. 1. Nomograph, representing equation (6a) and relating to each other the ratio of the mole fractions of the lighter component in still liquid and in distillate (X_S), the relative volatility (α), the reflux ratio (r), and the number of transfer units (A). Significance of symbols:

$$\epsilon = \frac{X_S}{X_{S\infty}} - 1\,; \quad m = (\alpha - 1)\, A\,;$$

$$z = \frac{1}{\alpha X_{S\infty}} = \frac{(\alpha - 1)(r + 1) + 1}{\alpha}$$

of the factor $(1 - X_S)/X_S$ in equation (7), which is equal to $\dfrac{(\alpha - 1)(r + 1) - \epsilon}{1 + \epsilon}$.

In the following discussion an approximate equation for $\dfrac{D}{W_0}$ is needed. To derive such an equation, equation (7) is written as

$$\ln \frac{x_S}{x_{S0}} = \ln \frac{x_D}{x_{D0}} = \frac{(\alpha - 1)(r + 1)}{1 + \dfrac{\epsilon}{1 - X_S}} \ln \frac{W}{W_0} \qquad (7a)$$

If X_S and $\dfrac{D}{W}$ are small, $\dfrac{\epsilon}{1 - X_S}$ may be replaced by ϵ and $\ln \dfrac{W}{W_0}$ by $\dfrac{-\dfrac{D}{W_0}}{1 - \frac{1}{2}\dfrac{D}{W_0}}$. Equation (7a) then results in:

$$\frac{D}{W_0} \approx \frac{\ln \dfrac{x_{S0}}{x_S}}{(\alpha - 1)(r + 1)} \left(1 + \epsilon - \tfrac{1}{2}\frac{D}{W_0}\right) \qquad (9)$$

Discussion

In the following discussion the economic aspects of the removal of the lighter component by batch rectification will take the central place.

As a measure of the labour which has to be spent on removing a volatile component by batch rectification with negligible holdup, may be taken

$$E = \frac{(r + 1)\, D/W_0}{1 - D/W_0}$$

The quantity E is the amount of vapour that has to be formed per unit amount of product (the least volatile component), and is,consequently, a measure of the heat consumption and of the time needed (if the diameter of the column is given) or the diameter of the column (if the time is given). Equation (9) leads to the following expression for E:

$$E \approx \frac{\ln (x_{S0}/x_S)}{\alpha - 1} \left(1 + \epsilon + \tfrac{1}{2}\frac{D}{W_0}\right) \qquad (10)$$

Usually, ϵ and $\frac{1}{2}\, D/W_0$ can easily be kept small, in which case E is not much greater than the smallest possible value. This is determined by $\ln (x_{S0}/x_S)$ and $\alpha - 1$.

Equation (9) shows that, to keep D/W_0 small, a sufficiently high r value should be chosen. An example will be given here which proves that a high value of r is soon suitable: if one puts $x_{S0}/x_S = 100$, $\alpha = 2$ and $D/W_0 = 0{\cdot}1$, one finds from equation (9), disregarding the terms ϵ and $\frac{1}{2}\ D/W_0$, a value of 45 for r.

If r exceeds a certain optimum value, E shows an increase instead of a decrease. This is caused by a shortage of transfer units, as a result of which the decrease of $\frac{1}{2}\ D/W_0$ is smaller than the increase of ϵ.

Next a comparison will be given of batch rectification and continuous rectification as methods of removing the lighter component, assuming this component to be present in low concentrations.

In a continuous rectification process x undergoes in a stripping section – which will, for the sake of convenience, be considered as consisting of theoretical plates – a change per theoretical plate which is approximately given by the factor $\alpha\ V/L\left\{ = \alpha\,\rho/(\rho+1)\right\}$ provided x does not differ too little from the fraction of the lighter component in the bottom product. Consequently, the change over N theoretical plates is approximately given by a factor $\left[\frac{\alpha\,\rho}{\rho+1}\right]^N$. To give this factor a desired value, N and ρ must be balanced against each other. The result will be e.g. that for ρ a value is chosen which is 1·5 times the minimum value, which is equal to $1/(\alpha-1)$. A different value of the aforementioned factor will have little influence upon the choice of ρ. It is seen that in the case of removal by continuous rectification N or A is strongly influenced by the requirement as to purity made with regard to the heavier component. The following antiparallel between batch rectification and continuous rectification will now be clear:

batch rectification: E is highly and A only slightly dependent on the degree of purity of the heavier component required*

continuous rectification: A is highly and ρ (comparable with E) only slightly dependent on the degree of purity of the heavier component required.

The increase of E with the degree of purity in batch rectification causes this process to be economically clearly inferior to continuous rectification if a high degree of purity is required. In addition, in the continuous rectification process the stream of vapour leaving the stripping section can be utilized in a rectifying section for obtaining the lighter component in a pure state. All this does not alter the fact that the removal of a light component by batch rectification is well feasible (if only the value of r is high enough) and is not as inapplicable as Lloyd [9] suggests.

Part II

Rectification in a Column with Non-negligible Holdup

Introduction

In Part I it has been found that if the amount of holdup may be neglected, the ratio between the mole fractions of the lighter component in still and distillate is constant. Of course, this implies constant ratios throughout the column. These ratios have other values if the amount of holdup is not negligible, but may then be constant too, a condition being, as will be shown later, that the ratio h between the amount of holdup and the amount of liquid in still and column remains constant. In practice this can be realized by constantly supplying the still with the pure heavier component. This state, characterized by constant ratios of the concentrations and approached asymptotically as time elapses, will be called the stationary state of the second order. In ordinary batch rectification this state will, in theory, not be reached, as during the rectification process h does not remain constant. Yet

* If it is assumed that ϵ is, at given A, directly proportional to $r+1$ (generally a rough approximation), D/W_0 is inversely proportional to $r+1$ (good approximation), r, at given A, has its optimum value, and dE/dA has a constant value determined by economical factors, the following simple relationship between A and $\ln(x_{S0}/x_S)$ can be derived:

$$\frac{d\,[(\alpha-1)\,A]}{d\,\ln(\ln x_{S0}/x_S)} = 3.$$

it will be assumed that, if h is small, the concentration will always be that characteristic of a stationary state of the second order. By this simplifying assumption the mathematical treatment of the problem of the influence of the amount of holdup in batch rectification is greatly facilitated.

Derivation of equations

To the assumptions made in Part I the following – relating to the holdup – should be added:

(i) The amount of holdup per transfer unit is constant (both as regards place (λ) and time).

(j) The holdup caused by the vapour may be disregarded.

(k) The holdup of the condenser may be neglected.

If there is an appreciable amount of holdup, a material balance leads to:

$$d(x_S W + x_H H) + x_H dD = 0$$

For ordinary batch rectification one must add:

$$dW + dD = 0$$

It is not difficult to derive from this, for the quantity S defined by:

$$S = -\frac{d \ln x^*_D}{(dD)/M}$$

in the case of rectification with constant W:

$$S = \frac{1}{\bar{X}} \qquad (11)$$

and in the case of ordinary batch rectification:

$$S = \frac{1 - X_S + h(1-h)\,dX_S/dh + h^2\,dX_H/dh}{\bar{X}} \qquad (12)$$

$$\left(\text{use is made of } \frac{dD}{M} = \frac{dh}{h}\right).$$

* One may also write $d \ln x_D / d \ln M$. If $h = 0$, $d \ln x_D = d \ln x_S$ and $M = W$. Then this form is the same as the left member of equation 3.

In ordinary batch rectification the concentration distribution will (if h is sufficiently small) slightly lag behind the distribution for the stationary state of the second order, the existence of which will be assumed however. For this reason there is no point in keeping strictly to the differential quotients in equation (12) and trying to meet serious mathematical difficulties. Therefore, an approximation will be made.

In numerical calculations it was found that from $h = 0$, X_S and X_H decrease nearly linearly with h over a comparatively large interval of h. Consequently, $h\,dX_S/dh$ can well be approximated by writing $X_S - X_{S,h=0}$, and the numerator of the right-hand member of equation (12) by writing: $1 - X_{S,h=0} + h^2(dX_H/dh - dX_S/dh)$. The latter term of this expression is quadratic in h and may therefore, for low values of h, be neglected with respect to $X_{S,h=0}$, which term itself is often small with respect to 1. Therefore the following equation, which gives a good approximation, may be written instead of equation (12):

$$S = \frac{1 - X_{S,h=0}}{\bar{X}} \qquad (13)$$

The value of $X_{S,h=0}$ follows from equation (6). Equation (13) becomes exact when r approaches infinity.

In the case of rectification with constant W, the quantities S, X_S and $\bar{X}$ are constant, so that integration of the equation defining S leads to

$$\ln(x_{D0}/x_D) = \ln(x_{S0}/x_S) = \ln(\bar{x}_0/\bar{x}) = S\frac{D}{M} \qquad (14)$$

In the case of ordinary batch rectification, the quantities S, X_S and $\bar{X}$ are not constant, so that the appropriate equation then is

$$\ln(x_{D0}/x_D) = \ln(x_{S0}\,X_S/x_S\,X_{S0})$$

$$= \ln(\bar{x}_0\,\bar{X}/\bar{x}\,\bar{X}_0) = \int_0^D S\frac{dD}{M} = \int_{h_s}^{h} S\frac{dh}{h} \qquad (15)$$

Often the integral form can with sufficient accuracy be replaced by $-S_m \ln(1 - D/M_0)$, in which expression S_m is the arithmetical mean of the initial and the ultimate value of S.

The quantities X_S, $\bar{X}$ and S must be related to α, r, A and h. To this end the differential equations describing the process in a column have to be solved. These equations can be derived from a material balance for an imaginary disk of a column and read:

$$\begin{cases} L\dfrac{\partial x}{\partial l} - v_L\dfrac{\partial x}{\partial t} = KO\,(y^* - y) \\ V\dfrac{\partial y}{\partial l} + v_V\dfrac{\partial y}{\partial t} = KO\,(y^* - y) \end{cases}$$

As appears from an article by BOWMAN and BRIANT [1]* and from another by JASWON and SMITH [7], the treatment of these equations to obtain a numerical solution is a complicated business, even if the existence of a straight equilibrium line is assumed. This is mainly due to the fact that an initial disturbance (e.g. taking off distillate after a long time of total reflux) returns periodically as a discontinuity in the course of the concentrations with time. However, the discontinuities are smoothed out as distillation proceeds (see Fig. 9 of JASWON and SMITH's article). In this article it will be assumed that the column has completely "forgotten" its initial state and has attained to a state which has been called the stationary state of the second order because of the constancy of the concentration ratios. A condition of this constancy is the passing of a straight equilibrium line through the origin ($y^* = \alpha x$), which will be assumed. Moreover the holdup due to the vapour will be neglected. In this way relatively simple equations result.

By introducing the dimensionless variables λ and τ (which is not new), the latter of which is defined by:

$$\tau = \frac{KO}{V}\cdot\frac{L}{v_L}\cdot t = \frac{L}{H/A}\cdot t$$

and by putting $v_V = 0$, the equations given above are changed to:

$$\begin{cases} \dfrac{\partial x}{\partial \lambda} - \dfrac{\partial x}{\partial \tau} = R\,(y^* - y) \\ \dfrac{\partial y}{\partial \lambda} = y^* - y \end{cases}$$

Elimination of y and $\dfrac{dy}{\partial \lambda}$ is now possible after an equation has been added by differentiation to λ of the first equation. The result of this elimination is:

$$\frac{\partial^2 x}{\partial \lambda^2} - \left(R\frac{dy^*}{dx} - 1\right)\frac{\partial x}{\partial \lambda} - \frac{\partial x}{\partial \tau} - \frac{\partial^2 x}{\partial \lambda \partial \tau} = 0 \quad (16)$$

If the concentration ratios are constant, x must be equal to $f(\lambda) \times g(\tau)$. Now X is chosen for $f(\lambda)$ and x_D for $g(\tau)$. Substitution in equation (16) $\left(\text{with } \dfrac{dy^*}{\partial x} = \alpha\right)$ leads to an equation for x_D and one for X:

$$-\frac{d\ln x_D}{d\tau} = A \quad (17)$$

$$\frac{d^2X}{d\lambda^2} - (\alpha R - 1 - A)\frac{dX}{d\lambda} + AX = 0 \quad (18)$$

(A is a constant).

It may be remarked that the derivation of the equation for the τ-independent mole fraction ratio X would not have been possible, if the differential equation (16) were not homogeneous. It will appear from the derivation and use of equation (21) that it is also necessary for the relation between y^* and x (equation (1)) to be homogeneous.

The solution of equation (16) which is incorporated in equation (17) and equation (18) is of such a nature that the terms of equation (16), multiplied by $\dfrac{1}{x}$, have values which are independent of τ. Therefore, it has to be considered as an asymptotic solution. It describes column conditions which are reached after an infinite time or which are maintained if already present at $t = 0$.

A in equations (17) and (18) is a constant, i.e. a quantity independent of λ and τ. However, it does depend on α, r, A and h. From this it follows that, strictly speaking, these equations

* BOWMAN and BRIANT use a different expression for the rate of mass transfer.

apply only if during the rectification h remains unchanged, i.e. if W is kept constant. We shall use, however, these equations also in the case of ordinary batch rectification, although A is not a constant in this case. This is essentially what was meant by saying that also in such a case a column is in a stationary state of the second order. It must be remarked that for an ordinary batch rectification this state corresponds to another value of A than it does for a rectification with constant W at the same h.

Application of the boundary conditions:

(1) for $\lambda = A \quad X = 1$

(2) for $\lambda = A \quad dX/d\lambda = (\alpha - 1)\,R - A$ (this follows from $x = y$)

leads to the following solution for equation (18):

$$X = \frac{a_1 - 1/r}{a_1 - a_2} \exp\left[-a_1 (A - \lambda)\right] + \frac{a_2 - 1/r}{a_2 - a_1} \exp\left[-a_2 (A - \lambda)\right] \qquad (19)$$

where a_1 and a_2 are the roots of the quadratic equation $a^2 - (\alpha R - 1 - A)\,a + A = 0$. There are some simple relationships between a_1 and a_2, which are useful in the reduction of expressions containing a_1 and a_2:

$$a_1 a_2 = A$$
$$a_1 + a_2 = \alpha R - 1 - A$$
$$(1 + a_1)(1 + a_2) = \alpha R$$

Starting from the equation for X we can easily find the expressions for Y, X_S and X_H:

$$Y = \alpha X - \frac{1}{R}\left(\frac{dX}{d\lambda} + AX\right) = \frac{(\alpha - 1) - a_2}{a_1 - a_2} \exp\left[-a_1 (A - \lambda)\right] + \frac{(\alpha - 1) - a_1}{a_2 - a_1} \exp\left[-a_2 (A - \lambda)\right] \qquad (20)$$

$$X_S = \frac{Y_{\lambda = 0}}{\alpha} = \frac{1}{\alpha}\left[\frac{(\alpha - 1) - a_2}{a_1 - a_2} \exp(-a_1 A) + \frac{(\alpha - 1) - a_1}{a_2 - a_1} \exp(-a_2 A)\right] \qquad (21)$$

$$X_H = \frac{1}{A}\int_0^A X\, d\lambda = \frac{1}{A\,rA}\left\{1 - \left[\frac{rA - a_2}{a_1 - a_2} \exp(-a_1 A) + \frac{rA - a_1}{a_2 - a_1} \exp(-a_2 A)\right]\right\} \qquad (22)$$

As regards the parameter A figuring in the above equations, it follows from equation (17) and the definitions of S and τ that

$$A\,rA = hS \qquad (23)$$

By elimination of h from the equations (23) and (11) or (13) the following equations for S are obtained:

in the case of rectification with constant W:

$$S = A\,rA + \frac{1 - A\,rA X_H}{X_S} = A\,rA + Q \qquad (24)$$

in the case of ordinary batch rectification:

$$S = A\,rA + \frac{1 - A\,rA X_H - X_{S,h=0}}{X_S} = A\,rA + Q - \frac{X_{S,h=0}}{X_S} \qquad (25)$$

For the quantity Q introduced into these equations a relatively simple equation holds:

$$Q = \alpha \times \frac{(rA - a_2)\exp(-a_1 A) + (a_1 - rA)\exp(-a_2 A)}{\{(\alpha - 1) - a_2\}\exp(-a_1 A) + \{a_1 - (\alpha - 1)\}\exp(-a_2 A)} = \alpha \frac{1 + \{(p - rA)/q\}\tanh q A}{1 + [\{p - (\alpha - 1)\}/q]\tanh q A} \qquad (26)$$

$$\left[p = \tfrac{1}{2}(a_1 + a_2); \quad q = \tfrac{1}{2}(a_1 - a_2) = \sqrt{p^2 - A}\right]$$

By means of the equations given above numerical values of S, X_S, X_H and $\bar{X}$ can be calculated if values of α, r, A and h are given. For this purpose the parameter A has to be assigned a certain value and S must be calculated by means of equation (24) or (25). From equation (23) the value of h corresponding to the chosen value of A is then found. Subsequently, another value is to be assigned to A, etc. In the range of low values of h numerical calculations can be

shortened by assuming X_S and X_H to be linearly dependent on h.

Special forms of the equations

The forms which the equations assume in boundary cases ($r \to 0$, $r \to \infty$, $A \to 0$, $A \to \infty$) will, for the sake of brevity, be omitted, except in cases where they will be needed in the discussions. They can be derived through the introduction of new parameters, being the limits of Ar or AA; in those cases where $A \to 0$ and $A \to \infty$, $\lim \lambda/A$ has to be introduced to denote the place in the column. It will be seen that S can be expressed as an explicit function of h, except for the case where $A \to 0$.

Also for some specific values of A the equations assume special forms.

(1) By assuming $A = 0$ equations are obtained which apply to the case where h is equal to zero, which means that the holdup has no influence.

(2) With $A = \dfrac{\alpha - 1}{r}$ the equations for X, Y, S and h assume the following simple forms:

$$X = Y = e^{-(\alpha-1)(A-\lambda)}$$

$$S = \alpha + (\alpha - 1)A$$

$$h = \frac{1}{1 + [\alpha/(\alpha - 1)A]}$$

These equations occasion the following remarks:

(a) The reflux ratio r does not appear.

(b) X and Y are equal and have the same value as with total reflux. Y can be shown to be smaller than X at values of h exceeding the one mentioned above.

(c) Elimination of A leads to the equation $S = \dfrac{\alpha}{1 - h}$, which equation also gives the relation between S and h if $r = 0$ (W constant).

(3) Both for $A = (1 - \sqrt{\alpha}\,R)^2$ and for $A = (1 + \sqrt{\alpha}\,R)^2$, q is equal to zero. The equations applying to these cases must be found as limits. For values of A lying between the two values mentioned above, q is imaginary. However, after replacement of q by ig ($g = \sqrt{(A - p^2)}$) and introduction of goniometric functions the equations assume real forms again. The case in which $A = (1 - \sqrt{\alpha}\,R)^2$ coincides with the case mentioned in (2) if $r = \dfrac{1}{\alpha - 1}$; it occurs at other values of r if $A > \dfrac{\alpha - 1}{r}$ and r is not too great. The case in which $A = (1 + \sqrt{\alpha}\,R)^2$ can be encountered with constant W only if A is very small ($A < (3 + 2\sqrt{2})^{-1}$ for $\alpha > 1$).

The influence of the amount of holdup

The influence of the amount of holdup is of a complicated nature. Various effects may be distinguished. Before discussing them we will first explain some figures illustrating the influence of the holdup. W is assumed to be constant.

Fig. 2 gives X as a function of λ for the case ($\alpha = 1{\cdot}5$, $r = 40$, $A = 10$) at various values of A and hence of h. The curve for $A = 0$ ($h = 0$) shows the general course. The influence of A can

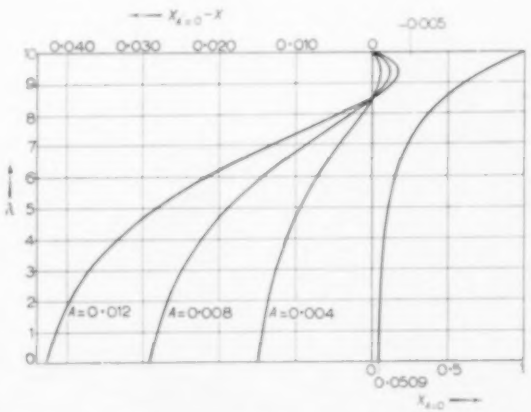

FIG. 2. X as a function of λ at different values of A ($\alpha = 1{\cdot}5$, $r = 40$, $A = 10$). The values 0, 0·004, 0·008 and 0·012 of A correspond with values of h equal to 0, 0·077, 0·158, 0·390 respectively, for rectification with constant W. The right-hand side of the figure shows the curve for $A = 0$, the left-hand side shows the deviations from this curve on an enlarged scale.

be seen from the deviation curves plotted on an enlarged X scale. The influence of the holdup on $X_{\lambda=0}$ and hence on X_S proves to be strong: $X_{\lambda=0}$ decreases strongly as A and h rise.

A remarkable aspect of Fig. 2 is that the deviation curves for a value of λ, which is 1·513 smaller than A, have a common point of intersection lying on the λ axis. At this value of λ, X has the same value as if there were no influence of the amount of holdup and from there the influence of the amount of holdup on X is reversed. In reality the curves do not intersect in one mathematical point. For, numerical calculations show that $(dX/dA)_{A=0}$ and $(dX/dA)_{A=(\alpha-1)/r}$ are equal to zero not at the same value of λ but at values differing by 0·00044.

As X is a function of $A - \lambda$ Fig. 2 after shifting of the zero-point of the λ axis also holds for other values of A. It should be borne in mind, however, that at other values of A the values of A correspond with other values of h.

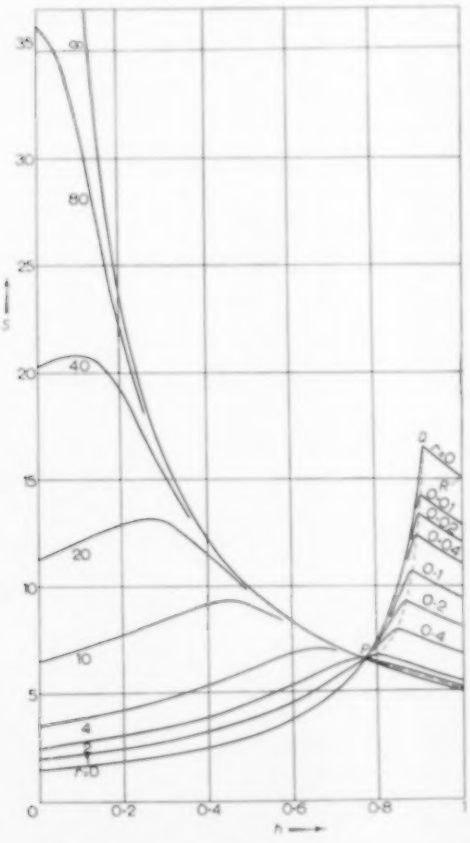

FIG. 3. S as a function of h at different reflux ratios for rectification with constant W ($\alpha = 1{\cdot}5$; $A = 10$).

Fig. 3 shows, for the case ($\alpha = 1{\cdot}5$, $A = 10$) the ratios between S and h for a number of values of r.

From this figure it is seen that below a certain value of r – lying between 40 and 80 – maxima occur, which are shifted to higher values of h as r decreases. A similar picture is shown in Fig. 2 of HOUTMAN and HUSAIN's article [6]. This figure applies to ordinary batch rectification in the case where $x_D = 0{\cdot}5$*. It is seen that an analogy exists between the situation for $x_D = 0{\cdot}5$ and the situation for small values of x_D. A difference is in the fact that the curves of Houtman and Husain have a practically symmetrical course near a maximum. Another and moreover remarkable difference is that in Fig. 3 the curves have a common point of intersection (P) (see p. 113, (2)), and that the series of maxima continues to the right of P towards higher values of S.

To the right of P the highest value of S, viz. $\alpha(1 + A)$, is reached by the curve for $r = 0$. However, in this case the maximum has degenerated to a discontinuity. Moreover, a study of the equations shows that the highest point (Q) corresponds with a situation in the column at which $x = 0$ for $\lambda < A$. This also is a degeneration. The same is true for the branch QR (a hyperbole corresponding to the equation $hS = \alpha A$). Here the limit of the assumption of a stationary state of the second order has been reached. It is assumable that this is indicated already in the region below QR, by the length of the time needed in rectification with constant W for approaching to the stationary state of the second order if the initial state deviates from it. This implies that the assumption of a stationary state of the second order existing in ordinary batch rectification is inadequate at high values of h and low values of r.

* The quantities plotted on the axes of HOUTMAN and HUSAIN's figure are $S_{x_D=0.5}$ (twice the pole height) and 0·5 h.

The two dotted curves starting from P enclose an area in which A is greater than $(1 - \sqrt{\alpha}\,R)^2$ (see p. 113, (3). One curve connects P with Q and is intersected by the curves for values of r ranging from 0 to 2 $(= 1/(\alpha - 1))$. The maxima of these curves do not lie on the curve PQ, but slightly to the left of it. The other curve is intersected at a small angle by curves (not shown in the figure) for values of r ranging from 2 to about 3.

Fig. 4 shows the relation between S and h for a number of values of r at a small value of A (0·5) ; here also, $\alpha = 1{\cdot}5$. For practical purposes this figure has little importance, but it is interesting from a mathematical point of view.

After passing through the common point of intersection P, the curves appear to intersect again, this time not in one point, but, for not too low values of r, still in a very small area (G). It is not accidental that in this area S is only little greater than α. The curve for $r = 0$ lies rather far outside this area. At the curve for $r = 0{\cdot}1$ a shifting in the direction of the curve for $r = 0$ is already perceptible. This shifting is accompanied by the occurrence of minimum values of S which are reached (for given values of h) at certain values of r.

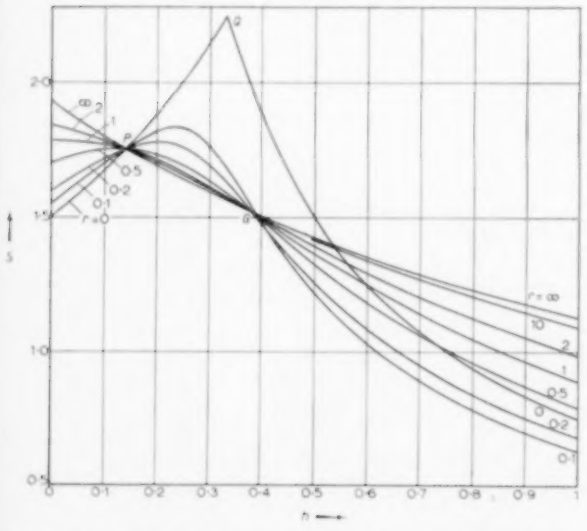

FIG. 4. S as a function of h at different reflux ratios for rectification with constant W ($\alpha = 1{\cdot}5$; $A = 0{\cdot}5$).

Several aspects of the influence of the amount of holdup come to light clearly in the extreme cases where $r = 0$, $r \to \infty$, $A = 0$, $A \to \infty$, which will be discussed below.

$r = 0$. If $r = 0$ and h may be put equal to zero the (stagnant) liquid in a column is in equilibrium with the vapour and has the same composition throughout the column. This changes as soon as h becomes greater than zero. For a given cross-section of the column the liquid composition then lags behind the vapour composition which changes with time. Now the liquid tries to accommodate itself to the vapour by giving off volatile matter to the passing vapour. As a consequence a concentration gradient is maintained in the longitudinal sense of the column, on account of which X_S is lower than $X_{S,h=0}$. This is manifest in an increase of S (cf. equation (27)).

This effect of the holdup, lowering X_S and consequently raising S, might be called the *accommodation effect*. It occurs under all circumstances, except when r approaches to infinity and, consequently, a stationary state of the first order results, and also when A is equal to zero, which means that there is no possibility of accommodation. This effect agrees in nature with the " flywheel effect " of PIGFORD *et al.* [10].

$r \to \infty$. In the case of $r \to \infty$ one is concerned with a stationary state of the first order. The change in the concentration from the still to the top of the column is then independent of h. However, there is an influence of h on $\bar{X}$ $(= X_S + h\,(X_H - X_S))$; an increase of h causes $\bar{X}$ to rise and hence S to decrease. This effect of the holdup, lowering S, which proceeds from the accumulation of volatile matter in the holdup (term $h\,(X_H - X_S)$), might be called the *accumulation effect*. In nature, it corresponds with the " depletion effect " of Pigford *et al.*

The accumulation effect occurs under all circumstances, as X_H is always greater than X_S, which is a result of :

(1) the rectifying power of a column (the only cause if $r \to \infty$),

(2) the accommodation effect,

(3) a third cause, which is the only one if $A = 0$ (see sub $A = 0$).

If $A \to \infty$ or $r = 0$, X_H, at not too high values of h, is only slightly greater than X_S, so that the

accumulation effect then has little significance (see sub $A \to \infty$).

The accumulation and accommodation effects oppose each other. This is manifest in the occurrence of maxima in most of the curves shown in Fig. 3 and in the fact that these curves have a common point of intersection (P).

$A = 0$. In this case the column serves only as a temporary storage for the liquid fed in as reflux at the top, there being no effective contact between vapour and liquid. It is remarkable that the concentration of the lighter component in the liquid now increases in the downward direction (at a given moment). This is caused by the steady decrease of the concentration in the reflux and by the absence of mixing in the direction of flow (assumption (f) p. 106). It will be clear that in this case $X_H > \alpha X_S$. Consequently, the accumulation effect occurs here. In view of the special cause of this effect if $A = 0$ it might here be termed the *dead space effect*.

The dead space effect also occurs in normal cases, when it may be considered as that part of the accumulation effect which is due to the tendency of the liquid contained in the column to lag behind in concentration. In normal cases there is, admittedly, no question of an increase in the downward direction of the concentration of the lighter component, but there is as a rudiment a rise of X with respect to $X_{h=0}$ near the top of the column (see Fig. 2).

The dead space effect disappears if A or r approaches infinity, and is felt more strongly as A or r decreases. It is clearly observed in Fig. 4, in that the curve for $r \to \infty$ is intersected for the second time by the other curves at G and in that at high values of h, S is highest if r approaches infinity.

$A \to \infty$. In this case X and Y undergo a stepwise change at the top of the column. It can be proved that X jumps from $X_{S,h=0}$ to 1 and that, in the column, for small values of h, X increases approximately linearly from $(1 - h)\, X_{S,h=0}$ $(\lambda = 0)$ to $X_{S,h=0}$ $(\lambda \to A)$ (this increase is caused by the accommodation effect). This means that at small values of h the main change in the concentration is at the top of the column, so that X_H differs little from X_S. At low values of h the accumulation effect is consequently felt only slightly and the column behaves, as far as this effect is concerned, almost as if the holdup were part of the contents of the still.

Equating of $\bar{X}$ and X_S, which implies neglect of a term containing h^2 (accumulation effect) with respect to a term containing h (accommodation effect) leads to:

$$S = \frac{S_{h=0}}{1 - h} \qquad (27)$$

A derivation in which no approximations are used leads to the same equation.

The case with $r = 0$ (A finite) is alike in character to the case where $A \to \infty$. If $r = 0$, there is no concentration jump at the top of the column; x_D and $x_{\lambda=A}$ do differ, however. Equation (27) applies, provided $h < A/(A + 1)$.

The cases $A \to \infty$ and $r = 0$ also agree in that if h approaches zero, the liquid assumes the same concentration throughout the column (except the top in the case that $A \to \infty$) and the column is in a so-called "pinch" state. The weakening of the accumulation effect as a result of a small difference between X_H and X_S might therefore be termed the *pinch effect*.

It will be clear that this effect is stronger according as A is greater and r is smaller.

Numerical example

Given: a column with five transfer units, by means of which, in an ordinary batch rectification at a reflux ratio of 12, a substance is removed for which $\alpha = 2$; the mole fraction of this substance in the distillate is equal to 0·02 at the moment when $h = 0{\cdot}1$.
Find:

(1) the value of $\bar{x}$ at this moment;

(2) the value of $\bar{x}$ reached when 5 per cent of the still contents has been distilled off.

After 5 per cent of the contents of the still has been distilled off, h is equal to $0{\cdot}1 : 0{\cdot}95 = 0{\cdot}105263$. Consequently, calculations have to be made for $h = 0{\cdot}1$ and $h = 0{\cdot}105263$. Calculation shows (a choice of A values has been made with the aid of preceding calculations):

for $A = 0{\cdot}022362$: for $A = 0{\cdot}023362$:

$X_S = 0{\cdot}052595$	$X_S = 0{\cdot}051722$ (eq. (21))
$X_H = 0{\cdot}221725$	$X_H = 0{\cdot}221349$ (eq. (22))
$Q = 13{\cdot}3569$	$Q = 13{\cdot}3354$
$S = 13{\cdot}3167$	$S = 13{\cdot}3318$ (eq. (25))
$h = 0{\cdot}100755$	$h = 0{\cdot}105141$ (eq. (23))

whence it follows for dX_S/dh and dX_H/dh in a range close to $h = 0{\cdot}1$:

$$\frac{dX_S}{dh} = -0{\cdot}1990\,; \quad \frac{dX_H}{dh} = -0{\cdot}0857$$

From small extrapolations it now follows that:

$$\left.\begin{aligned} X_S &= 0{\cdot}052745 \\ X_H &= 0{\cdot}221790 \end{aligned}\right\} \text{for } h = 0{\cdot}1$$

$$\left.\begin{aligned} X_S &= 0{\cdot}051698 \\ X_H &= 0{\cdot}221339 \end{aligned}\right\} \text{for } h = 0{\cdot}105263$$

This leads to:

$$\left.\begin{aligned} \bar{X} &= 0{\cdot}069649 \\ S &= 13{\cdot}3141 \end{aligned}\right\} \text{for } h = 0{\cdot}1$$

$$\left.\begin{aligned} \bar{X} &= 0{\cdot}069555 \\ S &= 13{\cdot}3321 \end{aligned}\right\} \text{for } h = 0{\cdot}105263$$

At the moment when $x_D = 0{\cdot}02$ and $h = 0{\cdot}1$, $\bar{X} = 0{\cdot}069649$, so that $\bar{x}$ is equal to $0{\cdot}02 \times 0{\cdot}069649 = 0{\cdot}0013930$ (answer to point 1).

Applying equation (15) and considering S to be a constant having the value 13·3231, one finds:

$$\frac{\bar{x}}{\bar{x}_0} \times \frac{\bar{X}_0}{\bar{X}} = 0{\cdot}50491$$

so that at the moment when $h = 0{\cdot}105263$ (i.e. after 5 per cent of the still contents has been distilled off) $\bar{x} = 0{\cdot}50491 \times 0{\cdot}0013930 \times 0{\cdot}069555 : 0{\cdot}069649 = 0{\cdot}0007024$ (answer to point 2).

Remarks. (1) From the values found for dX_S/dh and dX_H/dh it follows that the value of the neglected term $h^2(dX_H/dh - dX_S/dh)$ (see p. 110) is 0·001133. As this term is much smaller than $X_{S,h=0}$ it was, indeed, permissible to neglect it. The numerical results show more decimal places than is permitted in view of the neglect of this term, however.

(2) That X_S and X_H show an almost linear change with h from $h = 0$ to $h = 0{\cdot}1$ is seen from the fact that the decrease of X_S and X_H from $h = 0$ to $h = 0{\cdot}1$ is 0·01994 and 0·00836 respectively, which numbers, after division by 0·1, deviate but little from the values found for $-dX_S/dh$ and $-dX_H/dh$. The parameter A also shows a linear change. From the definition of $\bar{X}$ it is clear that a similar remark does not apply to this quantity; it tends to a minimum (and hence S tends to a maximum).

Notation*

a_1, a_2 = roots of the quadratic equation $a^2 - (\alpha R - 1 - A)a + A = 0$

h = amount of holdup as a fraction of the amount of liquid contained in still and column, $= H/M$

l = distance from the bottom end of a column (metres)

$m = (\alpha - 1)A$

$p = \frac{1}{2}(\alpha R - 1 - A) = \frac{1}{2}(a_1 + a_2)$

$q = \sqrt{(p^2 - A)} = \frac{1}{2}(a_1 - a_2)$

r = reflux ratio, $= \dfrac{L}{V - L}$

t = time (seconds)

v_L = amount of holdup formed by liquid per metre of column (moles/metre)

v_V = amount of holdup formed by vapour per metre of column (moles/metre)

x = mole fraction of the lighter component in the liquid

x_H = mean mole fraction of the lighter component in the holdup formed by the liquid

$\bar{x} = (1 - h)x_S + hx_H$

y = mole fraction of the lighter component in the vapour

$y^*(x)$ = mole fraction of the lighter component in the vapour that is in equilibrium with liquid in which the mole fraction of the lighter component is equal to x.

$z = \dfrac{1}{\alpha X_{S\infty}}$

* For the sake of convenience amounts are expressed in moles and consequently fractions are considered as being mole fractions. One is free to use other units for expressing amounts (the use of a volumetric unit requires the introduction of a proportionality factor). Instead of "meter" and "second" may be read "unit length" and "unit time."

A = parameter
D = amount of distillate (moles)
$E = (r+1)\dfrac{D}{W_0}\Big/\left(1-\dfrac{D}{W_0}\right)$
H = amount of holdup (moles)
K = mass transfer coefficient (moles/m² sec)
L = rate of flow of liquid through horizontal cross-section of a column (moles/sec)
M = amount of liquid contained in still and column (moles), $= W + H$
N = number of theoretical plates
O = area of interface between liquid and vapour per metre of column (metres)
$Q = \dfrac{1 - A\,r\,AX_H}{X_S}$
$R = \dfrac{r+1}{r}$
$S = -\dfrac{d\ln x_D}{\dfrac{dD}{M}}$
V = rate of flow of vapour through horizontal cross-section of a column (moles/sec)
$X = x/x_D$
$X_H = x_H/x_D$
$\bar{X} = \bar{x}/x_D$
$Y = y/x_D$
α = relative volatility, proportionality constant in the relation $y^* = \alpha x$
$\epsilon = (X_S/X_{S\infty}) - 1$
λ = distance from bottom end of a column, measured in transfer units
τ = dimensionless measure of time, $= \dfrac{L}{V}\cdot\dfrac{KO}{v_L}\cdot t$
ρ = reboil ratio (= moles of vapour per mole of bottom product)
Λ = number of transfer units

Indices

D = distillate
H = holdup
S = still
0 = $t = 0$
∞ = $A \to \infty$

References

[1] Bowman J. R. and Briant R. C. *Industr. Engng. Chem.* 1947 **39** 745.

[2] Bowman J. R. and Cichelli M. T. *Industr. Engng. Chem.* 1949 **41** 1985.

[3] Chilton T. H. and Colburn A. P. *Industr. Engng. Chem.* 1935 **27** 255, 904.

[4] Colburn A. P. *Industr. Engng. Chem.* 1941 **33** 459.

[5] Colburn A. P. and Stearns R. F. *Trans. Amer. Inst. Chem. Engrs.* 1941 **37** 291.

[6] Houtman J. P. W. and Husain A. *Chem. Engng. Sci.* 1956 **5** 178.

[7] Jaswon M. A. and Smith W. *Proc. Roy. Soc.* A 1954 **225** 226.

[8] Lewis W. K. *Industr. Engng. Chem.* 1936 **28** 399.

[9] Lloyd L. E. *Petrol. Refiner* 1950 **29** No. 2 135.

[10] Pigford R. L., Tepe J. B. and Garrahan C. J. *Industr. Engng. Chem.* 1951 **43** 2592.

[11] Lord Rayleigh *Phil. Mag.* 1902 **4** 521. Copy consulted in *A Source Book of Technical Literature on Fractional Distillation*. Gulf Research and Development Company.

[12] Rose A. and Rose E. *Technique of Organic Chemistry* (edited by A. Weissberger) Interscience, Inc., London and New York 1951. Part IV (*Distillation*), Chap. I.

[13] Rose A., Johnson R. C. and Williams Th.J. *Industr. Engng. Chem.* 1951 **43** 2459.

[14] Rose A. and Johnson R. C. *Chem. Engng. Progr.* 1953 **49** 15.

[15] Zuiderweg F. J. *Chem.-Ing.-Tech.* 1953 **25** 297.

Chemical Engineering Science, 1958, Vol. 9, pp. 119 to 129. Pergamon Press Ltd.

Mass-transfer from single solid spheres—I

Transfer at low Reynolds numbers

F. H. Garner and R. B. Keey

(*Received* 13 *January* 1958)

Abstract—A low-speed water-tunnel is described to enable dissolution rates of pelleted organic acid spheres to be measured. Results are obtained for the overall and local mass-transfer rates from $\frac{3}{4}$ in. diameter benzoic acid spheres to water at 30·0°C between Reynolds numbers of 2·3 and 255. Comparison with similar data enables the upper limit to be extended to 900. Results show that the bulk flow depresses the mass-transfer rate over a certain flow range and that free-convective effects are not entirely absent until $N_{Re} = 750$. This effect is the more pronounced in downflow. At Reynolds numbers greater than 250 the overall transfer results tend towards the theoretical relationship

$$N_{Sh} = 0{\cdot}94\, N_{Re}^{1/2}\, N_{Sc}^{1/3}.$$

Résumé—L'auteur décrit un tunnel à eau, de faible vitesse, permettant la mesure des vitesses de dissolution de sphères d'acide organique. Les vitesses de transfert massique, globales et locales, entre des sphères d'acide benzoïque de 1·9 cm de diamètre et l'eau à 30·0°C, ont été obtenues pour des nombres de Reynolds de 2·3 à 255. La comparaison de ces mesures avec d'autres résultats similaires a permis d'extrapoler la valeur limite du nombre de Reynolds jusqu'à 900. Les résultats montrent, que dans un certain domaine l'écoulement diminue la vitesse de transfert massique et que les influences de la convection libre n'ont entièrement disparues qu'au dessus d'un nombre de Reynolds de 750. Cet effet est le plus important pour l'écoulement descendant. Pour les nombres de Reynolds supérieurs à 250, les résultats du transfert global tendent à obéir à l'équation théorique

$$N_{Sh} = 0{\cdot}94\, N_{Re}^{1/2}\, N_{Sc}^{1/3}.$$

Zusammenfassung—Zur Messung der Auflösungsgeschwindigkeit von kompakten Kugeln aus oganischen Säuren wurde win Wasserkanal für geringe Geschwindigkeiten errichtet. Gemessen wurde die gesamte und die örtliche Stoffübertragungsgeschwindigkeit von Kugeln aus Benzoesäure von 19 mm Durchmesser an Wasser von 30°C im Bereich der Reynoldszahl von 2·3 bis 255. Durch Vergleich mit ähnlichen Messungen konnte die obere Grenze auf 900 ausgedehnt werden. Die Versuchsergebnisse zeigten, dass die Hauptströmung in gewissen Geschwindigkeitsbereichen die Stoffübergangszahl herabsetzt und dass bis Re = 750 auch der Einfluss der freien Konvektion nicht zu vernachlässigen ist, insbesondere bie abwärtsgerichteter Strömung. Bei Reynoldszahlen über 250 erreicht die Stoffübergangszahl die theoretische Beziehung

$$N_{Sh} = 0{\cdot}94\, N_{Re}^{1/2}\, N_{Sc}^{1/3}.$$

Introduction

Operations in which one fluid phase is dispersed throughout another are common and the limiting case of infinite drop viscosity (a solid dispersed phase) is of some importance. This limit is approached, whenever droplets are contaminated with surface-active compounds, which include many greases.

Whenever there is a concentration gradient, there is a migration of ions or molecules in the direction of decreasing concentration. This is known as mass-transfer. If such a process takes place uninfluenced by extraneous forces, this movement is termed molecular diffusion. In practice the differences in concentration result in differences of density, which cause a flow due to gravitational forces. This motion convects material from the phase boundary and so promotes mass-transfer. Such a flow is known as free or natural convection. The solute laden

material at the interfacial boundary will either fall or rise, depending upon whether this solution is heavier or lighter than the solvent. There may be a relative motion between the drop and the continuous phase due to centripetal, gravitational or inertial forces on the drop and the inertia of the fluid. For solid drops, analysis of this type of motion can be simplified by rigidly supporting the drop and allowing a controlled flow to wash over it. The latter motion is called forced convection.

While some attention has been given to these processes separately, there is little information about transfer when all modes of transfer are equally significant. In general, the amount of material transferred by molecular diffusion alone is small. The present paper will deal with some aspects of the problem of transfer when both free and forced convection occur. The work in this paper is confined to spheres, which approximate to drop shapes.

Theory

An estimate of the rate of mass-transfer in forced convection alone gives a datum for comparison with the total mass-transfer rate. Previous "exact" methods are time-consuming and demand tedious numerical integrations [6, 26]. Others based on the concept of the boundary-layer (see below) are limited in scope. The only method [1] available to predict mass-transfer rates from the whole surface assumes that this layer is constant throughout the wake behind the sphere. Since at low Reynolds numbers ($N_{Re} < 450$) the wake consists of a toroidal vortex [8], this assumption cannot be sound. A new method is therefore proposed:

A mass balance over any volume of an incompressible fluid, in which there are neither sources nor sinks, gives

$$\nabla \cdot \mathbf{U} = 0. \qquad (1)$$

When Newton's law of fluid stress holds, the equation of motion becomes for steady flows:

$$\mathbf{U} \cdot \nabla \mathbf{U} = \mathbf{F} - \frac{1}{\rho} \nabla P + \nu \nabla^2 \mathbf{U}. \qquad (2)$$

Equations (1) and (2) have no known elegant solution. These equations may be simplified by the concept of a boundary-layer over a surface. It is postulated that all viscous effects are confined to a thin zone near the surface and the flow outside this layer is inviscid. It is assumed that the thickness of this layer, δ is small compared to the characteristic dimension of the surface and quantities of order δ are thus neglected. Equations (1) and (2) then become:

$$\frac{\partial (ru)}{\partial x} + \frac{\partial (rv)}{\partial y} = 0,$$

$$u \frac{\partial u}{\partial x} + v \frac{\partial u}{\partial y} = \nu \frac{\partial^2 u}{\partial y^2} - (\nabla p = 0) \qquad (3)$$

These have been solved by Tomotika [22] for flow around a sphere. He assumes that the motion outside the boundary-layer is described by inviscid flow over a spherical surface. The solution may be written

$$Z = \frac{1}{u_1} g(\Lambda) + Z^2 u_1'' h(\Lambda) - \frac{r_0'}{r_0} \frac{1}{u_1'} h^*(\Lambda) \qquad (4)$$

where

$$Z = \frac{\delta^2}{\nu} = \Lambda / u_1', \quad u_1' = \frac{du_1}{dx}, \text{ etc.}$$

and $g(\Lambda)$, $h(\Lambda)$ and $h^*(\Lambda)$ are algebraic functions of Λ. Equation (4) can be used over the surface before separation of the forward-flow, but begins to break down when the flow in the boundary-layer decelerates.

Certain theoretical considerations [12] indicate that the skin-friction in the back-flow region is small over the flow range: $40 < N_{Re} < 1000$

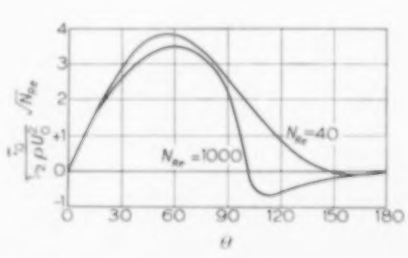

Fig. 1. Variation of skin-friction over sphere surface.

(Fig. 1). If the skin-friction in the wake is neglected, then, assuming a quartic velocity distribution in the boundary-layer, we get:

$$\tau_0 = \mu \left[\frac{\partial u}{\partial y}\right]_{y=0} = \left[\frac{12 + A}{6}\right] \frac{\mu}{\delta}. \qquad (5)$$

It follows that $A = -12.$ (6)

This is a sufficient solution of wake flow for the present purposes.

For solute of low solubility it is presumed that the diffusion has no significant effect on the hydrodynamics of the problem. Thus equations (3) and that of mass-transfer can be regarded as independent equations.

It is assumed there are no ionic effects and the diffusion is isothermal and isobaric. If the solvent velocity is small, an analysis of the resultant flux due to diffusion over an elemental volume of fluid under steady conditions is given by:

$$\mathbf{U} \cdot \nabla c = \mathscr{D} \nabla^2 c. \qquad (7)$$

To solve the problem, following the method suggested by Grafton [11], we assume all concentration changes occur over a thin layer near the surface. For convenience we define the variables:

$$\psi = \frac{c - c_1}{c_0 - c_1} \text{ and } \eta = y/\delta_M. \qquad (6)$$

It is assumed that the concentration distribution in this layer can be given by a simple algebraic expansion, viz:

$$\psi = a_0 + a_1 \eta + a_2 \eta^2 + \ldots + a_n \eta^n.$$

In practice only the first five terms are taken. The coefficients, $a_0 \ldots a_n$, are found from boundary conditions; four of these can be written down straightway:

At $\eta = 1$,

$$\psi = \psi_1, \frac{\partial \psi}{\partial \eta} = 0, \frac{\partial^2 \psi}{\partial \eta^2} = 0.$$

At $\eta = 0$,

$$\psi = \psi_0.$$

The fifth condition is found from equation (7). At the surface this becomes:

$$v \left(\frac{\partial c}{\partial y}\right)_{y=0} = \mathscr{D} \left(\frac{\partial^2 c}{\partial y^2}\right)_{y=0}.$$

Replacing ρv by m, the radial mass flux per unit surface, we get

$$\left(\frac{\partial^2 \psi}{\partial \eta^2}\right)_{\eta=0} = \frac{m}{\rho \mathscr{D}} \left(\frac{\partial \psi}{\partial \eta}\right)_{\eta=0}$$

Whence the unknown coefficients become:

$$a_0 = 0, \qquad a_2 = \frac{6m_0}{6 + m_0},$$

$$a_1 = -\frac{12}{6 + m_0}, \quad a_3 = \frac{4(3 + 2m_0)}{6 + m_0},$$

$$a_4 = \frac{3(2 + m_0)}{6 + m_0},$$

where $m_0 = \dfrac{m}{\rho \mathscr{D}} \delta_M.$

The rate of dissolution, m, is given by

$$m = -\mathscr{D} \rho \left(\frac{\partial \psi}{\partial \eta}\right)_{\eta=0},$$

i.e. $m_0 = -a_1(\psi_0 - \psi_1) = \dfrac{12}{6 + m_0}(\psi_0 - \psi_1),$

whence

$$m_0 = -3\left[1 - \sqrt{1 + \frac{4}{3}(\psi_0 - \psi_1)}\right]. \qquad (8)$$

The positive root is extraneous, as this implies that mass is being transferred to the sphere. For solutes of low solubility equation (8) can be simplified by retaining the first two terms of the binomial expansion, this gives:

$$m_0 = 2(\psi_0 - \psi_1). \qquad (9)$$

To solve equation (9) we must evaluate the thickness of the mass-transfer layer, δ_M. Formal calculations [14, 15] for a flat plate and a rotating disk give $\delta_M = \delta N_{Sc}^{-1/3}$. This expression agrees with the condition that the mass- and momentum-transfer film thicknesses are equal at $N_{Sc} = 1$. It is unlikely that such a relationship depends upon the geometry of the system and this is presumed to be valid in the present case.

The hydrodynamic boundary-layer thickness can be expressed in terms of a single flow parameter by:—

$$\Lambda = \frac{\delta^2}{\nu} u_1'. \qquad (10)$$

Following Tomotika's method, we find the variation of u_1' with angular distance from the forward stagnation point from the velocity potential of a sphere in inviscid flow :—

$$\phi_1 = U r \cos\theta \left[1 + \frac{1}{2}\left(\frac{a}{r}\right)^3\right],$$

whence $$u_1 = \frac{1}{r}\frac{\partial \phi_1}{\partial \theta} = \frac{3}{2} U \sin\theta.$$

and from equation (10)

$$\Lambda = \frac{3\delta^2}{\nu}\frac{U}{d}\cos\theta = 3\left(\frac{\delta_M}{d}\right)^2 N_{Re} N_{Sc}^{\frac{1}{3}} \cos\theta. \qquad (11)$$

By definition the mass-transfer coefficient K_L is $m/\rho\ (\psi_0 - \psi_1)$ and thus by combining equations (9) and (11), we obtain the local Sherwood number at an angle θ from the forward pole :—

$$N_{Sh} = \frac{K_L d}{\mathscr{D}} = 2\sqrt{3}\sqrt{\frac{\cos\theta}{\Lambda}}\, N_{Re}^{\frac{1}{2}} N_{Sc}^{\frac{1}{3}}. \qquad (12)$$

To obtain the average mass-transfer rate over a band from $\theta = \theta_1$ to $\theta = \theta_2$, equation (12) is integrated over that surface :

$$\left[N_{Sh}\right]_{\theta_1}^{\theta_2} = \left\{2\sqrt{3}\, N_{Re}^{\frac{1}{2}} N_{Sc}^{\frac{1}{3}}\right\} \frac{\int_{\theta_1}^{\theta_2} \sqrt{\frac{\cos\theta}{\Lambda}} \cdot 2\pi a^2 \sin\theta\, d\theta}{\int_{\theta_1}^{\theta_2} 2\pi a^2 \sin\theta\, d\theta}$$

$$= \left\{2\sqrt{3}\, N_{Re}^{\frac{1}{2}} N_{Sc}^{\frac{1}{3}}\right\} \frac{\int_{\theta_1}^{\theta_2} \left[\frac{\sin^2\theta\cos\theta}{\Lambda}\right]^{\frac{1}{2}} d\theta}{\cos\theta_2 - \cos\theta_1} \qquad (13)$$

In this manner overall transfer rates and those for the forward-flow and wake areas can be calculated using values of Λ calculated from equations (4) and (6). The integrands can be evaluated graphically and such values are compared to those presented by GARNER and SUCKLING [9]. These were obtained experimentally in a 3 in. diameter, horizontal water-tunnel over the range: $80 < N_{Re} < 900$, when the results are recalculated on the basis of constant Schmidt number as used in the experimental section. A rectilinear correlation between N_{Sh} and $\sqrt{N_{Re}}$ is found, and thus forced convection is assumed to predominate in this case.

Table 1. *Comparison of experimental and theoretical rates of mass-transfer in forced convection*

Area	$N_{Sh} N_{Re}^{-\frac{1}{2}} N_{Sc}^{-\frac{1}{3}}$		$\frac{T-E}{T}$ %
	theoretical (*T*)	*experimental* (*E*)	
overall	0·94	0·95	− 1·1
forward-flow	1·025	1·08	− 5·4
wake	0·785	0·67	+ 14·7
forward stagnation point	1·59	1·68	− 6·3
rear stagnation point	1·00	0·87	+ 13·0
ratio, forward/wake	2·5	2·8	− 12·0

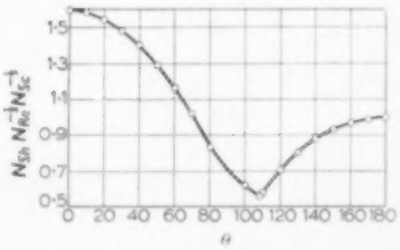

FIG. 2. Theoretical local mass-transfer rates in forced convection.

The close agreement between the values for overall transfer is somewhat fortuitous, as theoretical values compared to experimental ones are low in the forward-flow area and high in the wake. The distribution of local transfer rates is given in Fig. 2. Within the rear hemisphere there is a pronounced minimum, which corresponds to the separation ring. Nevertheless the theoretical relationship provides an adequate basis for comparisons with further experimental work.

Apparatus

Most water-tunnels have been designed primarily for hydraulic studies on cavitation [16]. Applications of such tunnels include free-stream propeller testing, the study of hydrofoils and the hydroballistic design of missile noses. Recently tunnels to study the dissolution of solid spheres [7] and to investigate diffusion-controlled chemical reactions [12] have been reported.

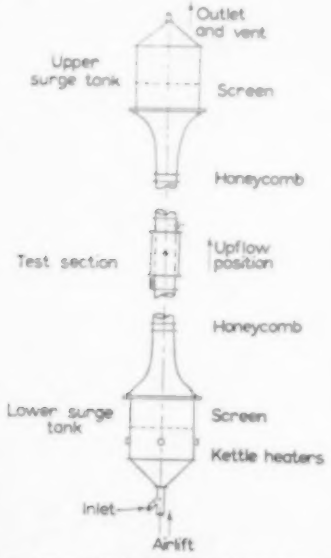

Fig. 3. Simplified diagram of water tunnel.

The plant consists of two water-tunnels placed endwise so that there would be similar hydrodynamic conditions for both upflow and downflow. A flowsheet of the plant is given in Fig. 3. It is designed for flow rates between 1·3 and 150 gal/hr and working temperatures between 50° and 100°F.

Water from the recirculation system discharges into one of the surge-tanks, fabricated from spun 18 S.W.G. copper sheet and holding about 20 gal. This allows viscous effects to damp out eddies in the incoming fluid. The inlet water is distributed through concentric rows of orifices and a 200 × 200 mesh bronze screen. Furthermore by reducing the fluid velocity to nearly zero, the increase in kinetic head athwart any cross-section is almost constant in the transition from the surge-tank to test-section diameter. The contraction is therefore smooth and of such a form that there is a uniform pressure distribution [13]. The water then passes through a honeycomb, consisting of 2 in. × 10 mm hexagonal brass tubes. From these, fluid filaments emerge parallel to the tube walls. A honeycomb like a screen of large free cross-sectional area, reduces the intensity of any upstream turbulence, but increases the scale of it.

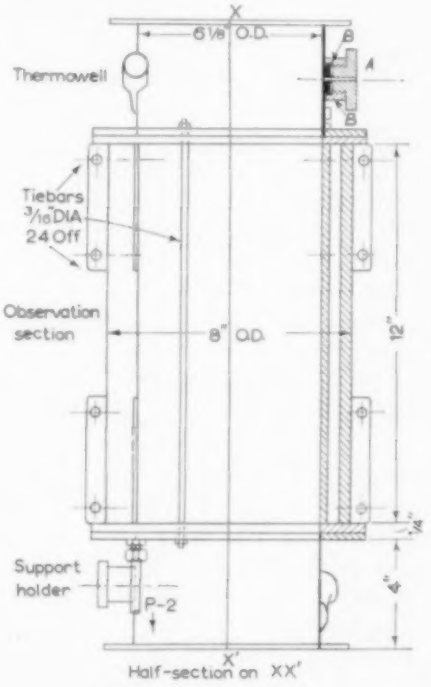

Fig. 4. Test section.

The test-section (Fig. 4) was designed for ease of dismantling for cleaning and for good observation of the flow field. This section consists essentially of a 12 in. × 6 in. Pyrex glass tube held between two end-plates by $\frac{3}{16}$ in. diameter tie-bars. These also secure $\frac{3}{8}$ in. Perspex sheets, which form a jacket round the test-section so that refractive distortion can be eliminated.

Flow control is achieved by throttling the by-pass valve and, at low flow rates, by reducing the voltage input to the pump motor with a variable autotransformer. For all runs the controllability, expressed as the average standard deviation from the mean flow rate, was 5·1 per cent.

Due to the slow circulating rate temperature control was fairly difficult. In the lower surge tank, four 2 kW kettle heaters are let in symmetrically together with a bimetallic temperature controller. The latter is connected in parallel to one of the heaters and the contacts of a hot-wire vacuum-switch. Cooling is effected by a single-pass, finned exchanger, having twenty-four $\frac{1}{2}$ in. fins on a $1\frac{1}{8}$ in. O.D. tube. To reduce the heat flux through the walls of the column, all the principal pipes are covered with a cellular asbestos-aluminium insulation of thermal conductivity 0·05 B.t.u/hr ft °F. The surge-tanks are lagged with a magnesia-asbestos cement and coated with retarded hemihydrate gypsum plaster to give a smooth finish. It is evident that the temperature control depends upon the flow rate and ambient temperature. For example, the temperature range is $\pm$ 0·1 °C at a circulation rate of 125 gal/hr and a working temperature of 30°C (86°F). The average standard deviation for all runs with up-flow was 0·2°C and for those with down-flow 0·4°C.

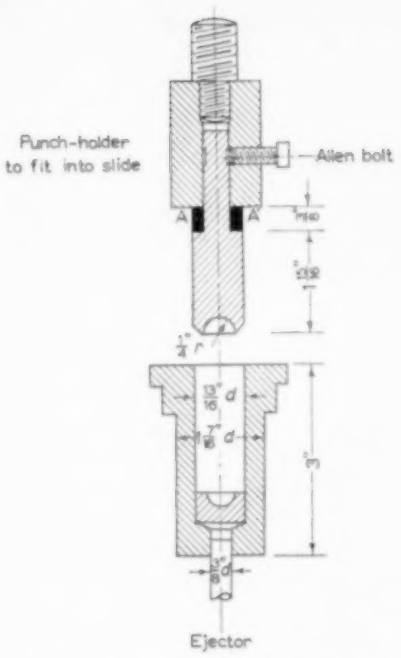

Fig. 5. Die and punch to make half-in. spheres.

Experimental Method

Materials used in the making of solid spheres are usually crystalline. Compression of the solid is preferable to casting, as the latter process tends to give diffential orientation to the crystals [17]. The material to be pelleted was compressed in a fly-press, which gave a maximum impact pressure of 5 tons/in². Excess solid was trimmed from the ejected pellet and it was recompressed several times, at first with extra material, but later alone. The die and punch holders are shewn in Fig. 5 and the faces AA′ are machined so that the punch and die face remain parallel. A clearance of about 0·003 in. gives a minimum flash, consistant with avoiding damaging the machined surfaces. It was satisfactory to use the materials as supplied by the manufacturer, since the random size distribution gave good pelleting properties [17]. In all cases any diameter of the pellet was within 1 per cent of the mean diameter and, in general, pellets of uniformly high density could be obtained to within 1 per cent of the commonly accepted value of the solid density.

To minimize disturbance to the flow, each sphere was supported at the rear stagnation point [10]. The one chosen consisted of a $1\frac{1}{2}$ in. $\times$ 0·015 in. diameter nichrome wire, soldered into a $9\frac{1}{4} \times \frac{1}{16}$ in. diameter brass rod, which was bent into an ell and fitted into the support holder (Fig. 4).

Before the spheres were mounted in the test-section, they were dipped into Teepol-B to ensure that the surface became completely wetted. This procedure is claimed to have no apparent effect upon the rate of dissolution [13, 19].

During each experiment the temperature and rotameter reading were noted at regular intervals and weighted mean values were used in evaluating the physical properties of the system.

Dissolution of the spheres was studied photographically using a double-extension bellows, plate camera of 170 mm focal length in conjunction with a supplementary lens of + 3 diopt. A uniformly-lit, matt background was used.

A number of $\frac{3}{4}$ in. diameter benzoic acid spheres were prepared with a little red azo-dye, Rhodamine-B, added in the final stages of compression. As orthochromatic material is

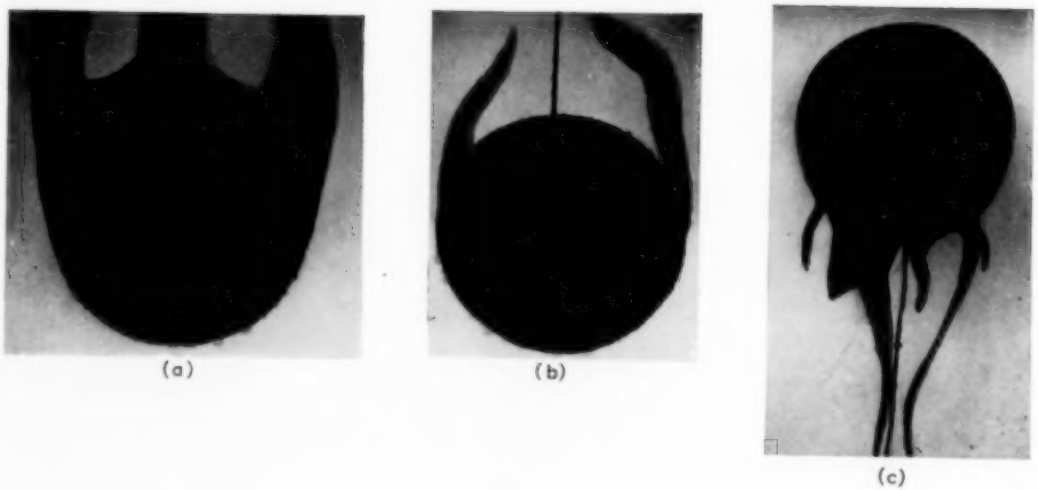

FIG. 6. Sphere in forced convection-dye traces.
(a) $N_{Re} = 82$ upflow
(b) $N_{Re} = 76$ upflow
(c) $N_{Re} = 82$ downflow

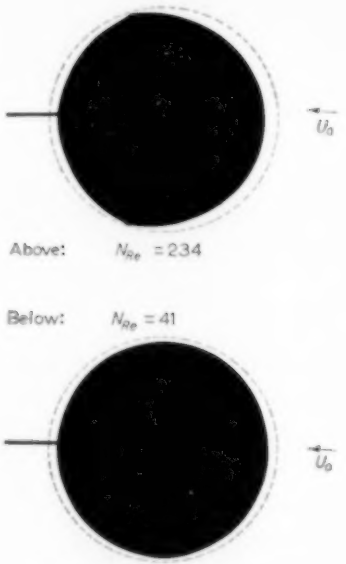

FIG. 7. Dissolution of benzoic acid spheres in upflow.

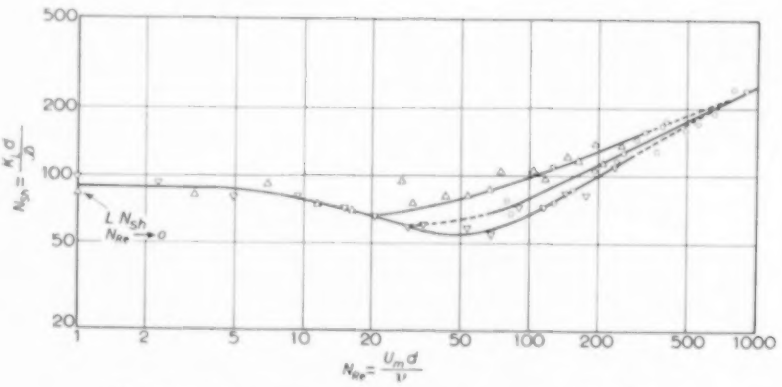

FIG. 8. Overall mass-transfer rates. $N'_{Ra} = 2{\cdot}74 \times 10^7$.
△ Upflow ▽ Downflow ○ Horizontal flow

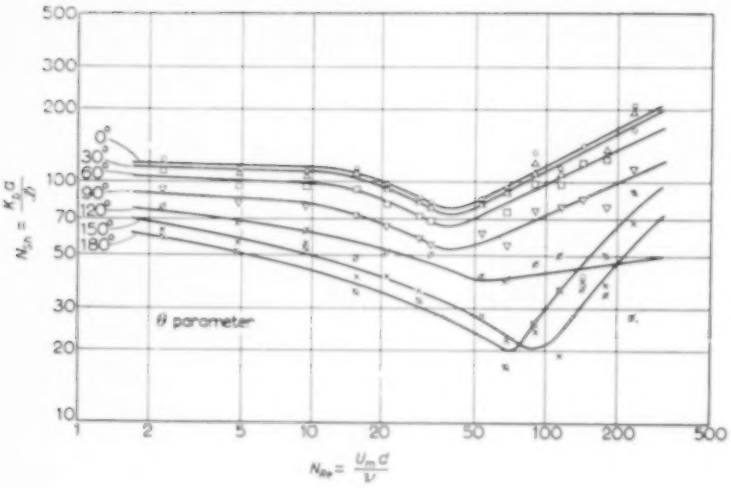

FIG. 9(a). Local mass-transfer rates in downflow at $N'_{Ra} = 2{\cdot}74 \times 10^7$.

○ 0°
△ 30°
□ 60°
▽ 90°
○ 120°
× 150°
○ 180°

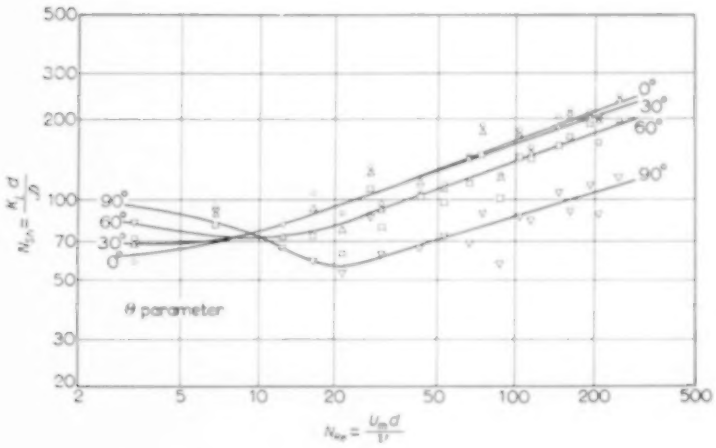

FIG. 9(b). Local mass-transfer rates in upflow over forward surface $N'_{Ra} = 2{\cdot}74 \times 10^7$.

○ 0°
△ 30°
□ 60°
▽ 90°

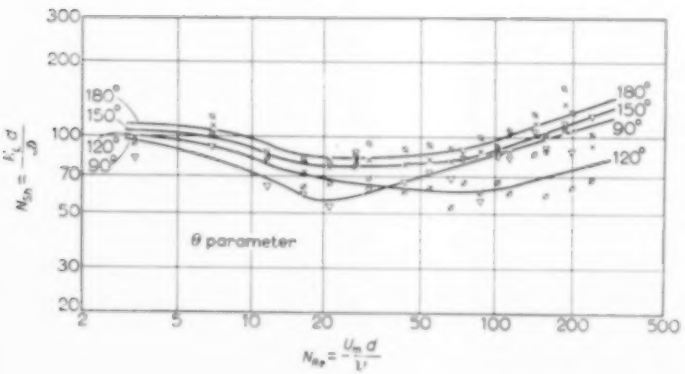

▽ 90°
○ 120°
× 150°
○ 180°

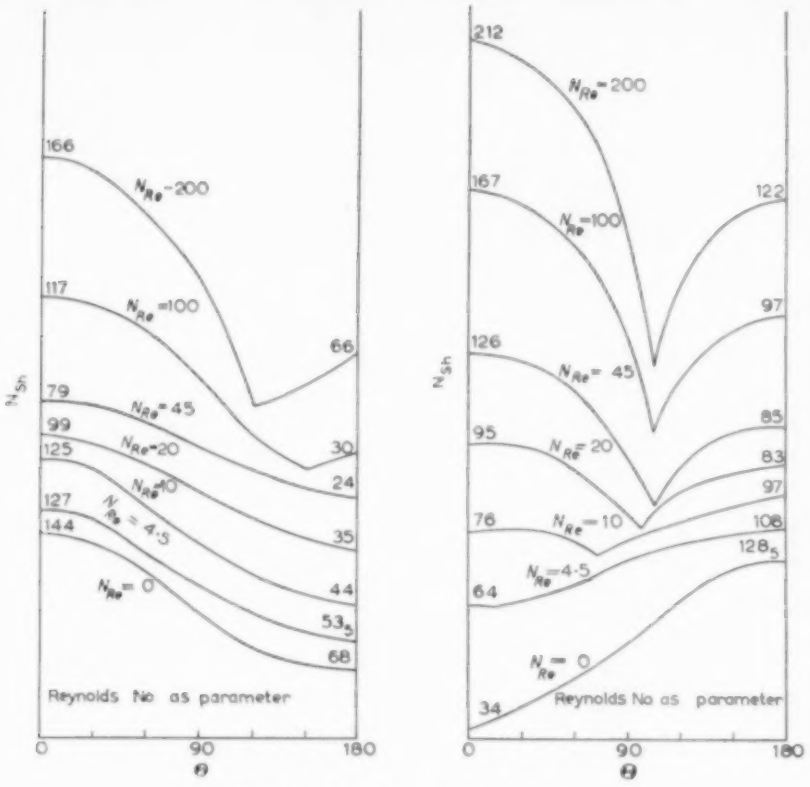

Fig. 9(c). Local mass-transfer rates.
(On the left, $N_{Re} = 200$)

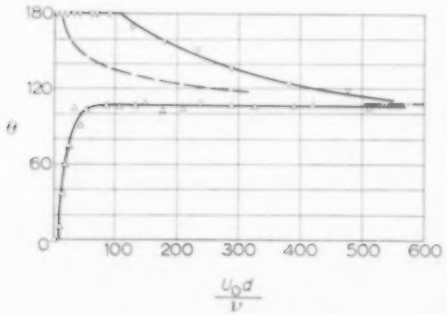

Fig. 10. Position of minimum mass-transfer rate.
▽ Downflow
△ Upflow
– – – Separation angle
Present Work
— · — Separation angle
Tomotika [22]

blind to red, this was used to obtain photographs of the dye streaming from the sphere surface. Dye traces taken from such photographs are presented in Fig. 6.

In the quantitative work one exposure was made at the beginning and end of the dissolution on panchromatic plates. The processed negative plates were projected by a diascope, giving a resultant magnification of 20 × and the outlines of the pellets drawn out. These were superimposed and the diminution of radii at successive 10° intervals was then measured around the periphery of the silhouettes. For an average diminution of 0·020 in., this change could be measured to within ± 5 per cent.

Mass-transfer coefficients could then be calculated readily from this diminution (h), since

$$\frac{W}{t} = \frac{h\,S\,\rho_s}{t} = K_L\,S\,\Delta c$$

$$\therefore K_L = \frac{h\,\rho_s}{c_0 t}\,(\Delta c = c_0 - 0) \quad (14)$$

and overall coefficients are found by integrating over the surface:—

$$\bar{K}_L = \left(\frac{\rho_s}{2\,c_0 t}\right)\left[2\pi a^2 \int_0^{\pi} h \sin\theta\, d\theta / 4\pi a^2\right]$$

$$= \frac{\rho_s}{2\,c_0 t}\int_0^{\pi} h \sin\theta\, d\theta \quad (15)$$

The integrand can be evaluated graphically.

To solve the problem we need the following data: pellet density, the solubility and diffusivity of the solute in the solvent and the viscosity of the saturated solution.

Benzoic acid of "Analar" grade was used, as this was available commercially in high purity and possesses good pelleting properties. Pellet density was measured by Archimedes' principle. Solubility of benzoic acid in water was calculated from Bourgoin's data [3]. Due to the paucity of experimental data, liquid diffusivities are usually estimated from semi-empirical correlations. The one chosen is that proposed by Wilke and Pin Chang [23], as this makes the most satisfactory allowance for solvent association. The viscosity of the solutions are assumed to be the same as that for pure water.

The Reynolds number of the sphere, $U_m d/\nu$ varied from 2·3 to 255 and all results are expressed on a constant Schmidt number basis ($N_{Sc} = 788$, $T = 30{\cdot}0$°C). Other data at slightly higher Reynolds numbers in horizontal flow are recalculated on this basis [9]. Both sets of data are plotted in Fig. 8; local mass-transfer rates are given in Figs. 9 (a, b and c). The position of the minimum mass-transfer rate is compared to the locus of separation, which was found by injecting red ink into the boundary-layer flow. (Fig. 10).

Discussion

The pellet surface after each experiment was free from pitting, which suggests that the spheres dissolved rather than eroded away. This is due to the low voidage in the compressed spheres. The curves for the overall transfer rate (Fig. 8) show a high degree of correlation with low mean probable errors (downflow ± 4·6 per cent; upflow 7·6 per cent). These errors are of the same order as those introduced in the method of estimating the diminution of radii.

Below $N_{Re} = 4$ the Sherwood number seems to be the same as that for molecular diffusion and free convection alone. At higher Reynolds number the mass-transfer rate is depressed and above $N_{Re} = 20$ the curve for upflow falls above those for horizontal- and down-flow. Such a separation has been noticed previously in experiments on packed beds [2a]. Since the data for horizontal flow fall between those for up- and down-flow, the latter can be justifiably extrapolated to their upper point of intersection, which appears to be about $N_{Re} = 750$. Thus, in this case, above $N_{Re} = 750$ forced convection alone is significant.

Since the theoretical equation (13) agrees very well with the experimental curve for forced convection and that for horizontal flow, it seems that free-convective effects can promote or hinder mass-transfer rates in forced convection. Conversely a bulk flow can hinder mass-transfer by free convection. This mutual depression of transfer rate will be termed "interference."

It might appear that the true convective velocity could be obtained by adding vectorially the velocity associated with the free convection to that of the forced convection. However, the experiments with dye-containing pellets showed that this transitional region is one of metastability. Below $N_{Re} = 120$ the steady wake behind the sphere began to break up and the dye effusing from the wake in upflow tended to drift downstream at about one sphere diameter from the surface. Typical stages of the unsteady motion of the wake are given in Fig. 6 of a sphere of benzoic acid, in which a little dye had been impressed in the surface. As the caption indicates, these pictures are not strictly comparable, but they give a good indication of the changeover from a wake shewing a toroidal vortex to a tundish-shaped tail. It is thought the latter is more characteristic of free-convective flow. As the flow rate decreased the latter flow pattern was more persistant, but unsteadiness was still detected at a Reynolds number of 10. It is known that free-convection is subject to a capacity lag (23) and possibly the aforementioned motion is due to inherent transients in the transport process.

Since the overall transfer results fall on a smooth curve between the limits where forced and free convection predominate, it follows that in this transitional region there are time-averaged values of the variables, which define the process. With this in mind we can examine the flow field and give a resultant velocity to each point within it.

In understanding the way in which this interference occurs it is necessary to have some knowledge of the flow patterns in free convection. Since in the present case motion is caused by the solute laden fluid falling from the sphere under the influence of gravitational forces, from considerations of continuity there must be an upflow some distance from the sphere, as shown in Fig. 11. It is important to note that in forced convection the maximum free-stream velocity is reached only at some distance from the sphere.

Now in upflow the motion in the wake near the surface is in the same direction as the free convective currents. Outside the boundary

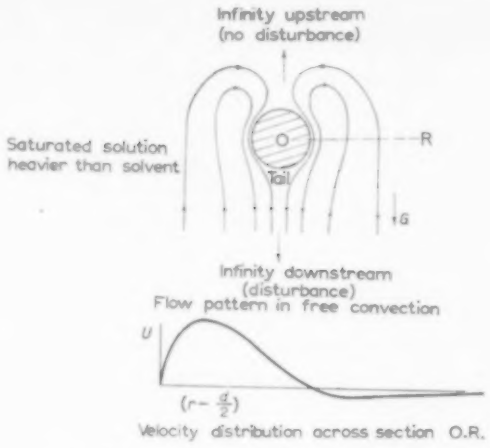

Fig. 11. Flow Pattern in free convection.

layer, which encloses the wake, the free and forced convection streams aid one another (see Fig. 11). They also aid each other over the area before separation of the flow. The reverse is true in the case of downflow. It is thus expected that interference in mass-transfer will result in the lowering of the mass-transfer rate until the general flow has increased to a critical magnitude. Since the ring of separation is over the rear hemisphere, this opposition is the greater in downflow. This may be regarded primarily as an area effect. (The actual numerical values of this depression are 25 per cent in upflow and 38 per cent in downflow). From Figs. 9 (a) and (b) it is seen that there is a considerable depression of the mass-transfer rate over the rear hemisphere in downflow. When the flow is reversed the depression is largest at the equator. This indicates that the direction of circulation within the wake has an important bearing upon the extent of interference.

The transition between the two convection regimes is illustrated in Figs. 9 (c) and 10. It is seen that the pronounced minimum mass-transfer rate, which occurs near the position of break-away of forward-flow, becomes less marked at lower Reynolds number. This change is also demonstrated by the silhouettes of dissolved pellets given in Fig. 6. The dotted curves give the original outline of the spheres.

The only data known to the authors on mass-transfer in this region refer to packed beds. Winterkamp [24] notes that at a critical Reynolds number of 1·7, dye from his spherules moved downwards against the bulk upflow. Gaffney and Drew [7] show that the direction of flow is important at low fluid speed. Mass-transfer rates in upflow were found to be higher than those in downflow and this difference appeared to a function of the modified Grashof number. A similar difference is noted by Dryden *et al.* [5]. Recently Bar-Ilan and Resnick [2] have presented data on the sublimation of naphthalene in fixed beds and show at $N_{Re} \sim 1$ the j-factor is a maximum, whence the Sherwood number is a minimum. If it is assumed that, in general, the overall transfer curves form a family with a parameter depending upon the level of the Grashof and Schmidt number, then this result is consistant with the present work.

Dropkin and Carni [4] find that heat-transfer coefficients for a rotating cylinder are independent of the speed of rotation until a certain critical value. At higher speeds both free convection and angular speed are important until eventually only the latter is important. Similar three regions are found in the present case.

The problem of estimating mass-transfer rates in the transitional region remains. It is evident that methods such as treating the limiting values i.e. transfer by free or forced convection as vectors [16] and defining an equivalent free-convective velocity to use in a Reynolds number [27] represent gross over-simplifications. While the present data are insufficient to draw up any general correlation for mass-transfer in this transitional region, the overall transfer results suggest that forced convection can be assumed to be dominant until the Sherwood number is equal to that in free convection. Now we have,

$$[N_{Sh}]_1 = 2 + A\,(N'_{Gr})^{\frac{1}{4}}\,N_{Sc}^{\frac{1}{4}}$$

—free convection alone

$$[N_{Sh}]_2 = 2 + B\,N_{Re}^{\frac{1}{2}}\,N_{Sc}^{\frac{1}{3}}$$

—forced convection alone

Equating $[N_{Sh}]_1$ to $[N_{Sh}]_2$ we find that forced-convective effects will be solely significant when the Reynolds number exceeds a limiting value given by:

$$N_{Re} > 0{\cdot}4\,(N'_{Gr})^{\frac{1}{2}}N_{Sc}^{-1/6} \qquad (16)$$

when $A = 0{\cdot}6$ and $B = 0{\cdot}95$

Conclusions

Minimum mass-transfer rates do not occur at zero flow rate, since the bulk flow can sometimes interfere with that caused by gravitational forces. The depression of the mass-transfer rate is particularly marked over the rear hemisphere, especially in down-flow.

Over the range $900 > N_{Re} > 250$ the overall transfer results are in approximate agreement with the theoretical relationship:

$$\bar{N}_{Sh} = 0{\cdot}94\,N_{Re}^{\frac{1}{2}}\,N_{Sc}^{\frac{1}{3}}.$$

Notation

a	= sphere radius	L
A, B	= constants, defined in text	—
c	= concentration	ML^{-3}
d	= sphere diameter	L
D	= diffusivity	L^2T^{-1}
F	= extraneous force	MLT^{-2}
h	= diminution of radius	L
K_L	= mass-transfer coefficient	TL^{-1}
m, m_0	= transfer rates (defined in text)	—
N_{Gr}'	= Grashof number (modified for mass-transfer)	—
N_{Re}	= Reynolds number	—
N_{Sc}	= Schmidt number	—
p	= external pressure	$ML^{-1}T^{-2}$
r	= radial distance	L
r_0	= distance from axis of revolution	L
S	= surface area	L^2
t	= time interval	T
u, v	= velocities in x- and y directions	LT^{-1}
U	= velocity	LT^{-1}
U_m	= average velocity	LT^{-1}
W	= total mass transferred	M
x, y	= distances mutually at right-angles	L
Z	= Pohlhausen parameter (defined in text)	—
δ	= boundary-layer thickness (momentum-transfer)	L
δ_m	= boundary-layer thickness (mass-transfer)	L
η	= dimensionless distance normal to surface (defined in text)	—
θ	= angle from forward stagnation point	—
Λ	= Pohlhausen parameter, defined in text	—
μ	= shear viscosity	$ML^{-1}T^{-1}$
ν	= kinematic viscosity	L^2T^{-1}

ρ_s = solid density	ML^{-3}	
τ_0 = skin-friction intensity	$ML^{-1}T^{2}$	
ϕ = dimensionless concentration (defined in text)	—	

Subscripts :—

0 = at surface

1 = at edge of boundary-layer

s = saturation

Operators :—

∂ = partial differential

d = total differential

∇ = nabla

Δ = finite-difference

References

[1] Aksel'rud G. A. *J. Phys. Chem., Moscow* 1953 **27** 1446.

[2] Bar-Ilan M. and Resnick W. *Ind. Engng. Chem.* 1957 **49** 313.

[2a] Bosworth R. C. L. *Heat Transfer Phenomena.* Assoc. Gen. Publ. Ltd., Sydney 1952.

[3] Bourgoin R. *Ann. Chim. (Phys.)* 1878 **15** 161.

[4] Dropkin D. and Carni A. *Trans. Amer. Soc. Mech. Engrs.* 1957 **79** 741.

[5] Dryden C. E., Strang D. A. and Withrow A. E. *Chem. Engng. Prog.* 1953 **49** 191.

[6] Frössling N. *Lunds Univ. Årssk.* 1940 **36.**

[7] Gaffney B. J. and Drew T. B. *Ind. Engng. Chem.* 1950 **42** 1120.

[8] Garner F. H. and Grafton R. W. *Proc. Roy. Soc.* 1954 **A224** 64.

[9] Garner F. H. and Suckling R. D. *Amer. Inst. Chem. Engrs. J.* 1958.

[10] Goldsteins S. *Modern Developments in Fluid Dynamics,* Oxford Univ. Press, London 1938.

[11] Grafton R. W. Ph.D. Thesis, Birmingham University 1953.

[12] Jenson V. G. Ph.D. Thesis, Birmingham University 1957.

[13] Kiser K. M. and Hoelischer H. E. *Ind. Engng. Chem.* 1957 **49** 970.

[14] Levich V. *Actaphysicochem. U.S.S.R.* 1944 **19** 117 133.

[15] Pohlhausen E. *Z. Angew. Math. Mech.* 1921 **1** 115.

[16] Ranz W. E. and Marshall W. E. *Chem. Engng. Progr.* 1952 **48** 141.

[17] Robertson J. M. *Trans. Amer. Soc. Mech. Engrs.* 1956 **78** 95.

[18] Rousse H. *Mech. Engng.* 1949 **71** 213.

[19] Spalding D. B. *Proc. Roy. Soc.* 1954 **A221**, 78.

[20] Stewart H. *Engineering, Lond.* 1950 **169** 175, 203.

[21] Stirba C. and Hurt D. M. *Amer. Inst. Chem. Engrs. J.* 1955 **1** 178.

[22] Tomotika S. *Aero. Res. Coun. Rep. and Memo* 1938 1678.

[23] Wilke C. R. and Pin Chang *Amer. Inst. Chem. Engrs. J.* 1955 **1** 264.

[24] Winterkamp F. H. M.Sc. Thesis, Ohio State University 1950.

[25] Yuge T. *Inst. High-Speed Mech.,* Tohoku University 1956 **6** 115.

[26] Yuge T. *ibid.* p. 173.

[27] Zijnen B. G. van der Hegge *Appl. Sci. Res., Hague* 1956 **A6** 129.

Chemical Engineering Science, 1958, Vol. 9, pp. 130 to 134. Pergamon Press Ltd.

Some properties of the activity coefficient

I. Sorgato

Istituto di Impianti Industriali Chimici, Università di Padova, via Marzolo, Padova

(*Received* 2 *May* 1958)

Abstract—In previous papers the author has described the isobaric maximum of the activity coefficient by means of the molecular parameters and interactions. He has demonstrated the universal character of the generalized function.

In this paper he shows that at this singular state the compressibility factor is numerically equal to the activity coefficient. This empirical correlation has been found useful in the determination of other properties of the activity function.

Résumé—L'auteur a décrit dans des articles antérieurs le maximum isobare du coefficient d'activité par les paramètres et les interactions moléculaires. Il a démontré le caractère universel de la fonction généralisée.

Dans cet article l'auteur montre que dans ce cas particulier le facteur de compressibilité est numériquement égal au coefficient d'activité. Cette relation empirique est utile dans la détermination d'autres propriétés de la fonction activité.

Zusammenfassung—In früheren Arbeiten hat der Autor das isobare Maximum des Aktivitätskoeffizienten mit Hilfe von molekularen Parametern und Wechselwirkungen beschrieben. Der universelle Charakter der generalisierten Funktion wurde betont.

In dieser Arbeit zeigt der Verfasser, dass bei diesem besonderen Zustand der Kompressibilitätsfaktor numerisch gleich dem Aktivitätskoeffizienten ist. Diese empirische Beziehung erweist sich als brauchbar bei der Bestimmung anderer Eigenschaften der Aktivitätsfunktion.

The activity function describes in a simple way the deviations from the ideal state. The activity coefficient γ represents the excess of the actual Gibbs function G over the ideal value G^* at the same temperature:

$$\ln \gamma = -\frac{G_p^* - G}{RT} = \int_0^P (C - 1)\, d \ln P \qquad (1)$$

In previous publications [1, 2, 3] we have pointed out that when plotted as a function of the temperature at a constant pressure, the activity coefficient shows a maximum:

$$\left(\frac{\partial \ln \gamma}{\partial T}\right)_P = \frac{H^* - H}{RT^2} = 0 \qquad (2)$$

This state of maximum activity is a singular state; it may be considered to be a point of ideality, since the difference $(H^* - H)$ between the enthalpies is zero.

Using a statistical treatment we have studied the activity from the molecular point of view and written in differential form the equation of the line of maximum activity [4].

This line is represented in Fig. 1 in reduced co-ordinates using the molecular parameters σ and ϵ_m, defined by the Lennard-Jones 6-12 equation. It is a straight line and it is surprising to observe that the linearity extends into the dense state, in the critical regions and at high pressures, for example about 2000 atm for the gas N_2.

In addition the experimental values represented in Fig. 1 are the only ones available, but are not numerous; nevertheless the agreement is good and shows the universal character of this generalized function.

The state of maximum activity as any other singular state may be used as the basis of important correlations, and the property of linearity should be important in this respect.

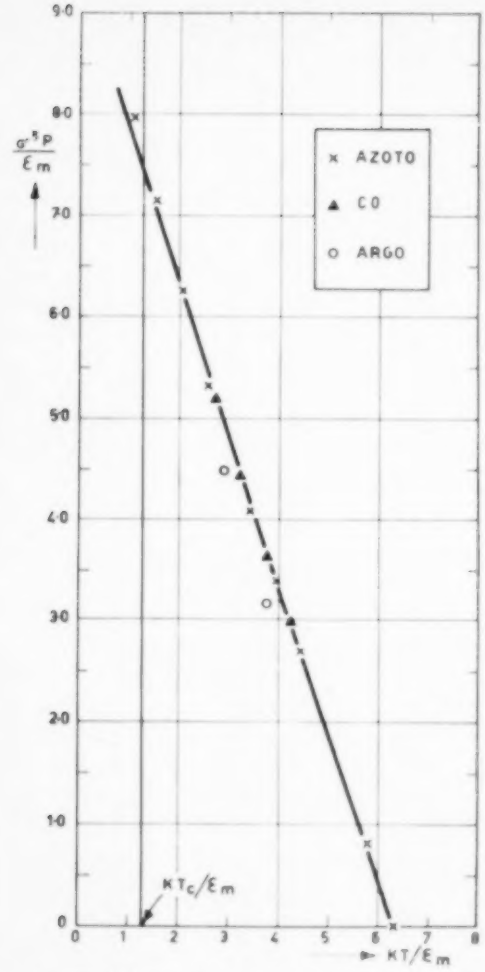

FIG. 1. The state of maximum activity in reduced co-ordinates.
× Nitrogen
▲ Carbon monoxide
○ Argon

THE EQUATION DEFINING THE STATE OF MAXIMUM ACTIVITY

We can also obtain the equation of the line using the virial theory, i.e. in terms of the intermolecular forces; these forces determine the values of the second virial coefficient $B(T)$, the third virial coefficient $C'(T)$ and so on.

Since the coefficient may be conveniently calculated by the compressibility factor C with the equation (1), we shall employ the virial expansion in powers of P:

$$C = \frac{PV}{RT} = 1 + B(T)\frac{P}{RT} + C'(T)\frac{P^2}{RT} + D(T)\frac{P^3}{RT} + \cdots \quad (3)$$

Combining with equation (1) we obtain the relative contribution of each virial coefficient to the magnitude of the function γ:

$$\ln \gamma = B(T)\frac{P}{RT} + \frac{1}{2}C'(T)\frac{P^2}{RT} + \frac{1}{3}D(T)\frac{P^3}{RT} + \cdots \quad (4)$$

Now combining equations (2) and (4) we have the equation of the line of maximum activity:

$$\left(\frac{\partial}{\partial T}\frac{B(T) + 1/2\,C'(T)P + 1/3\,D(T)P^2 + \cdots}{T}\right)_P = 0 \quad (5)$$

First we can utilize it to obtain:

The intercept of the line of maximum activity with the T-axis

Putting $P = 0$:

$$T_{P=0} = B(T) \Big/ \frac{d}{dT}B(T) \quad (6)$$

that is the curve $B(T)$ as a function of T must have only one tangent, which passes through the origin. In order to obtain the temperature for $P = 0$, we may express the 2nd and the 3rd virial coefficients for the gas N_2 as power series:

$$B(T) = a + bT + cT^2$$
$$a = -19{\cdot}2.10^{-4};\ b = 0{\cdot}081.10^{-4};\ c = -5{\cdot}2.10^{-9}\ \text{Amagat} \quad (7)$$

$$C'(T) = d + eT + fT^2$$
$$d = 7{\cdot}7.10^{-4};\quad e = -2{\cdot}0.10^{-6};\quad f = 1{\cdot}18.10^{-11}\ \text{Amagat} \quad (8)$$

Then $T_{P=0} = (a/c)^{\frac{1}{2}} = 608°K$. This is in reasonable agreement with the measurement of the Joule–Thomson effect ($T = 621K°$) [1] and with the experimental values of $B(T)$ [5] plotted in equation (6) ($T = 600°K$). The slight difference between these experimental values is attributal to the difficulty in measuring the 2nd virial coefficient with high accuracy.

The slope of the line at the origin

$$\left(\frac{dP}{dT}\right)_{P=0} = \frac{4\,c\,T^2}{d - f\,T^2} \qquad (9)$$

In reduced co-ordinates we calculated for the gas N_2 the slope $-13{\cdot}8$ instead of the value $-13{\cdot}4$, obtainable graphically from Fig. 4 of the previous paper [3]. We cannot verify that the slope remains constant into the region of high pressures because we would require the 4th, the 5th . . . . virial coefficients, which are not well known.

If we neglect the 3rd coefficient $C'(T)$, then all the values of γ_{max} fall at the same temperature given by equation (6) and defined by the maximum value of $B(T)/T$. The line of γ_{max} would be a straight line and the function independent of the pressure. Fig. 1 shows that the influence of the higher coefficients is to produce a line sloping to the left, i.e. $(\partial P/\partial T)\gamma_{max}$ is negative.

The Coefficient of Maximum Activity is Equal to the Compressibility coefficient

Let us first consider the low pressure region, in which we can neglect the 3rd, the 4th . . . virial coefficients. Since in the equation (4) $\ln \gamma = B(T)\,P/RT$ is numerically small, it is possible to write:

$$\gamma = 1 + B(T)\,\frac{P}{RT} \qquad (10)$$

and using equation (3) we obtain $\gamma = C$.

Therefore the isobars of the function γ tend to converge with the isobars of the function C, little by little, as the pressure $P \to O$. This is also true for the maximum values, knowing that also the C curves show isobaric maxima at low pressures.

For pressures less than 200 atm the compressibility of N_2 shows an isobaric maximum (Table 1); the increase of temperature decreases the values of the maxima, owing to the idealizing effect of the temperature. The value of the maxima tends to zero, as indicated by Table 1, in the range between 300° and 400°C. We remember that previously we have shown the experimental values of 600° and 621°K.

Table 1.
Compressibility coefficients for the gas N_2 [9]

Pressure (atm)	200°C	300°C	400°C
1	1·000296	1·000360	1·000323
10	1·003932	1·004313	1·004176
20	1·008029	1·008696	1·008476
30	1·012241	1·013269	1·012817
100	1·045074	1·046710	1·044452
200	1·103240	1·101682	1·093935

We conclude that at the limit, when $P = 0$, the two maxima have the same value. Further we recognize this property for any other pressure along the line of maxima:

$$\gamma_{max} = C = PV/RT \qquad (11)$$

To verify it let us consider the figures of Table 2, calculated from the tables of Michels [7, 8]. We have found the points at which $(H^* - H) = 0$ and the corresponding temperatures and pressures are shown in Table 2, alongside the values of C and γ_{max}, calculated by the functions PV and $(G^* - G)$.

Table 2. *Demonstration of the equation* (11) $\gamma_{max} = C$. *The figures at* 250°C *are calculated from the tables of* Perry [9]

T (°C)	P (atm)	C	γ_{max}	γ calcul. by eq. (3)
		Gas CO [7]		
0°	1306·0	2·485	2·471	—
50°	1113·5	2·060	2·026	—
100°	929·2	1·755	1·722	—
150°	753·9	1·531	1·525	—
		Gas N_2 [8]		
− 50°	1470·7	3·022	3·182	—
− 25°	1342·3	2·654	2·694	—
0°	1233·1	2·347	2·354	—
50°	1025·1	1·950	1·910	—
150°	685·3	1·475	1·437	1·462
250°	335·0	1·170	1·181	1·170

Table 2 indicates that equation (11) is applicable in the whole range of maximum activity, for pressures up to 1·500 atm. The differences between C and γ_{max} are of the order of $1 - 2$ per cent and are due to the inevitable inaccuracy in reading in the Tables of Michels the values of the functions. In addition, while the values H^* and $(PV)^*$ are read at $P = 0$, the values of G^* must be read at $P = 1$, being $G = -\infty$ at $P = 0$. This increases the differences between C and γ_{max}. The values of γ calculated by equation (3) are in good agreement with the experimental ones at not so high a pressure.

We were not able to find a satisfactory theoretical explanation for equation (11). Anyhow, it may be useful to know some properties. For instance, let us separate the function $(C - 1)$ as given by equation (3) in two parts: one, which represents $\ln \gamma$, the other which represents the Helmholtz function A:

$$\tfrac{1}{2} C'(T) \frac{P^2}{RT} + \frac{2}{3} D(T) \frac{P^3}{RT} + \cdots = \frac{A_P^* - A}{RT} \qquad (12)$$

At the point γ_{max}, the overall behaviour of the function C is expressed only by the second part:

$$\left(\frac{\partial C}{\partial T}\right)_P = \frac{d}{dT}\left(\frac{A_P^* - A}{RT}\right)_P \qquad (13)$$

since the first part, which refers to $\ln \gamma$, does not feel at this point the influence of T. Therefore the variation of one part describes the variation of all the virial coefficients. As the virial coefficients are related to the intermolecular forces, this point may be of interest.

Other Properties at the Singular Point

The relationship $\gamma_{max} = C$ gives further possibilities of illustrating the function activity.

As we stated, at the state of maximum activity every system (N, P, V) of N molecules shows the excess $(G - G_P^*)$ of Gibbs function over the ideal system (N, P, V_P^*), which at the same pressure has the same Gibbs function G. In addition we may apply the relationship of G. N. Lewis:

$$G - G^\circ = RT \ln f \qquad (14)$$

$f = \gamma P$ = fugacity.

We also may refer the real system (N, P, V) to a second ideal system (N, P_V^*, V) with the same Gibbs function G and the same volume V (instead of the same pressure P).

Now let us consider the reciprocal position of the two ideal states. We easily obtain:

$$G_P^* - G_V^* = RT \ln \frac{P}{P_V^*} = RT \ln C \qquad (15)$$

At the point of maximum activity, when $\gamma = C$, equation (1) gives:

$$G - G_P^* = G_P^* - G_V^* \qquad (16)$$

that is the point of γ_{max} is characterized by the equivalence of the real state over the two ideal states (Fig. 2). The excess of free energy, $(G - G_P^*)$ is equal to the energy $(G_P^* - G_V^*)$, that the gas receives during the ideal compression from the state (N, P_V^*, V) to the state (N, P, V_P^*). In other words, the compression of ideal molecules in the ratio $C = (P/P_V^*)$ gives the magnitude of the gain, when the ideal state becomes a real state, owing to the appearance of co-volume and molecular interactions. We have elsewhere illustrated the mechanism of this path [2]. Here we point out that we have to speak only of gain and not of loss of energy, because it is always $\gamma_{max} > 1$ and hence $C > 1$.

Let us now mention another application of equation (11) and take into consideration the activity coefficient γ_c, which refers to the concentrations as stated in the statistical theory by Mayer and Mayer [10]. We consider the situation at $V = \text{cost}$ and define γ_c:

$$\gamma_c = \frac{N^*}{V} \Big/ \frac{N}{V} = \left(\frac{N^*}{N}\right)_{G,V} \qquad (17)$$

N^* = number of ideal molecules with the same value of the Gibbs function G, in the same volume, as the real molecules N.

Substantially we refer the actual situation to the ideality condition (N^*, f, V). The concentrations for the two ideal states are shown in Fig. 2; taking in consideration that we are dealing with ideal gases, it is easy to obtain from Fig. 2:

$$\gamma = \frac{f}{P} = \frac{N^*}{V} \Big/ \frac{N}{V_P} = \frac{\gamma_c}{C} \qquad (18)$$

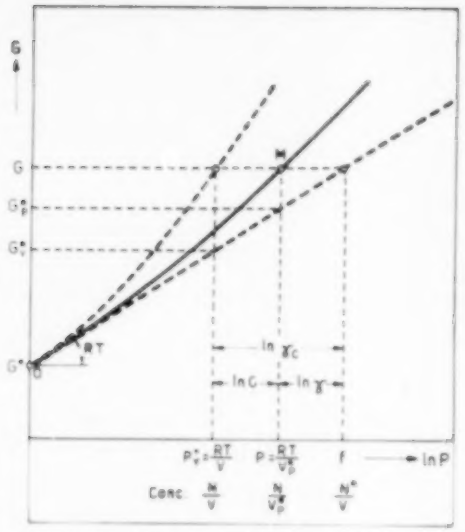

Fig. 2. Gibbs function of a real gas (curve OM) referred to the ideal states. — Point M = state of maximum activity.

We have deduced equation (18) using a statistical treatment [4]. From this simple ratio between the two activity coefficients we obtain the general correlation:

$$\ln \gamma_c = \ln \gamma + \ln C \qquad (19)$$

At the point of maximum activity $\gamma_c = (\gamma_{max})^2$; in all other cases γ is different from C and the values of $\ln \gamma$ and $\ln C$ could also be zero or negative.

Notation

A = Helmholtz function

$B(T)$, $C(T)$, $D(T)$ ... = 2nd, 3rd, 4th .... virial coefficient

C = compressibility factor

f = fugacity

G = Gibbs function

H = enthalpy

N = number of molecules

ϵ_m = maximum energy of interaction

γ = activity coefficient

σ = molecular diameter

Superscript * = the ideal state.

The index for a quantity in the ideal state, for instance V_p^*, shows the function, in this case the pressure P, which is the same for the ideal and the real state.

References

[1] Sorgato I. *Chim. Industr.* 1954 **36** 171.

[2] Sorgato I. *Chim. Industr.* 1956 **38** 14.

[3] Sorgato I. *Chim. Industr.* 1956 **38** 173.

[4] Sorgato I. *Chim. Industr.* 1956 **38** 844.

[5] Guggenheim E. A. *Thermodynamics* (2nd Ed.) p. 95. North-Holland Publ. Co., Amsterdam.

[6] Taylor H. and Gladstone S., *States of Matter* p. 323. Van Nostrand, New York 1952.

[7] Michels A., Lunbeck R. and Wolkers G. *Appl. Sci. Res.* A 1952 **3** 253.

[8] Lunbeck R., Michels A. and Wolkers G. *Appl. Sci. Res.* A 1952 **3** 197.

[9] Perry J. *Chemical Engineers' Handbook* (3rd Ed.) p. 206. McGraw-Hill, New York 1950.

[10] Mayer J. and Mayer M. *Statistical Mechanics* p. 292. John Wiley, New York 1950.

Chemical Engineering Science, 1958, Vol. 9, pp. 135 to 144. Pergamon Press Ltd.

Kinetics of water-gas conversion reaction

P. Bortolini

Institute of Industrial Chemical Plants—University of Padua, Italy

(*Received* 28 *March* 1958)

Abstract—A description is given of experimental investigations into the kinetics of the water-gas conversion reaction as a function of the gas composition and its specific flow-rate. The results obtained are compared with the calculated reaction rate, assuming that the mechanism determining the kinetics of the process as a whole is diffusion of the gas reagents in the catalyst surface and of the catalysis products in the gas. It is found that, at least at temperatures of about 500°C and higher, this diffusion mechanism actually does determine the kinetics of the entire process.

For experimental purposes the reactions of oxidation and reduction occurring between the gas and the catalyst were also studied as a function of the temperature and the H_2O : CO ratio.

Useful data are derived for the design and the running of commercial reactors.

Résumé—L'auteur décrit son travail expérimental sur la cinétique de la réaction de conversion du gaz à l'eau, en fonction de la composition du gaz et de sa vitesse d'écoulement spécifique. Les résultats obtenus sont comparés avec la vitesse de réaction calculée, en supposant que le mécanisme déterminant la cinétique du procédé, est la diffusion des gaz réagissant à la surface du catalyseur, et des produits de la catalyse dans le gaz. Il a trouvé, au moins pour les températures de 500°C et plus, que le mécanisme de diffusion détermine la cinétique du procédé entier.

Dans un but expérimental, les réactions d'oxydation et de réduction se produisant entre le gaz et le catalyseur ont aussi été étudiées en fonction de la température et du rapport H_2O : CO.

L'auteur en tire des données utiles pour le calcul et le practique des réacteurs industriels.

Zusammenfassung—Der Verfasser beschreibt eine Experimentaluntersuchung über die Reaktionskinetik der Wasser-Gas-Konvertierung als Funktion der Gaszusammensetzung und des spezifischen Mengenstroms. Die erhaltenen Ergebnisse werden mit der berechneten Reaktionsgeschwindigkeit verglichen, wobei angenommen ist, dass der Mechanismus, der die Kinetik des Prozesses im ganzen bestimmt, die Diffusion der reagierenden Gase an der Oberfläche des Katalysators und der Produkte im Gas ist. Es wird gefunden, dass mindestens bei Temperaturen in der Gegend von 500°C und mehr der Diffusionsmechanismus tatsächlich die Kinetik des gesamten Vorgangs bestimmt. Für experimentelle Zwecke werden auch die Reaktionen der Oxydation und Reduktion zwischen dem Gas und dem Katalysator untersucht, und zwar als Funktion der Temperatur und dem Verhältnis H_2O : CO.

Für Entwurf und Betrieb üblicher Reaktoren werden brauchbare Werte abgeleitet.

Introduction

In a previous paper [1] a study was made of a commercial conversion unit from the thermal and thermodynamic viewpoints; it now became convenient to continue the research into this reaction and to examine the kinetics and study the behaviour of the relevant catalyst.

A complete study of the kinetics would be long and difficult, in view of the very different physical conditions of pressure and temperature accompanying this reaction in commercial practice, the variation of the type and size of the catalysts, and the wide variety of compositions of the reacting gases.

The reaction was studied at atmospheric pressure only and the tests were limited to gases without impurities and to a single type of catalyst. Work was also confined to a relatively high temperature, mainly in order to have a sufficiently high residual CO content at equilibrium for the converted gases to be analysed with sufficient accuracy.

These restrictions to the experiments did not, however, prevent us from drawing certain important conclusions.

EXPERIMENTAL SECTION

Method adopted

Firstly we will indicate the experimental method adopted, employing the usual formula for the reaction rate for reactions on a solid catalyst:

$$G\,dx = r\,dW \text{ (material balance)}$$

$$r = \frac{dx}{d\,(W/G)} \qquad (1)$$

where G indicates the mole of gas/hr, W the g of the catalyst, x the concentration of a product (in this case the CO_2 or H_2 partial pressure) and r the reaction rate in mole/hr, g of catalyst.

In order to employ equation (1), we should charge our experimental reactor with a very small bed dW of catalyst and measure under certain conditions of flow G the very small variation dx in composition. But the analytical methods at our disposal do not enable us to obtain sufficiently accurate data from these tests.

Equation (1) also illustrates the slope of the x vs. W/G curve: we can then charge the reactor with a given bed W of catalyst and analyse the composition x of the converted gas under various conditions of G in order to draw the required curve and hence find the reaction rate r.

Experimentally, instead of finding the curve of x (CO_2 or H_2 partial pressure) directly, it is expedient to find the curve K/R, where K is the equilibrium constant at the test temperature and R is the ratio between the partial pressures, calculated from analysis of the converted gas. The magnitude of K/R is a unique function of x: in fact, indicating by A the initial H_2O/CO ratio of the gas that is converted:

$$R = \frac{P_{CO}\,P_{H_2O}}{P_{CO_2}\,P_{H_2}} = \frac{[1/(1+A)-x]\,[A/(1+A)-x]}{x^2} \qquad (2)$$

Knowing K/R is therefore equivalent to knowing x, but the function K/R has certain important advantages over x. Whereas for W/G tending towards infinity x tends towards the equilibrium partial pressure, that is closely linked with the initial composition of the gas and with the temperature, the function K/R always tends towards unity, irrespective of inevitable variations in the experimental conditions. Moreover, since the asymptote of K/R, unlike that of x, remains the same for all the various test series, it can be stated that a variation in the course of K/R vs. W/G curves down under different conditions is entirely due to the different kinetic conditions of the reaction.

Description of apparatus

The apparatus used is simple and very similar to that of BARKLEY *et al* [2], who studied the kinetics of the reverse reaction.

The CO, obtained by decomposing formic acid by concentrated sulphuric acid at about 60°C, is collected in a large 40l. flask discharging from the bottom, acting as a gasometer. The flow of gas is constant and can be closely controlled; the water flow is measured by a rotameter.

From the gasometer the CO passes into a saturator completely immersed in a large thermostat. The thermal inertia of the thermostat keeps the fluctuations in temperature of the saturator to within several tenths of a degree Centigrade, and the height of the saturation column is such that it guarantees almost complete saturation of the gas, so that the value of the H_2O/CO ratio can be found simply by reading off the temperature.

The outlet tube passes through the side wall of the thermostat and then enters immediately an electrically-heated tubular metal container. The gas thus arrives in the reactor with a constant water content and is already heated. The reactor is a glass tube with an inside diameter of 24 mm, with a vertical furnace at the centre containing two sets of electrical resistances that are controlled separately. A large metal tube inside the reactor makes the heating uniform. The lower half of the reactor is filled with sandstone rings in order to aid in heating the gas up to the reaction temperature; immediately above, separated by an

asbestos cap, is the bed of catalyst. The BAMAG catalyst (about 85 per cent Fe_2O_3, 15 per cent Cr_2O_3) consists of uniform particles with a mean diameter of about 3 mm. In order to reduce the wall effect, asbestos fibre is placed around the inside of the reactor near the catalyst.

Despite the exothermic nature of the reaction, the gas must not be heated beyond the predetermined temperature; thus heating in the upper half of the furnace is restricted, so that the reaction heat is largely drawn off from the gas by thermal dispersion effects. The temperature along the bed of the catalyst is kept constant to within about 10°C. This liability to variation in temperature is the weak point of the apparatus.

The outlet temperature of the gas from the catalyst is kept at the predetermined level to within $\pm$ 3°C. The head of the reaction tube is kept very hot by means of electrical resistances in order to prevent any condensation; the gas thus reaches a cooling condenser or a tube containing anhydride for water-vapour analysis, and from this the gas is drawn off for analysis.

The gas balances on entry and on exit agree to within 1 per cent.

In the tests we did not find noticeable quantities of CH_4.

Reduction and oxidation of the catalyst

We shall consider briefly the possibility of interference between gas and catalyst.

We know that the catalyst, marketed as Fe_2O_3 (we shall ignore the other components, that under our test conditions cannot contribute to oxidation or reduction), is reduced under normal conditions to Fe_3O_4. Moreover, depending on the oxidizing potential of the gas in equilibrium with the catalyst, it is possible for all the oxide forms and metallic iron to appear and attain stability. We will now study this oxidation potential in relation to the gas composition and determine the form of iron oxide in equilibrium with a gas of any composition.

If we assume that the equilibrium conditions for the formation of H_2O from H_2 and of CO_2 from CO are satisfied, and indicate by K_{H_2O} and K_{CO_2} the equilibrium constants of these two reactions, we can write:

$$P_{O_2}^{0.5} = \left(\frac{1}{K_{H_2O}}\right)\left(\frac{H_2O}{H_2}\right) =$$

$$P_{O_2}^{0.5} = \left(\frac{1}{K_{CO_2}}\right)\left(\frac{CO_2}{CO}\right) \quad (2a)$$

where the chemical symbols are taken as representing concentrations.

Multiplying these together, we obtain:

$$P_{O_2} = \left(\frac{1}{K_{H_2O}\,K_{CO_2}}\right)\left(\frac{H_2O\;CO_2}{CO\;H_2}\right) \quad (3)$$

In the case being considered, all the CO_2 and H_2 come from the reaction, through which their ratio is unity. At 500°C for example, we can write [3]:

$$\log P_{O_2} = -28{\cdot}398 + \log\left(\frac{H_2O}{CO}\right)$$

and draw a logarithmic diagram with a straight line of unit ratio that gives the oxidizing potential as a function of the H_2O/CO ratio (Fig. 1).

In order to calculate the oxidizing potentials of the various iron oxides, we resort to the classical methods. For example, for the reaction in which we are mainly interested:

$$3\,FeO + 0{\cdot}5\,O_2 = Fe_3O_4\,(K = 1/O_2^{0.5})$$

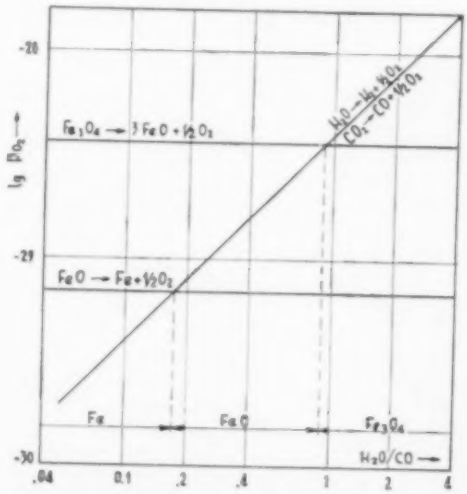

FIG. 1. Oxidizing potentials of gaseous reaction mixtures and of the various oxide forms of the catalyst. P_{O_2} is given in atm and the ratio H_2O/CO is moles/moles. Temperature 500°C.

from PERRY's [4] data we find at 500°C:

$$\log K = 14{\cdot}219 \qquad \log P_{O_2} = -28{\cdot}438.$$

In addition to this value of P_{O_2} in Fig. 1 we shall mark the pressure corresponding to the reduction of FeO. The oxygen potential of Fe_2O_3 is $\log P_{O_2} = -23{\cdot}0$, i.e. considerably higher. The diagram shows clearly the limit between the regions of stability of Fe_3O_4 and of FeO, and indicates how oxide mixtures can no longer occur in equilibrium.

For experimental verification a test lasting many hours was carried out, in which the temperature of the saturator was varied in stages, from 84°C ($H_2O/CO = 1{\cdot}21$) to about 60°C ($H_2O/CO = 0{\cdot}25$) and back to 84°C.

From 84° to about 77° the analyses of the converted gas were regular; below 77° there was a continuously increasing surplus of CO_2 compared with H_2, indicating that the CO reduced the catalyst; above 79° again, the situation was reversed and the part of the catalyst reduced earlier was reoxidized, analysis clearly showing the presence of a surplus of H_2 compared with CO_2.

A temperature of 78°C on the saturator corresponds to a ratio $H_2O/CO = 0{\cdot}76$; this experimental value agrees very well with the value

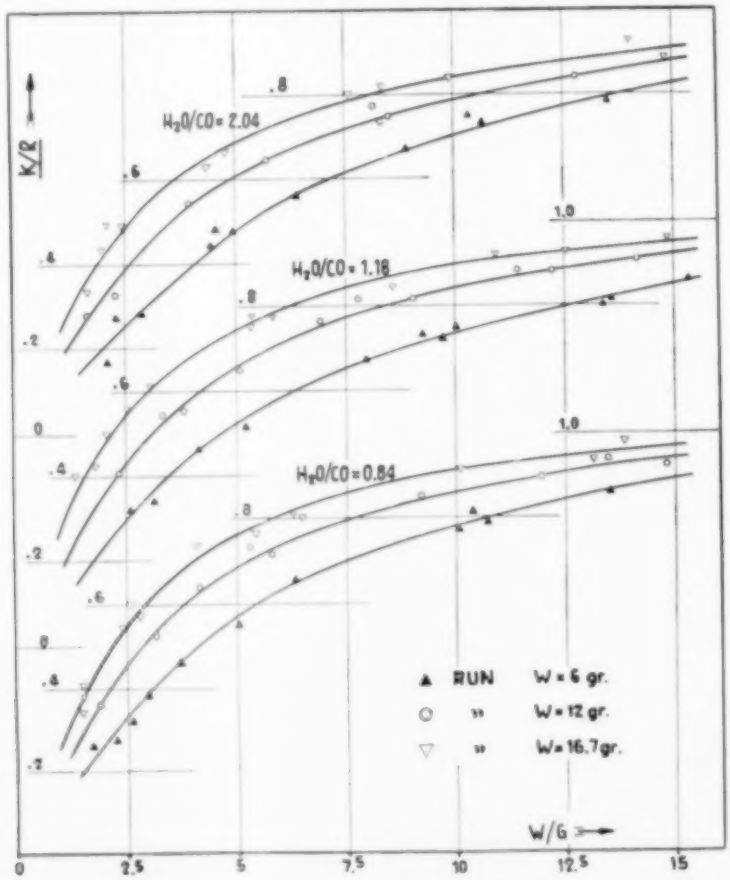

FIG. 2. Experimental diagrams of the ratio K/R (K/R is a function of the degree of conversion) as a function of the reciprocal of the space velocity W/G. The curves are based on the quantity of catalyst W in g. G is the flow of gas ft³/hr calculated at 20°C. The reaction temperature is 500°C.

0·9 calculated thermodynamically and confirms the accuracy of the original thermodynamic data.

It is worth while to consider some important points concerning *the running of industrial plant*. It is obvious that the transformation from Fe_3O_4 to FeO and vice versa is harmful to the catalyst; according to our experience the activity of the catalyst remains practically unchanged after a reduction to FeO and a reoxidation to Fe_3O_4; but—especially if the quantity of the catalyst is large, as it is in commercial reactors—it loses its mechanical properties as a result of the chemical and physical transformations, and breaks easily.

It should be pointed out that in calculating equation (3) it is supposed that $CO_2 = H_2$, but often, especially in cracking gas, there is a large surplus of H_2 that causes the stability region of Fe_3O_4 to rise to far higher values of the H_2O/CO ratio. In such cases particular care must be taken not to reduce the catalyst and deteriorate it. It is a good rule to conduct operations with a surplus of steam and at a rather low temperature. Lowering the temperature causes the limits between the stability regions of FeO and Fe_3O_4 to fall to lower values of the H_2O/CO ratio.

Experimental Results and their Elaboration

It is clear that for our kinetic study the tests must be limited to the stability region of the Fe_3O_4 form and thus be confined to a gas with a sufficiently high H_2O/CO ratio; in fact the various test series were carried out with gas having H_2O/CO ratios of 0·84, 1·18 and 2·04.

Since it was seen that the degree of conversion, and hence the reaction rate, does not depend on the ratio W/G only, as had been expected, but also on the absolute value of W (or of G) at the same space velocity G/W, the conversion conditions were examined experimentally for each of the compositions given above, and with $W = 6$, 12 and 16·7 g.

Figure 2 gives experimental curves showing K/R as a function of W/G (g catalyst/1 moist gas, hr) with various initial gas compositions (H_2O/CO ratio) and different amounts of catalyst. Each test run was carried out keeping the saturator temperature, and hence the H_2O/CO ratio, constant, and thus it was possible to relate the volume of CO recorded on the flowmeter to the volume of moist gas entering into reaction, which is the volume referred to in the diagrams.

All these diagrams relate to tests conducted with a reaction furnace at 500°C.

From the K/R vs. W/G curves it is easy, using equation (2) to obtain the corresponding x vs. W/G curves. Using equation (1) all curves of the reaction rate r can finally be expressed as a function of x; these are given as full-line curves in Fig. 3.

Theoretical calculation of the reaction rate

If the kinetics of the process were controlled by the chemical reaction or by the adsorption or desorption mechanism of any one chemical component in the catalyst, the rate, defined as the quantity of CO_2 produced per unit of time per unit of catalyst (see equation (1)), would depend entirely on the degree of conversion or the composition of the gas, and of course on the temperature and the pressure, but should not be directly affected by the flow-dynamic conditions of the gas stream and hence by the quantity of gas treated in the infinitesimal reactor dW. Similarly the degree of conversion (or the ratio K/R in Fig. 2) obtained in a reactor of finite dimensions W would depend entirely on the space velocity G/W and would not be affected by the absolute values of G and W.

The experimental diagrams in Figs. 2 and 3 clearly show on the contrary that in the reaction process as a whole, the flow-dynamic conditions of the gas current in the reactor are of fundamental importance. It is thus logical to assume that the diffusion mechanism of the reagents in the gaseous mass in the catalyst surface and of the surface products in the gas current do not play a negligible part in the kinetics of the process.

In order to study the correctness of this hypothesis we propose to calculate what would be the reaction rate if the diffusion processes alone controlled the process. Of the authors who have studied and developed methods of calculating the effect of diffusion on the kinetics of a process based on a catalyst, we should mention Colburn [5], Chilton [6, 7], Gamson [8], Wilke [9],

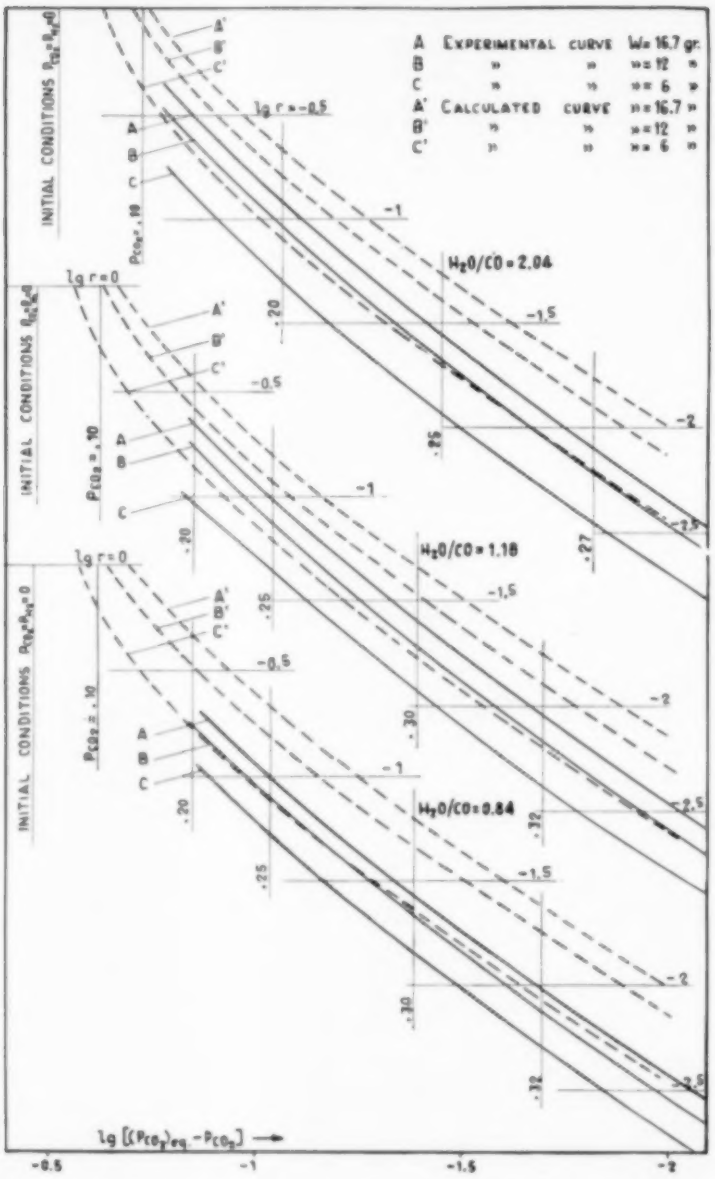

FIG. 3. Diagrams of reaction rate r, expressed in mole/hr, g of catalyst, as a function of the degree of conversion or partial pressure $P_{CO_2} = P_{H_2}$. The reaction temperature is 500°C.

LINTON [10], HOBSON [11] and LEVA [12, 13]. We shall carry out our calculation according to the method developed by HOUGEN and WATSON in their well-known book [14].

The chemical kinetics of the process is however obviously linked with the composition on the catalyst surface, a composition differing from the mean value for the gas stream in view of the difficulty of diffusion of the various individual gaseous elements between the centre of the stream

and the catalyst surface. It is then necessary to calculate the difference in partial pressure of the various components of the mixture between the gas stream and the reaction surface as a function of the following variables: the gas velocity, its density, viscosity and diffusivity; the catalyst particle dimensions and the reaction rate, that influence the diffusion mechanism.

Extending the analysis and employing the non-dimensional method, we obtain the following relationships:

$$\Delta P_A = \frac{r\,\rho_b\,M_m\,P}{G}\,H_{d_A} \tag{4}$$

$$H_{d_A} = \frac{1}{a_v\,\gamma_d}\left[\frac{\mu}{\rho\,D_{Am}}\right]^{2/3} \tag{5}$$

Suitable tabulation of the available data gives:

$$\gamma_d = 1{\cdot}82\,(D_e\,G/\mu)^{-0{\cdot}51} \tag{6}$$

If the rate of chemical reaction on the catalyst surface were such that there were practically equilibrium conditions on the catalyst, the rate of the process as a whole would be controlled solely by the diffusion mechanism. Knowing ΔP_A, we should then be able to calculate the reaction rate, substituting (4) for r:

$$r = \frac{G}{M_m\,P\,\rho_b\,H_{d_A}}\,\Delta P_A \tag{4'}$$

In order to obtain ΔP_A, we must calculate the partial pressures of the different components on the catalyst surface. Indicating these by a dash (P'_A, ...), letting P_A indicate the pressure in the centre of the gas and indicating by A and B the reactants and by R and S the products, we can write:

$$\frac{P'_R\,P'_S}{P'_A\,P'_B} = K \tag{7}$$

where K is the equilibrium constant of the reaction. Moreover, according to (4):

$$\left.\begin{aligned}\Delta P_A : \Delta P_B : \Delta P_R : \Delta P_S &= \\ = H_{d_A} : H_{d_B} : H_{d_R} : H_{d_S} &= \\ = \left[\frac{1}{D_{Am}} : \frac{1}{D_{Bm}} : \frac{1}{D_{Rm}} : \frac{1}{D_{Sm}}\right]^{2/3}&\end{aligned}\right\} \tag{8}$$

The four equations (7) and (8) are soluble in the four unknowns $\Delta P'_A$, ... and thus ΔP_A, and finally by means of formulae (4'), (5) and (6) the reaction rate r should be calculable.

The importance of this value of r is clear; it represents the maximum rate of the process, which cannot be exceeded at the predetermined temperature no matter how high the rate of the actual chemical reaction may be, unless of course the flow-dynamic system of the reactor is changed.

The diffusivity was calculated by the method of Gilliland [15], according to whom D_{Am}, ... can be calculated as the mean by weight of the coefficients relating to the possible pairs of pure components. These binary coefficients may be calculated with the aid of the following semi-empirical relationship:

$$D_{AB} = 0{\cdot}0043\,\frac{T^{3/2}}{P\,(v_A^{1/3} + v_B^{1/3})^2}\sqrt{\frac{1}{M_A} + \frac{1}{M_B}} \tag{9}$$

where D_{AB} is in cm²/sec, T in °K, P in atm, V_A and V_B are the molecular volumes of A and B, M the corresponding molecular weights.

The fact that these diffusion coefficients vary with the composition of the mixture somewhat complicates our calculations, but does not introduce any difficulty regarding concepts.

Writing equation (7) we wish to take into account our hypothesis, according to which the gas is in equilibrium at the catalyst surface. It must be noted, however, that the stabilized equilibrium will be that relating to the temperature of the catalyst surface, and this is higher than the temperature of the gas stream (and of the control thermometer), in view of the exothermic nature of the reaction. In order to calculate this difference in temperature we must write:

$$\Delta T = Q/h \tag{10}$$

where Q is in cal/hr, cm² of catalyst surface; h in cal/hr, °C, cm². Calculation of Q is easy when the reaction rate r (mole/hr, g of catalyst) and the heat of reaction H_r (cal/mole) are known:

$$Q = \frac{r\,\Delta H_r\,\rho_b}{a_v} \tag{11}$$

In order to calculate the heat transfer coefficient h, just as was done to calculate the diffusion or

mass transfer of material we can derive the following relationships:

$$h = \gamma_h C_P G \left(\frac{C_P \mu}{\lambda}\right)^{2/3} \quad (12)$$

$$\gamma_h = 1{\cdot}95\, Re^{-0{\cdot}51} \quad (13)$$

where C_P is in cal/mole, °C; G is the volume specified in mole/cm², hr, $C_P \mu/\lambda$ is Prandtl's non-dimensional number.

To use equations (12) and (13) presupposes a knowledge of the reaction rate and, hence, the surface temperature: we must therefore proceed by successive approximations. In order to lower the work of calculation we note that the diffusion factor γ_d (or the reaction rate) and the heat transmission factor γ_h (or the heat transfer coefficient of convection h) depend on the same power of the Reynold's number (cf. equations (6) and (13)), an algebraic consequence of the fact that the mechanisms of the two processes are identical, the temperature gradient from the catalyst surface and the centre of the gas being independent of the gas flow rate, and hence it will suffice to perform the calculation for any value of the flow rate G.

The characteristics of the catalyst are: $a_v = 7\text{cm}^2/\text{cm}^3$ (outer surface of the particles); $\rho_b = 1{\cdot}3$ g/cm³ (apparent density); $D_e = 0{\cdot}3$ cm (mean equivalent diameter of the particles). For the gas mixture we shall suppose that $C_P = 7{\cdot}0$ cal/mole, °C and Prandtl $(C_P \mu/\lambda) = 0{\cdot}74$ are invariable with the temperature and the composition. For calculating the diffusivity we shall use the molecular volumes given by ARNOLD [16].

The results of these calculations are given in Fig. 4, where the curves of r as a function of P_{CO_2} for a constant specific flow rate G are shown as full lines. This means (according to our initial hypothesis) that, for a certain pressure P_{CO_2} and a certain flow rate G at a given point in the reactor the reaction rate at this point is r. The broken-line curves on the other hand are for constant W (g of catalyst). These curves have the same significance as the continuous experimental curves in Fig. 3. In order to draw these curves for constant W, we have to integrate equation (1). Expressing G in g/hr, cm², equation (1) becomes:

$$W = \frac{G S}{M_m} \int_0^x \frac{\mathrm{d}x}{r}$$

where S indicates the cross-section of the reaction tube in cm². Substituting equation (4′) in this relationship we obtain an equation by means of which can be calculated the necessary amount of catalyst W for obtaining under certain conditions (e.g. of flow rate) a given degree of conversion x, or looking at it in a different way the degree of conversion obtainable from a bed W of catalyst as a function of the flow rate of gas G. This second point of view enables us to draw the curves for constant W.

CONCLUSIONS

The full-line curves in Fig. 3 give the experimental results of our work and the broken-line curves give the theoretical results, based on the hypothesis that the reaction rate is controlled by the diffusion processes between the catalyst surface and the surrounding gases.

The reaction rate depends very closely on the flow-dynamic conditions in the reactor, hence on the gas volume per unit of reactor cross-section and the particle-size of the catalyst.

These differences in the rate with the flow rate can be explained quantitatively if we suppose that the kinetics of the process are controlled by diffusion of the reactants and the products between the catalyst surface and the gases.

The experimental curves of the reaction rate as a function of the degree of conversion are correspondingly parallel to the curves calculated taking the process of diffusion only into account.

All this enables us to state with certainty that in the reaction process as a whole, under the investigation conditions, the diffusion processes are of overriding importance. If in addition to diffusion the purely chemical kinetics of the reaction had had any appreciable influence, we should not have been able to explain the position in the above manner.

We still have to explain however why the experimental and theoretical values of the reaction rate differ by a factor 1·7. This may be due to various factors—viz. the approximation of the

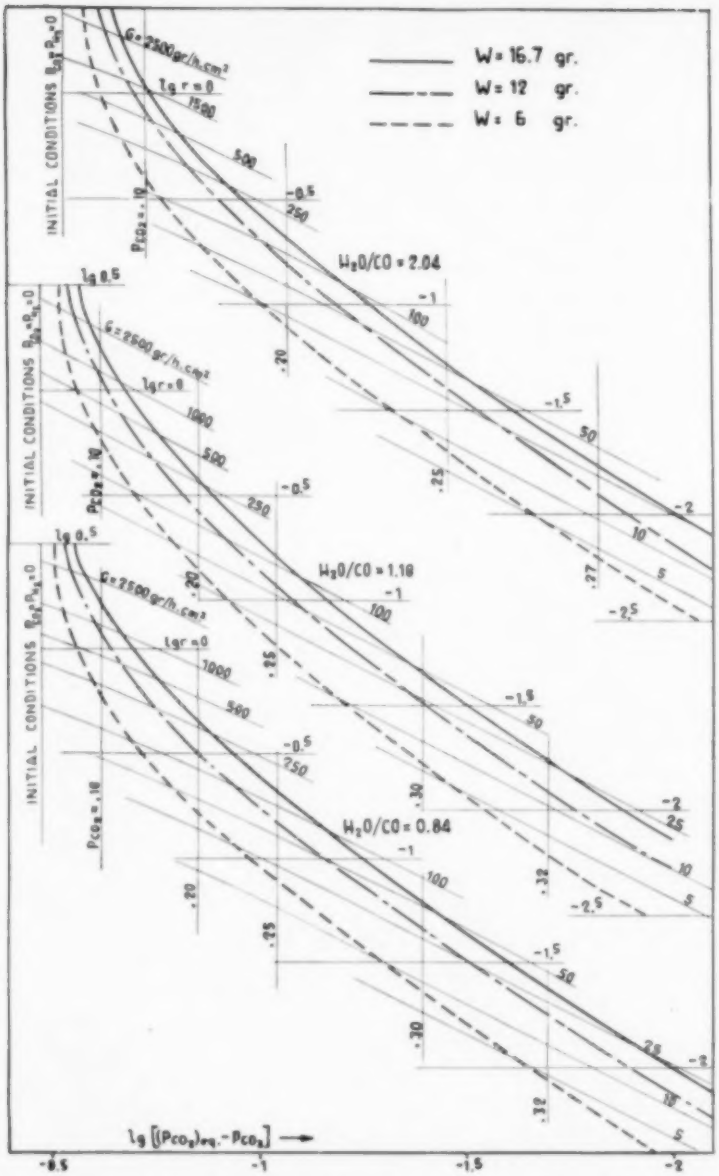

FIG. 4. Diagrams of the theoretical reaction rate r (mole/hr, g of catalyst) as a function of the degree of conversion or partial pressure $P_{CO_2} = P_{H_2}$. W is the weight of catalyst in g; G is the flow rate in g/hr, cm².

methods of calculation; the very extensive wall effect, in view of the small diameter of the reaction tube, and the relatively low thickness of the bed of catalyst compared with the size of the catalyst particles and the consequent heterogeneity in the bed cause a fairly irregular distribution of gas. It is easy to foresee that any irregularity in the flow of gas leads to an apparent reduction in the reaction rate.

From the industrial point of view our conclusions lead us to affirm that, in order to improve the activity of conversion catalysts, great care must

be given to studying their composition, their macroscopic structure, and hence their specific weight, the size and shape of the particles, the outer surface, etc. In addition the shape of the reactor is very important; provided that this does not unduly restrict the amount of the charge, long reaction tubes are always preferable.

The results of this investigation must not be extended indiscriminately to other cases. It can however be stated that diffusion is of overriding importance for temperatures of 500° and over. At lower temperatures the chemical reaction proper has such a retarding action that it in turn predominates. The number of experiments made by us at relatively low temperatures is insufficient to enable us to draw any definite conclusions on this point, but it is significant, that at a temperature of 400° it is found that the reaction rate diminishes, the fall not being due entirely to a decrease in diffusivity or gas velocity.

(Translated by R. Hardbottle.)

Notation

A = initial molar H_2O/CO ratio
a_v = catalyst surface per unit of volume, cm^2/cm^3
C_p = molar heat of gas, cal/mole, °C
D_{Am} = diffusivity of component A of mixture, cm^2/sec
D_e = equivalent diameter of grains of catalyst, cm
G = flow rate of gas, mole/hr or cu. ft/hr or g/hr, cm^2
h = heat transfer coefficient, cal/hr, cm^2, °C
Hd_A = size of a unit of diffusion for component A, cm
ΔH_r = molar heat of reaction, cal/mole
γ_d = diffusion factor
γ_h = heat transfer factor
K = equilibrium constant
M_m = mean molecular weight of gas, g/mole
ΔP_A = difference in partial pressure of component A between catalyst surface and gas stream, atm
Q = heat released by the reaction, cal/hr, cm^2
r = reaction rate, mole/hr, gr
R = ratio between the partial pressures of the gases after reaction
S = section of reaction tube, cm^2
ΔT = temperature difference between catalyst surface and gas stream, °C
W = quantity of catalyst, g
x = molar concentration of CO_2 or H_2
λ = thermal conductivity of gas, cal/hr, cm, °C
μ = viscosity of gas, g/cm, sec
ρ = density of gas, g/cm^3
ρ_b = density of catalyst, g/cm^3

References

[1] Bortolini P. *Chim. e Industr.* 1956 **38** 857.
[2] Barkley L. W., Conigan T. E., Wainwright H. W. and Sands A. E. *Industr. Engng. Chem.* 1952 **44** 1066.
[3] Steiner L. E. *Introduction to chemical thermodynamics*, McGraw-Hill.
[4] Perry J. H. *Chemical engineers' handbook*, McGraw-Hill.
[5] Colburn A. P. *Trans. Amer. Inst. Chem. Engrs.* 1933 **29** 174.
[6] Chilton T. H. and Colburn A. P. *Industr. Engng. Chem.* 1934 **26** 1183.
[7] Chilton T. H. and Colburn A. P. *Industr. Engng. Chem.* 1935 **27** 255.
[8] Gamson B. W., Thodos G. and Hougen, O. A. *Trans. Amer. Inst. Chem. Engrs.* 1943 **39** 1.
[9] Wilke C. R. and Hougen O. A. *Trans. Amer. Inst. Chem. Engrs.* 1945 **41** 445.
[10] Linton W. H. Jr. and Sherwood T. K. *Chem. Engng. Progr.* 1950 **46** 258.
[11] Honson M. and Thodos G. *Chem. Engng. Progr.* 1949 **45** 517.
[12] Leva M. and Grummer M. *Chem. Engng. Progr.* 1947 **43** 713.
[13] Leva M. *Industr. Engng. Chem.* 1947 **39** 857.
[14] Hougen O. A. and Watson K. M. *Chemical process principles* J. Wiley, London.
[15] Gilliland E. R. *Industr. Engng. Chem.* 1934 **26** 681.
[16] Arnold J. H. *Industr. Engng. Chem.* 1930 **22** 1091.

Chemical Engineering Science, 1958, Vol. 9, pp. 145 to 152. Pergamon Press Ltd.

The thermal conductivity of catalyst particles

ROBERT A. SEHR

Research and Development Laboratory, Socony Mobil Oil Company, Inc., Paulsboro, New Jersey

(*Received* 17 *July* 1957)

Abstract—Three different methods for the measurement of thermal conductivity of catalyst particles have been developed and are compared using silica–alumina cracking catalyst. Values of the thermal conductivity of a number of practical catalyst particles are reported also.

Résumé—L'auteur développe et compare trois méthodes différentes de mesure de la conductivité thermique de particules de catalyseurs, en utilisant un catalyseur de cracking du type silice-alumine. Des valeurs de la conductivité thermique d'un certain nombre de particules de catalyseurs pratiques sont également présentées.

Zusammenfassung—Zur Messung der Wärmeleitfähigkeit von Kontaktkörnern wurden drei verschiedene Methoden entwickelt und unter Verwendung eines Crack-Kontaktes aus Aluminiumsilikat miteinander verglichen. Für mehrere, in der Praxis verwendete Kontakte werden die Wärmeleitfähigkeiten angegeben.

I. INTRODUCTION

THE thermal conductivity of porous catalyst particles can play an important role in reactions occurring within the particle. This situation arises because the heat of reaction can change the temperature within the particle to an extent determined in part by the thermal conductivity of the catalyst. In turn, this temperature change may modify the reaction kinetics within the catalyst in an undesirable manner; furthermore, highly exothermic reactions could lead to to such high internal temperatures that the catalyst itself would be damaged.

There are two classical methods for measurement of thermal conductivity on single particles: (1) the steady state method in which the heat flux is measured through a body of well-defined geometry, and, (2) the temperature transient method in which the time course of the temperature is measured when the boundary conditions on the object are suddenly changed. Because of the poor geometrical form and small size of the usual catalyst particle these methods cannot be applied without some modification.

Conceptually, the steady state is the simpler of two methods. The poor geometry of the catalyst particles can be overcome in some cases by grinding the particles into cylinders. This technique, along with other modifications, made it possible to apply the steady state method to a single particle of one catalyst.

As for the temperature transient method, the transient times are too short with the size of catalyst particles usually encountered for this method to be applied easily to individual particles. To show this, consider an experiment in which the particle is heated to a temperature T_1 and then immersed in a well-stirred fluid bath at a temperature T_0. The temperature rise in the bath as a function of time is sufficient to determine the thermal conductivity of the particle. For the theoretical treatment of this problem see CARSLAW and JAEGER [1]. The larger the diameter and the smaller the thermal conductivity, the slower will be the temperature change. Consider a catalyst particle having a radius of 0·4 cm and a thermal conductivity of 10^{-4} cal/cm sec °C. This represents an optimum case. Applying equation 5 and the graph given in Fig. 23 on p. 206 of reference [1] to this data shows that the transient is essentially over in about 10 sec. Such short times make it difficult to satisfy the well-stirred conditions necessary to obtain meaningful data. It becomes apparent that

temperature transient experiments on the particle itself cannot be easily employed to determine its conductivity.

Both the steady state and temperature transient methods, however, may be used to measure the conductivity of large, heterogeneous bodies consisting of catalyst dispersed in a suitable matrix. The continuous phase should be a solid in order to prevent heat transfer by gross convection. For example, it may consist of a castable plastic or a matrix of finely powdered material. Thus, by fabricating large pieces of cast material or enclosing large volumes of porous materials in a vessel of convenient shape, it becomes possible to obtain the conductivity of the mixture by conventional methods. From the conductivity of the mixture it is possible to deduce the conductivity of the components.

II. THEORETICAL

A. Thermal conductivity measurements on single particles

The thermal conductivity of a single cylindrical particle can be determined by measuring the heat flux through it when its ends are maintained at temperatures T_1 and T_2, respectively. If no heat loss through the sides is allowed, the heat flux, dQ/dt, across the particle is then given by :—

$$\frac{dQ}{dt} = K A \frac{\Delta T}{\Delta x} \qquad (1)$$

Here K is the thermal conductivity (cal/sec-cm-°C),
Δx is the length (cm),
A is the cross-section (cm^2),
ΔT is the temperature difference ($T_1 - T_2$) (°C).

B. Thermal conductivity using heterogeneous mixtures

The thermal conductivity of mixtures will depend on the thermal conductivity of the components in the same way as the dielectric properties of a mixture depend on the dielectric properties of the individual components. In a recent paper by W. F. BROWN, Jr. [2] this problem is formulated rigorously for dispersed particles of any shape and solved in series form. The solution is given as follows :—

$$\frac{K}{K'} = 1 - \frac{1}{3}\alpha\beta\left(\frac{\delta}{K'}\right)^2 + \left(-\frac{1}{3}\alpha^2\beta + \frac{1}{9}\alpha\beta^2\lambda\right)\left(\frac{\delta}{K'}\right)^3 + \cdots \qquad (2)$$

Here α = the volume fraction of the embedded particles,
$\beta = 1 - \alpha$ = the volume fraction of the continuous phase,
K = the observed conductivity of the mixture.

K' and δ are defined by :—

$$K' = \alpha K_d + \beta K_c \qquad (3)$$

$$\delta = K_d - K_c$$

where K_d is the conductivity of the dispersed phase and K_c is the conductivity of the continuous phase. The quantity λ appearing in the third and higher order term is a particle shape factor of the dispersed phase.

In deriving this equation the following assumptions were made :—

(a) The particle size is small compared to the dimensions of the heterogeneous body,
(b) K_d and K_c are not too different,
(c) Uniform dispersion exists, and,
(d) no thermal resistance exists at the interface between the two phases.

These assumptions have to be borne in mind for experimental application.

The first term of equation (2), which is independent of particle shape, gives a simple averaging formula. This can be improved by taking higher order terms into account. The second term is still independent of the particle geometry. The shape factor contributes relatively little to the correction even in the third term.

Several special cases of (2) have been proposed in earlier literature. Maxwell derived an approximate expression for the dielectric constant of mixtures on the assumption that the dispersed particles are small spheres. With the symbols used in this paper, Maxwell's equation becomes :–

$$\frac{K - K_c}{2K + K_c} = \alpha \frac{K_d - K_c}{2K_d + K_c} \qquad (4)$$

Using the definitions (3) and expanding equation (4) as series, one finds agreement between (2) and (4) up to the third order term if λ is assigned the value zero.

For arbitrarily shaped particles the geometry factor in (2) remains unknown. If it is neglected, equation (4) may be considered an approximation for randomly shaped particles also. In this paper, equation (4) will be used to determine K_d from the measured values of K and K_c.

Both transient and steady state methods will be used to determine catalyst conductivity via a heterogeneous system. The transient method is applied to spheres of a plastic material containing the embedded catalyst particles. A thermocouple is placed in the centre of the sphere and the sphere heated to a temperature T_0. At time $t = 0$ this sphere begins to cool off by radiation into a medium at a temperature $T = 0$. The temperature $T(t)$ at time t is given by :—

$$T(t) = 2\,T_0 \frac{\sin R\alpha - R\alpha \cos R\alpha}{R\alpha - \sin R\alpha \cos R\alpha} \exp(-k\alpha^2 t) \qquad (5)$$

where R is the radius of the sphere,
t the time,
k the thermal diffusivity,
and α a constant.

In order to evaluate this expression, it is written :

$$T(t) = T(0)\,2\,N \exp(-nt)$$

The value of n is obtained from two different temperatures $T(t_1)$ and $T(t_2)$ at the times t_1 and t_2 using :—

$$\frac{T(t_1)}{T(t_2)} = \exp\left[-n\,(t_1 - t_2)\right]$$

Using this n from above, N is obtained from

$$T(t_1)/2\,T(0) = N \exp(-n\,t_1)$$

With known N, α is obtained by means of a table of the function

$$N = \frac{\sin x - x \cos x}{x - \sin x \cos x} \qquad (5a)$$

which were computed by means of a digital computer. Finally, k is given by the equation :—

$$n = k\,\alpha^2$$

For the steady state method, the continuous phase consists of finely powdered catalyst for which the conductivity is to be measured along with the air spaces between the particles. This choice of continuous phase was made so that condition (*b*) could be more easily satisfied. The dispersed phase then consists of large particles of the same material uniformly distributed throughout the finely divided material. This mixture is placed in the annular ring formed by two concentric cylinders of radius r_1 and r_2. A radial temperature gradient is established by maintaining r_1 at a temperature T_1 and r_2 at T_2. The ratio of l, the length of the cylinder, to the radius r_2 is chosen greater than 5 so that the heat flow in axial direction is much less than that in radial direction and may be neglected.

Assuming then that only radial heat flow occurs, the basic differential equation of heat conductions $k\Delta^2 T = \partial T/\partial t$ reduces to :—

$$\frac{d}{dr}\left(r \frac{dT}{dr}\right) = 0 \qquad (6)$$

$r_1 < r < r_2$ when a steady state temperature gradient is established. Upon integration, equation (6) yields

$$r\,(dT/dr) = \text{constant} \qquad (7)$$

i.e., the heat flow in radial direction $F = 2\,\pi\,r\,lK\,dT/dr$ is constant within $r_1 < r < r_2$. Let H_0 be the heat per unit length produced by the heater. Since all the heat originates from the central heating rod, equation (7) can then be written

$$H_0 + 2\,\pi\,r\,K\,(dT/dr) = 0 \qquad (8)$$

Denoting the temperatures at r_1 and r_2 by T_1 and T_2, respectively, it follows from (8) :—

$$H_0 \ln(r_2/r_1) = 2\,\pi\,K\,(T_1 - T_2) \qquad (9)$$

If the heat is produced electrically in the heating rod, H_0 simply becomes $\gamma\,J^2R$ (cal sec^{-1}) where R is the resistance of the rod per unit length, J the current through it and $\gamma = 0{\cdot}239$ (cal W^{-1}).

Thus, the final expression for the thermal conductivity is given by :—

$$K = \gamma \frac{J^2 R}{2\pi (T_1 - T_2)} \ln (r_2/r_1) \quad (\text{cal sec}^{-1}\ \text{cm}^{-1}\ ^\circ\text{C}^{-1}) \qquad (10)$$

III. EXPERIMENTAL

A. Single particle

It was found that by skilful grinding on a lathe, cylinders 0·4 cm in diameter and 0·4 cm long could be formed from the larger particles of a commercial silica–alumina cracking catalyst. These cylinders were used to determine the conductivity in the apparatus shown in Fig. 1.

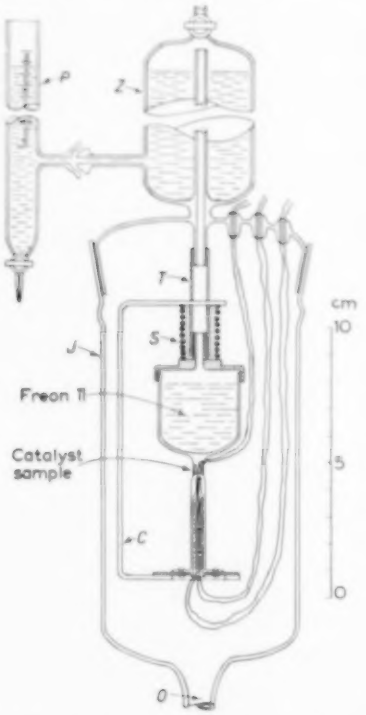

FIG. 1 Apparatus for measuring the thermal conductivity of single cylindrical catalyst particles.

The hot plate is a hollow copper rod which contains a tungsten heater wound on a piece of glass tubing. A thermocouple measures the temperature just below the contacting surface. The cold plate, also made of copper, is shaped to form a receptacle which holds a low boiling liquid; the latter maintains the temperature constant at this plate. The temperature is monitored by a thermocouple near the contacting plane.

The heat flux through the cylindrical particle is measured by the rate of evaporation of Freon 11 from the receptacle. This liquid was chosen because of its boiling point of 16°C and its low heat of evaporation of 43·8 cal/g. The vapour escapes through tube T (Fig. 1) and is collected above water in cylinder Z. The volume of water displaced is measured by the pipette P. The heat flux is given by :—

$$F = H \rho (dv/dt)$$

where H is the heat of evaporation of Freon 11
ρ is the vapour density
and dV/dt is the rate of evaporation of Freon 11.

To secure good mechanical contact, the two plates are pressed onto the end planes of the cylindrical catalyst particle by means of a helical spring S and clamp C. The thermal contact between the cylinder and plates is improved by a thin film of mercury. In order to prevent heat transfer from one plate to the other by air conduction and convection, the entire device is suspended in the jar J which is evacuated by an oil diffusion pump at the outlet O. The pressure is measured by an ionization gauge.

Since the thermal interface resistance between the catalyst particle and the holding plates may well be of the same order as the thermal resistance R of the bead itself, as defined by $R = l/KA$, the two must be separated. This can be done by measuring the overall resistance for pieces of different length and extrapolating to zero length. If a residual resistance is found it may be ascribed to the interface.

Six different cylinders varying in length from 0·79 to 0·43 cm were measured. The applied temperature difference across the specimen was between 90 and 100°C. The evaporation rate due to the heat flux through the particle ranged from 3·6 to 7·8 cm^3 per minute while the background rate was 1·1 $\text{cm}^3\ \text{min}^{-1}$. Background and effect measurements were made alternately for

several hours in order to level out the fluctuation.

Figure 2 shows the results of the measurements. In this figure the thermal resistance R is plotted against the length of the specimen. According to equation (1) the measured points should fit a straight line through the origin if no interface resistance is present. The actual points are seen to scatter. The least square straight line shown in Fig. 2 intercepts the ordinate at a negative

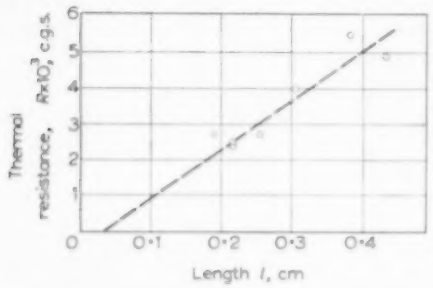

FIG. 2. The total thermal resistance of cylindrical catalyst particles of different length measured in the apparatus shown in Fig. 1.

value, namely -0.36. However, this value is of no aid in determining the presence or absence of contact resistance since a determination of its 95 per cent confidence limit by means of Student's distribution yields -0.36 ± 1.77. The possible sources of experimental errors which cause this scatter are :—

1. Additional heat transfer from the hot to cold plate by radiation.

2. Additional heat transfer due to conduction and convection of the surrounding medium.

3. Finite and fluctuating thermal interface resistance between bead and plates.

An upper limit of the first effect can easily be obtained. The total energy per second radiated from a body of temperature T_1 and surface S into a surrounding of temperature T_0 is given by :—

$$E = \Sigma \sigma (T_1^4 - T_0^4) S$$

where $\sigma = 5.7 \times 10^{-5}$ erg sec^{-1} °C^{-4} and Σ is a surface coefficient which is about 0·3 for machined copper. With the actual values $T_1 = 4 \times 10^2$ °K and $T_0 = 3 \times 10^2$ °K the above equation yields a total energy radiated by the hot plate

$$E = 2 \times 10^{-3} \text{ cal sec}^{-1}$$

Considering that only a fraction of this energy reaches the cold plate and that the heat flux through the bead is of the order of 0·5 cal sec^{-1}, it is evident that the radiation effect is negligible.

At the maintained pressure of 10^{-5} mm Hg heat transfer by convection may also be neglected. As is known from molecular theory, heat conduction of gases decreases linearly with pressure from about 1 mm Hg on downward. Thus, according to a rough calculation, air conduction at 10^{-5} mm Hg is less than 1 per cent of the conduction through the specimen.

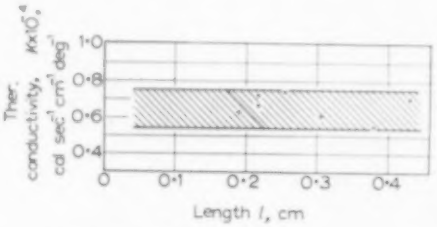

FIG. 3. The thermal conductivity of cylindrical catalyst particles of different length.

Having ruled out the first two sources of error, the interface resistance between plates and particle remains to be considered. Variation in thermal contact for different specimens could account for the fluctuation of the measured values. In Fig. 3 the thermal conductivity vs. length is plotted. There, instead of fitting a straight horizontal line, the points are scattered at random within a strip defining the range of fluctuation. If the interface resistance is the only source of error, the upper limit of such a scattered array should represent the value closest to the true conductivity of the particle. This upper limit seems to be about 0.75×10^{-3} cal/sec-cm-°C. However, the statistics of six points is not sufficient to established this upper limit with satisfactory accuracy.

B. Heterogeneous mixtures

1. *Transient measurements.* This method was only applied to a silica–alumina cracking catalyst. Spheres 1 in. in diameter were used with a hole drilled in the centre to receive a thermocouple. These spheres consist of a lucite continuous phase containing from 0 to 80 per cent of 16 to 40 mesh crushed catalyst particles. The lucite was used in the form of 1385 AB Transoptic mounting powder supplied by Buehler, Ltd., for preparing metallurgical specimens.

The lucite powder was thoroughly mixed with crushed catalyst in the proper proportions and moulded into cylinders one inch in diameter at a temperature of 230°F under 4,000 to 6,000 p.s.i. The cylinders were then machined into spheres one inch in diameter. No lucite penetrated into the pores of the catalyst particles, as could be shown by density measurement.

A sphere, with a thermocouple in place to measure the temperature at the centre, was heated to a uniform temperature of about 85°C in a small oven; it was then quickly lowered into a metal container completely surrounded by ice except for the hole in the top for the ball to pass through. This can was in the form of a cylinder 5 in. high and 3½ in. in diameter. The time course of the temperature at the centre of the sphere was recorded continuously on a Brown recorder. The thermal conductivity of the sphere was determined from the theoretical treatment described in II *B*.

Figure 4 shows the thermal diffusivity for varying fractional volumes resulting from the measurements. Each point is obtained from two or three different spheres with the same α. The curve ranges from $\alpha = 0$ to $\alpha = 0{\cdot}8$. Spheres of higher α cannot be made because (1) the continuous phase serves as adhesive for the granule, and (2) arbitrarily shaped particles cannot be packed to occupy a volume to more than about 80 per cent with a reasonable range of particle size.

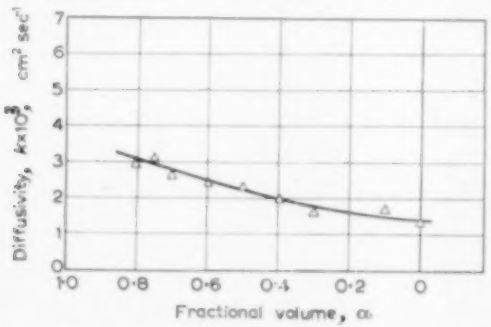

Fig. 4. The thermal diffusivity of heterogeneous spheres, consisting of catalyst granules and bonding lucite, as a function of the fractional volume α of the catalyst particles.

Strictly speaking, it is necessary to make measurements for only two different values of the volume fraction, namely, for $\alpha = 0$ and for any $\alpha > 0$. But, measurement of several values for different α's reduces the probable error, which is especially desirable in the present case, since the function $N(x)$ given by equation (5a) has a small slope.

After determining the conductivity of the mixture and the matrix phase, the thermal diffusivity of the embedded catalyst granules is then obtained by means of the Maxwell formula. It is found to be $3{\cdot}5 \times 10^{-3}$ cm^2 sec^{-1} for the silica–alumina catalyst used. With the measured specific heat of $C = 0{\cdot}19$ cal g^{-1} °C^{-1} and density of $\rho = 1{\cdot}25$ g cm^{-3} the thermal conductivity is then found to be $K_d = 0{\cdot}82 \times 10^{-3}$ cal sec^{-1} cm^{-1} °C^{-1}. The error is estimated to be not larger than 10 per cent.

2. *Steady state method.* Experimentally, the heterogeneous mixture forming the hollow cylinder is contained in a glass cylinder 32 cm long and 2·5 cm in diameter. The heater consists of a uniformly and densely wound tungsten coil axially supported by a glass rod. To provide uniform temperature distribution along the heater, the coil is covered by a thin copper tubing having a radius of $r_1 = 0{\cdot}15$ cm. The temperature T_1 at r_1 is measured by a thermocouple. A second thermocouple is placed at a point on a line parallel to the axis at $r_2 = 2{\cdot}0$ cm.

In order to render axial heat losses of the heater negligible, the supporting glass rod is pencil-shaped at the end to give a point-like bearing. Thus, the temperature at the ends did not differ by more than 1·5 per cent from that in the middle of the heater. Two hours were allowed from the time the inner cylinder was heated to the time the temperatures were taken.

Table 1

Catalyst	$K_{Particle}$ 10^{+3} (cal sec^{-1} cm^{-1} $°C^{-1}$)	K_{Powder} 10^{+3} (cal sec^{-1} cm^{-1} $°C^{-1}$)	*Density*	
			Particle (g cm^{-3})	*Powder* (g cm^{-3})
Ni/W	1·12	0·73	1·83	1·48
Co/Mo (Dehydrogenation* catalyst)	0·83	0·51	1·63	1·56
Cr/Al (Reforming catalyst)	0·70	0·42	1·4	1·06
Co/Mo (Dehydrogenation† catalyst)	0·58	0·33	1·54	1·09
Si/Al (Cracking catalyst)	0·86	0·43	1·25	0·82
Pt/Al_2O_3 (Reforming catalyst)	0·53	0·31	1·15	0·88
Activated carbon	0·64	0·40	0·65	0·52

* 3·6 per cent CoO and 7·1 per cent MoO_3 supported on alpha-alumina, 180 m^2/g.
† 3·4 per cent CoO and 11·3 per cent MoO_3 supported on beta-alumina, 128 m^2/g.

The resistance of the heater and the current through it were continuously controlled.

The pulverized particles forming the continuous phase were of mesh size smaller than 80 while the dispersed particles were between mesh 6 and 10. In these experiments the fractional volume ranged only between 50 and 68 in all experiments. Lower values were avoided because of sedimentation between particles and powder which would disturb the homogeneity of the mixture. The upper limit was set by the densest possible packing of the particles used. In order to determine α, the mixture was separated by a screen after the experiment. The fractional volume $\beta = 1 - \alpha$ of the powder was then measured in a graduated cylinder. To assure the same powder density in the volume measurement as in the experiment the containers were vibrated for a certain time by an electric shaker.

A typical set of measured data for a mixture of SiO_2–Al_2O_3 beads with its powder is given below :—

Temp. of the heating rod ($r_1 = 0{\cdot}16$ cm), $T_1 = 127°C$

Temp. at $r_2 = 2{\cdot}0$ cm, $T_2 = 48°C$

Electric input per cm heating rod, $I^2 R = 20$ W

Volume fraction, $\alpha = 0{\cdot}51$

After computing $K(\alpha)$ and K_c from such data by means of equation (10) the thermal conductivity of the embedded granules is obtained from equation (4). The values thus obtained for several different catalysts are given in Table 1.

IV. Discussion

From the three methods described the steady state method with heterogeneous mixtures was chosen for routine measurements. In this method the theoretical analysis is straightforward and contains no assumptions which are not fulfilled experimentally. Furthermore, the quantities occurring in the final formula from which K is calculated are either electrical or mechanical quantities and thus accurately measurable.

A comparison of the values of K for silica–alumina cracking catalyst as measured by the three methods are given in Table 2.

As is well known the thermal conductivity is a function of temperature. The mean temperature of each experiment is given in the last column of Table 2 and is seen to be slightly different in the last two experiments. Crandal [3] has recently reported some new values of the conductivity of sintered alumina for the temperature range in question. His data show that the conductivity approximately doubles on decreasing the temperature by 100°C. If one assumes that the alumina catalyst sample behaves in the same manner as the sintered alumina, this introduces approximately a 6 per cent difference between the results of the last two experiments.

The value we obtained for the catalyst particles

Table 2. Comparison of thermal conductivity measurements obtained by the three methods, using a silica-alumina cracking catalyst

Method	*K* (cal/sec cm °C × 10^{-3})	*T* (°C)
Steady state single particle	0·75	45
Transient heterogeneous mixture	0·82	44
Steady state heterogeneous mixture	0·86	38

is almost an order of magnitude lower in value than that obtained by CRANDAL for his alumina; that is, the catalyst gave 8×10^{-4} cal/cm sec °C compared to 6×10^{-3} cal/cm sec °C for sintered alumina.

The value obtained by the single particle method may be significantly lower in value than the other two. However, the experiments using the single cylindrical particle were made under vacuum, while in the other two methods the pores of the catalyst were filled with gas. The lower value obtained when no gases were present suggests that the gas filling contributes appreciably to the conductivity. This could be due to the fact that the pore diameter (about 10^{-7} cm) is small compared to the mean free path of the gas molecules (about 10^{-5} cm), which allows more rapid exchange of energy from wall to wall by gas molecules collisions. The influence of gases on the conductivity of porous solids has been discussed in the literature. (See for example KLING [4].

The use of this data to determine the temperature difference between the inside and outside of a catalyst particle during the course of a catalytic reaction is presented elsewhere [5].

REFERENCES

[1] CARSLAW H. S. and JAEGER J. C. *Conduction of Heat in Solids* p. 205 *ff.*

[2] BROWN W. F. *J. Chem. Phys.* 1955 **23** 1514.

[3] CRANDAL W. B. *Thermal Diffusivity in Ionic Solids.* Second Annual Symposium on the Defect Solid State, Alfred University, September 1957.

[4] KLING G. *Allg. Waermetechnik, Bd.* 3 167 1952.

[5] PRATER C. D. *Chem. Engng. Sci.* 1958 **8** 284.

Chemical Engineering Science, 1958, Vol. 9, pp. 153 to 163. Pergamon Press Ltd.

The non-homogeneous chromatographic column

A. S. Said

Department of Pathology, Columbia University, New York, N.Y.

(*Received* 15 *October* 1957; *in revised form* 15 *March* 1958)

Abstract—The theoretical plate concept in chromatography has been extended to the treatment of the non-homogeneous chromatographic column where the exchange coefficient k is not the same for all the plates in the column. The treatment is subject to the two basic assumptions of the theory, namely that the column is equivalent to a certain number of theoretical plates and that the eluent passes continuously through these plates. General deposition and elution equations have been derived and formulas for some special cases of practical interest were deduced. A numerical example illustrates the use of the derived equations.

Résumé—Le concept du plateau théorique en chromatographie a été étandu à l'étude d'une colonne de chromatographie non homogène, où le coefficient d'échange k n'est pas le même pour tous les plateaux de la colonne. L'étude est assujettie aux deux hypothèses fondamentales de la théorie que la colonne est équivalente à un certain nombre de plateaux théoriques et que l'éluant passe continuellement à travers ces plateaux. Des équations générales de dépôt et d'élution ont été établies et des formules, pour certains cas spéciaux d'intérêt pratique, ont été déduites. Un exemple numérique illustre l'emploi des équations établies.

Zusammenfassung—Die Vorstellung des theoretischen Bodens in der Chromatographie wurde auf die Behandlung der nicht-homogenen chromatographischen Säule ausgedehnt, bei welcher der Austauschkoeffizient k für alle Böden der Säule nicht gleich ist. Die Behandlung geht aus von zwei Grundannahmen der Theorie, nämlich dass die Säule einer bestimmten Anzahl theoretischer Böden äquivalent ist und dass das Elutionsmittel kontinuierlich durch diese Böden strömt. Die allgemeine Abscheidung und die Elutionsgleichungen werden abgeleitet und Formeln für einige Sonderfälle von praktischen Interesse mitgeteilt. Ein numerisches Beispiel verdeutlicht die Anwendung der abgeleiteten Gleichungen.

The differential equation which expresses the concentration on any plate in a homogeneous chromatographic column as a function of the column parameter n and the solution parameter u was derived in a previous paper [1] by means of a differential material balance around plate n. In deriving that equation it was assumed that the adsorption coefficient k is the same for all the plates in the column. On the other hand, when the column is not homogeneous, as in the case of a column made up of two or more layers of different adsorbents having different exchange coefficients, then a differential material balance around plate n gives

$$(k_n y_n - k_{n-1}\, y_{n-1})\, dw = -\frac{S}{N}\, dy_n$$

$$\therefore \frac{dy_n}{dx} + k_n y_n = k_{n-1} y_{n-1} \qquad (1)$$

y_n represents the concentration of solute on plate n, k_n is the adsorption or exchange coefficient at plate n, N is the total number of plates in the column, S is the total weight of adsorbent, w is the weight of eluent which has crossed plate n, and $x = N\,w/S$.

When k_n and k_{n-1} are constants or functions of x only as in the case of gradient elution, equation (1) can be solved as a first order linear differential equation and the following relation is obtained

$$y_n = \exp\left(-\int k_n dx\right) \left[\int k_{n-1}\, y_{n-1} \exp\left(\int k_n dx\right) dx + c\right] \qquad (2)$$

which is the recursion formula for plate n in the non-homogeneous chromatographic column. When k_n and k_{n-1} are constants equation (2) reduces to

$$y_n = \exp(-k_n x)\left[\int k_{n-1}\, y_{n-1} \exp(k_n x)\, dx + c\right] \quad (3)$$

The recursion formula for plate n in the homogeneous column can be deduced from equation (3) by substituting $k_n = k_{n-1} = k$ and one gets

$$y_n = \exp(-kx)\left[\int k y_{n-1} \exp(kx)\, dx + c\right] \quad (4)$$

In this paper equation (3) will be applied to deduce the deposition and elution relations for some simple cases of the non-homogeneous column.

The Deposition Case

A solute is deposited on a column containing N theoretical plates from a solvent where the adsorption coefficients between the solvent and the different plates of the column 1, 2, ... , n, ... N are k_1, k_2, ... k_n, ... k_N respectively.

Let us assume that the concentration of solute in the solvent entering the column is $\bar{y}_0$ and the column is free of solute at the beginning of the deposition process.

By a material balance around Plate 1

$$(\bar{y}_0 - \bar{y}_1)\, dw = \frac{S}{N}\, dy_1$$

$$(\bar{y}_0 - k_1 y_1)\, dx = dy_1 \quad \therefore \quad \frac{dy_1}{\bar{y}_0 - k_1 y_1} = dx$$

Integrating and substituting the boundary condition $y_1 = 0$ when $x = 0$, one gets

$$\frac{k_1 y_1}{\bar{y}_0} = 1 - \exp(-k_1 x)$$

or

$$\bar{R}_1 = 1 - \exp(-k_1 x)$$

In order to obtain the formula for Plate 2, one applies the recursion formula (3)

$$y_2 = \exp(-k_2 x)\left[\int k_1 y_1\, e^{k_2 x}\, dx + c\right]$$

$$= \exp(-k_2 x)\left[\int \bar{y}_0 \{1 - \exp(-k_1 x)\} e^{k_2 x}\, dx + c\right]$$

$$= \exp(-k_2 x)\left[\frac{\bar{y}_0}{k_2}\exp(k_2 x) - \frac{\bar{y}_0}{k_2 - k_1}\exp\{(k_2 - k_1)x\} + c\right]$$

when $x = 0$, $y_2 = 0$

substituting in the preceding equation

$$\therefore c = \frac{\bar{y}_0 k_1}{(k_2 - k_1)\, k_2}$$

and

$$\bar{R}_2 = \frac{k_2 y_2}{\bar{y}_0} = 1 - \frac{k_2}{k_2 - k_1}\exp(-k_1 x) - \frac{k_1}{k_1 - k_2}\exp(-k_2 x)$$

going to Plate 3 one can show that

$$\bar{R}_3 = 1 - \frac{k_2 k_3}{(k_2 - k_1)(k_3 - k_1)}\exp(-k_1 x) - \frac{k_1 k_3}{(k_1 - k_2)(k_3 - k_2)}\exp(-k_2 x) - \frac{k_1 k_2}{(k_1 - k_3)(k_2 - k_3)}\exp(-k_3 x)$$

and generally for Plate n

$$\bar{R}_n = 1 - \left[\frac{k_2 k_3 \cdot \cdots \cdot k_n}{(k_2 - k_1)(k_3 - k_1)\cdots(k_n - k_1)}\exp(-k_1 x) + \cdots + \frac{k_1 k_2 \cdot \cdots \cdot k_{n-1}}{(k_1 - k_n)(k_2 - k_n)\cdots(k_{n-1} - k_n)}\exp(-k_n x)\right]$$

Symbols. In order to simplify the writing of the above formula the following two symbols are introduced.

$k_g^{\,n} = k_1 k_2 k_3 \cdot \cdots \cdot k_n$ = the geometrical mean raised to the nth power and

$$k_{nr} = (k_1 - k_r)(k_2 - k_r)\cdots(k_{r-1} - k_r)(k_{r+1} - k_r)\cdots(k_n - k_r) = \prod_{s \neq r}^{n}(k_s - k_r)$$

$$\therefore \bar{R}_n = 1 - k_g^{\,n}\left[\frac{\exp(-k_1 x)}{k_1 k_{n1}} + \frac{\exp(-k_2 x)}{k_2 k_{n2}} + \cdots + \frac{\exp(-k_n x)}{k_n k_{nn}}\right] = 1 - k_g^{\,n}\sum_{r=1}^{n}\exp(-k_r x)/k_r k_{nr} \quad (5)$$

One deduces from this formula that the order of the plates is immaterial since by interchanging any two plates we wind up with the same equation.

Special case. k_n varies linearly with n

$$k_n = k_1 + (n-1)\,a \qquad a \text{ is a constant}$$

denoting $k_1 - a$ by k_0 $\therefore k_n = k_0 + na$

$$\overline{R}_n = 1 - k_g^n \left[\frac{\exp(-k_1 x)/k_1}{a \times 2a \cdots (n-1)a} + \frac{\exp(-k_2 x)/k_2}{-a \times a \cdots (n-2)a} + \cdots \right.$$

$$\left. \cdots + (-1)^{n-1} \frac{\exp(-k_n x)/k_n}{(n-1)a \times (n-2)a \cdots \times a} \right]$$

$$= 1 - \exp(-k_0 x)\, \frac{k_g^n}{a^{n-1}(n-1)!} \left[\frac{\exp(ax)}{k_1} - \frac{\exp(2ax)}{k_2}(n-1) \right.$$

$$\left. - \cdots + (-1)^{n+1} \frac{\exp(nax)}{k_n} \right]$$

$$= 1 - \frac{k_g^n}{a^{n-1}(n-1)!} \exp(-k_0 x) \sum_{r=1}^{n} (-1)^{r+1} c_{r-1}^{n-1} \frac{\exp(rax)}{k_r} \qquad (6)$$

Elution of a Zone Occupying One Plate Only

$$y_1 = y_1^0\, e^{-k_1 x}$$

Applying recursion formula (3)

$$y_2 = \exp(-k_2 x) \left[\int k_1 y_1 \exp(k_2 x)\, dx + c \right]$$

$$= \exp(-k_2 x) \left[\int k_1 y_1^0 \exp(-k_1 x) \exp(k_2 x)\, dx + c \right]$$

$$= \exp(-k_2 x) \left[y_1^0 \frac{k_1}{k_2 - k_1} \exp\{(k_2 - k_1)x\} + c \right]$$

when $x = 0$, $y_2 = 0$

$$\therefore c = \frac{k_1}{k_1 - k_2}$$

and

$$\frac{y_2}{y_1^0} = \frac{k_1}{k_2 - k_1} \exp(-k_1 x) + \frac{k_1}{k_1 - k_2} \exp(-k_2 x)$$

By applying the recursion formula again one can show that

$$\frac{y_3}{y_1^0} = \frac{k_1 k_2}{(k_2 - k_1)(k_3 - k_1)} \exp(-k_1 x) + \frac{k_1 k_2}{(k_1 - k_2)(k_3 - k_2)} \exp(-k_2 x) + \frac{k_1 k_2}{(k_1 - k_3)(k_2 - k_3)} \exp(-k_3 x)$$

and generally for plate n

$$\frac{y_n}{y_1^0} = \frac{k_g^{n-1}}{k_{n1}} \exp(-k_1 x) + \cdots + \frac{k_g^{n-1}}{k_{nn}} \exp(-k_n x)$$

and

$$\overline{R}_n = k_n \frac{y_n}{y_1^0} = \frac{k_g^n}{k_{n1}} \exp(-k_1 x) + \cdots + \frac{k_g^n \exp(-k_n x)}{k_{nn}} = k_g^n \sum_{r=1}^{n} \exp(-k_r x)/k_{nr} \qquad (7)$$

One can also see that as in the case of deposition, the order of the plates is immaterial.

Equation (7) is similar to the Bateman equation derived by Bateman [3] for the concentrations of different species during a chain radioactive decay process when only one species is present at the beginning of the process.

Special cases

(1) k_n varies linearly with n

$k_n = k_1 + (n-1)\,a$

Substituting in equation (7)

$$\overline{R}_n = k^n{}_g \left[\frac{\exp(-k_1 x)}{a \times 2a \cdots (n-1)a} - \frac{\exp(-k_2 x)}{a \times a \cdots (n-2)a} + \cdots + (-1)^{n+1} \frac{\exp(-k_n x)}{(n-1)a \times (n-2)a \cdots a} \right]$$

$$= \exp(-k_1 x)\frac{k_g^{\,n}}{a^{n-1}(n-1)!}$$
$$[1 - \exp(-ax)(n-1)$$
$$+ \exp(-2ax)c_2^{n-1} - \cdots\cdots +$$
$$(-1)^{n-1}\exp\{-(n-1)ax\}]$$
$$= \exp(-k_n x)\frac{k_g^{\,n}}{a^{n-1}(n-1)!}$$
$$[\exp(ax) - 1]^{n-1} \qquad (8)$$

The homogeneous column formula $R_n = \phi_{n-1}^{u}$ can be deduced as a limit to this formula as a tends to zero as follows:

$$\frac{\exp(ax)+1}{a} = x + \frac{ax^2}{2!} + \frac{a^2x^3}{3!} + \cdots\cdots$$

As a tends to 0, the right hand side tends to x

and $\lim_{a\to 0}\dfrac{\exp(ax) - 1}{a} = x$

also $k_n \to k$ and $k_g^{\,n} \to k^n$

$$\therefore \overline{R}_n \to \exp(-kx)\frac{k(kx)^{n-1}}{(n-1)!}$$

and

$$R_n = \frac{\overline{R}_n}{k} = \exp(-kx)\frac{(kx)^{n-1}}{(n-1)!} = \phi_{n-1}^{u}$$

(2) *The column is made up of two layers,* 1 *and* 2, *containing* n_1 *and* n_2 *plates with adsorption coefficients* k_1 *and* k_2 *respectively.*

$$y_{n_1} = y_1^0 \phi_{n_1-1}^{k_1 x} = y_1^0 \exp(-k_1 x)\frac{(k_1 x)^{n_1-1}}{(n_1-1)!}$$

Applying equation (5) for plate $n_1 + 1$

$$\therefore y_{n_1+1} = \exp(-k_2 x)\left[\int k_1 y_{n_1} e^{k_2 x}\,dx + c\right]$$
$$= y_1^0 \exp(-k_2 x)\left[\int a_1^{n_1}\phi_{n_1-1}^{u^*}\,du^* + c\right]$$

where

$$a_1 = \frac{k_1}{k_1 - k_2} \text{ and } u^* = (k_1 - k_2)x = u_1 - u_2$$

Integrating and substituting the boundary condition $y_{n_1+1} = 0$ when $x = 0$

$$\therefore y_{n_1+1} = y_1^0 \exp(-k_2 x)\, a_1^{n_1} P_{n_1}^{u^*}$$

going to plate $n_1 + 2$ and applying equation (3) again

$$y_{n_1+2} = \exp(-k_2 x)\left[\int k_2 y_1^0 \exp(-k_2 x)\, a_1^{n_1} P_{n_1}^{u^*}\exp(k_2 x)\,dx + c\right]$$
$$= \exp(-k_2 x)\left[y_1^0 a_1^{n_1} a_2 \int P_{n_1}^{u^*}\,du^* + c\right]$$

where

$$a_2 = \frac{k_2}{k_1 - k_2}$$

Integrating and substituting $y_{n_1+2} = 0$ when $x = 0$ we get

$$y_{n_1+2} = y_1^0 \exp(-k_2 x)\, a_1^{n_1} a_2 \int_0^{[1]} P_{n_1}^{u^*}$$

and for plate $n_1 + n_2$ one can show that

$$y_{n_1+n_2} = y_1^0 \exp(-u_2)\, a_1^{n_1} a_2^{n_2-1} \int_0^{[n_2-1]} P_{n_1}^{u^*} \qquad (9)$$

where

$$\int_0^{[m]} P_n^u \equiv \int_0^u \left(\int_0^{[m-1]} P_n^u\right) du = \int_0^u \cdots\cdots \int_0^u P_n^u\,(du)^m$$

It was shown by this author [2] that

$$\int_0^{[m]} P_n^u = \sum^{[m]} P_n^u$$

where

$$\sum^{[m]} P_n^u \equiv \sum_{r=n+1}^{\infty}\left(\sum^{[m-1]} P_r^u\right)$$
$$\equiv \sum_{r_m=n+1}^{\infty} \cdots\cdots \sum_{r_2=r_3+1}^{\infty}\sum_{r_1=r_2+1}^{\infty} P_{r_1}^u$$

$\sum^{[m]} P_n^u$ can be evaluated directly from the Poisson Tables as shown in Table 1 and hence $\int_0^{[m]} P_n^u$ can be obtained.

In constructing Table 1, use was made of the relation $\int_0^{[m]} P_0^u = \dfrac{u^m}{m!}$ which was also deduced by this author [2].

Table 1. *Values of* $\overset{[\infty]}{\Sigma} P_n^u$ *for different values of* u

1. $(u = 2)$

n	P_n^2	$\overset{[1]}{\Sigma} P_n^2$	$\overset{[2]}{\Sigma} P_n^2$	$\overset{[3]}{\Sigma} P_n^2$
0	1·000000	2·000000	2·000000	1·333333
1	·864665	1·135325	·864665	·468668
2	·593994	·541341	·323324	·145344
3	·323324	·218017	·105307	·040037
4	·142877	·075140	·030167	·009860
5	·052653	·022487	·007680	·002180
6	·016564	·005923	·001757	·000424

2. $(u = 2{\cdot}4)$

n	$P_n^{2\cdot4}$	$\overset{[1]}{\Sigma} P_n^{2\cdot4}$	$\overset{[2]}{\Sigma} P_n^{2\cdot4}$	$\overset{[3]}{\Sigma} P_n^{2\cdot4}$
0	1·000000	2·400000	2·880000	2·304000
1	·909282	1·490718	1·389282	·914718
2	·691559	·799159	·390123	·324595
3	·430291	·368868	·221255	·103340
4	·221277	·147591	·073664	·029676
5	·095869	·051722	·201942	·007734
6	·035673	·016049	·005893	·001841

3. $(u = 3{\cdot}0)$

n	P_n^3	$\overset{[1]}{\Sigma} P_n^3$	$\overset{[2]}{\Sigma} P_n^3$	$\overset{[3]}{\Sigma} P_n^3$
0	1·000000	3·000000	4·500000	4·500000
1	·950213	2·049787	2·450213	2·049787
2	·800852	1·248935	1·201278	·848509
3	·576810	·672125	·529153	·319356
4	·352768	·319357	·209796	·109560
5	·184737	·134620	·075176	·034384
6	·083918	·050702	·024474	·009910

4. $(u = 3{\cdot}6)$

n	$P_n^{3\cdot6}$	$\overset{[1]}{\Sigma} P_n^{3\cdot6}$	$\overset{[2]}{\Sigma} P_n^{3\cdot6}$	$\overset{[3]}{\Sigma} P_n^{3\cdot6}$
0	1·000000	3·600000	6·480000	7·776000
1	·972676	2·627324	3·852676	3·923324
2	·874311	1·753013	2·099663	1·823661
3	·697253	1·055760	1·043903	·779758
4	·484784	·570976	·472927	·306831
5	·293562	·277414	·195513	·111318
6	·155881	·121533	·073980	·037338

5. $(u = 4{\cdot}0)$

n	P_n^4	$\overset{[1]}{\Sigma} P_n^4$	$\overset{[2]}{\Sigma} P_n^4$	$\overset{[3]}{\Sigma} P_n^4$
0	1·000000	4·000000	8·000000	10·666667
1	·981684	3·018316	4·981684	5·684983
2	·908422	2·109894	2·871790	2·813193
3	·761897	1·347997	1·523793	1·289400
4	·566530	·781467	·742326	·547074
5	·371163	·410304	·332022	·215052
6	·214870	·195434	·136588	·078464

6. $(u = 4{\cdot}4)$

n	$P_n^{4\cdot4}$	$\overset{[1]}{\Sigma} P_n^{4\cdot4}$	$\overset{[2]}{\Sigma} P_n^{4\cdot4}$	$\overset{[3]}{\Sigma} P_n^{4\cdot4}$
0	1·000000	4·400000	9·680000	14·197333
1	·987723	3·412277	6·267723	7·929610
2	·933702	2·478575	3·789148	4·140462
3	·814858	1·663717	2·125431	2·015031
4	·640552	1·023165	1·102226	0·912765
5	·448816	·574349	·527917	0·384847
6	·280088	·294261	·233656	0·151191

7. $(u = 5)$

n	P_n^5	$\overset{[1]}{\Sigma} P_n^5$	$\overset{[2]}{\Sigma} P_n^5$	$\overset{[3]}{\Sigma} P_n^5$
0	1·000000	5·000000	12·500000	20·833333
1	·993262	4·006738	8·493262	12·340071
2	·959572	3·047166	5·446096	6·893975
3	·875348	2·171818	3·274278	3·619697
4	·734974	1·436844	1·837434	1·782268
5	·559507	·877337	·960097	·822166
6	·384039	·493298	·466799	·355367

8. $(u = 5{\cdot}4)$

n	$P_n^{5\cdot4}$	$\overset{[1]}{\Sigma} P_n^{5\cdot4}$	$\overset{[2]}{\Sigma} P_n^{5\cdot4}$	$\overset{[3]}{\Sigma} P_n^{5\cdot4}$
0	1·000000	5·400000	14·580000	26·244000
1	·995483	4·404517	10·175483	16·068517
2	·971094	3·433423	6·742060	9·326457
3	·905242	2·528181	4·213879	5·112578
4	·786709	1·741472	2·472407	2·640171
5	·626689	1·114783	1·357624	1·282547
6	·453868	·660915	·696709	·585838

Table 1 (*contd.*)

9. ($u = 5{\cdot}8$)

n	$P_n^{5\cdot8}$	$\sum^{[1]} P_n^{5\cdot8}$	$\sum^{[2]} P_n^{5\cdot8}$	$\sum^{[3]} P_n^{5\cdot8}$
0	1·000000	5·800000	16·820000	32·518667
1	·996972	2·803028	12·016972	20·501695
2	·979413	3·823615	8·193357	12·308338
3	·929489	2·895126	5·298231	7·010107
4	·830037	2·065089	3·233142	3·776965
5	·687282	1·377807	1·855335	1·921630
6	·521685	·856122	·999213	·922417

10. ($u = 6$)

n	P_n^{6}	$\sum^{[1]} P_n^{6}$	$\sum^{[2]} P_n^{6}$	$\sum^{[3]} P_n^{6}$
0	1·000000	6·000000	18·000000	36·000000
1	·997521	5·002479	12·997521	23·002479
2	·782649	4·019830	8·977691	14·024788
3	·938031	3·081799	5·895892	8·128896
4	·848796	2·233003	3·662889	4·466007
5	·714943	1·518060	2·144829	2·322178
6	·554320	·963740	1·181089	1·141089

11. ($u = 6{\cdot}2$)

n	$P_n^{6\cdot2}$	$\sum^{[1]} P_n^{6\cdot2}$	$\sum^{[2]} P_n^{6\cdot2}$	$\sum^{[3]} P_n^{6\cdot2}$
0	1·000000	6·200000	19·220000	39·721333
1	·997971	5·202029	14·017971	25·703362
2	·985388	4·216641	9·801330	15·902032
3	·946382	3·270259	6·531071	9·370961
4	·865771	2·404488	4·126583	5·244378
5	·740823	1·663665	2·462918	2·781460
6	·585887	1·077778	1·385140	1·396320

12. ($u = 6{\cdot}4$)

n	$P_n^{6\cdot4}$	$\sum^{[1]} P_n^{6\cdot4}$	$\sum^{[2]} P_n^{6\cdot4}$	$\sum^{[3]} P_n^{6\cdot4}$
0	1·000000	6·400000	20·480000	43·690667
1	·998338	5·401662	15·078338	28·612329
2	·987704	4·413958	10·664380	17·947949
3	·953676	3·460282	7·204098	10·743851
4	·881081	2·579201	4·624897	6·118954
5	·764930	1·814271	2·810626	3·308328
6	·616256	1·198015	1·612611	1·695717

13. ($u = 6{\cdot}6$)

n	$P_n^{6\cdot6}$	$\sum^{[1]} P_n^{6\cdot6}$	$\sum^{[2]} P_n^{6\cdot6}$	$\sum^{[3]} P_n^{6\cdot6}$
0	1·000000	6·600000	21·780000	47·916000
1	·998640	5·601360	16·178640	31·737360
2	·989661	4·611699	11·566941	20·170419
3	·960032	3·651667	7·915274	12·255145
4	·894849	2·756818	5·158456	7·096689
5	·787296	1·969522	3·188934	3·907755
6	·645327	1·324195	1·864739	2·043016

14. ($u = 7$)

n	P_n^{7}	$\sum^{[1]} P_n^{7}$	$\sum^{[2]} P_n^{7}$	$\sum^{[3]} P_n^{7}$
0	1·000000	7·000000	24·500000	57·166667
1	·999088	6·000912	18·499088	38·667579
2	·992705	5·008207	13·490881	25·176698
3	·970364	4·037843	9·453028	15·723660
4	·918235	3·119608	6·333430	9·390230
5	·827008	2·292600	4·040830	5·349400
6	·699292	1·593308	2·447522	2·901878

15. ($u = 8$)

n	P_n^{8}	$\sum^{[1]} P_n^{8}$	$\sum^{[2]} P_n^{8}$	$\sum^{[3]} P_n^{8}$
0	1·0000	8·0000	32·0000	85·3333
1	·9997	7·0003	24·9997	60·3336
2	·9970	6·0033	18·9964	41·3372
3	·9862	5·0171	13·9793	27·3579
4	·9576	4·0595	9·9198	17·4381
5	·9004	3·1591	6·7607	10·6774
6	·8088	2·3503	4·4104	6·2670

16. ($u = 9$)

n	P_n^{9}	$\sum^{[1]} P_n^{9}$	$\sum^{[2]} P_n^{9}$	$\sum^{[3]} P_n^{9}$
0	1·0000	9·0000	40·5000	121·5000
1	·9999	8·0001	32·4999	89·0001
2	·9988	7·0013	25·4986	64·5015
3	·9938	6·0075	19·4911	45·0104
4	·9788	5·0287	14·4624	30·5480
5	·9450	4·0837	10·3787	30·1693
6	·8840	3·1994	7·1793	12·9900

Table 1 (*contd.*)

17. ($u = 10$)

n	P_n^{10}	$\overset{[1]}{\Sigma} P_n^{10}$	$\overset{[2]}{\Sigma} P_n^{10}$	$\overset{[3]}{\Sigma} P_n^{10}$
0	1·0000	10·0000	50·0000	166·6667
1	1·0000	9·0000	41·0000	125·6667
2	·9995	8·0005	32·9995	92·6672
3	·9972	7·0033	25·9962	56·6710
4	·9897	6·0136	19·9826	36·6884
5	·9707	5·0429	14·9397	21·7487
6	·9329	4·1100	10·8297	10·9190

18. ($u = 12$)

n	P_n^{12}	$\overset{[1]}{\Sigma} P_n^{12}$	$\overset{[2]}{\Sigma} P_n^{12}$	$\overset{[3]}{\Sigma} P_n^{12}$
0	1·0000	12·0000	72·0000	288·0000
1	1·0000	11·0000	61·0000	227·0000
2	·9999	10·0001	50·9999	176·0001
3	·9995	9·0006	41·9993	134·0008
4	·9977	8·0029	33·9964	100·0044
5	·9924	7·0105	26·9859	73·0185
6	·9797	6·0308	20·9551	52·0634

19. ($u = 14$)

n	P_n^{14}	$\overset{[1]}{\Sigma} P_n^{14}$	$\overset{[2]}{\Sigma} P_n^{14}$	$\overset{[3]}{\Sigma} P_n^{14}$
0	1·0000	14·0000	98·0000	457·3333
1	1·0000	13·0000	85·0000	372·3333
2	1·0000	12·0000	73·0000	299·3333
3	·9999	11·0001	61·9999	237·3334
4	·9995	10·0006	51·9993	185·3341
5	·9982	9·0024	42·9969	142·3372
6	·9945	8·0079	34·9890	107·3482

20. ($u = 16$)

n	P_n^{16}	$\overset{[1]}{\Sigma} P_n^{16}$	$\overset{[2]}{\Sigma} P_n^{16}$	$\overset{[3]}{\Sigma} P_n^{16}$
0	1·0000	16·0000	128·0000	682·6667
1	1·0000	15·0000	113·0000	569·6667
2	1·0000	14·0000	99·0000	470·6667
3	1·0000	13·0000	86·0000	389·6667
4	·9999	12·0001	73·9999	310·6668
5	·9996	11·0005	62·9994	247·6674
6	·9986	10·0019	52·9975	194·6699

Illustrative Example

To illustrate the applications of these equations let us consider the simple case of a column made up of two layers; layer 1 equivalent to 6 theoretical plates and having an exchange coeff. k_1, and layer 2 equivalent to 4 theoretical plates and an exchange coeff. k_2 such that $k_1/k_2 = 2$. At the start of the elution process, the solute is adsorbed on the first plate only and its concentration is y_1^0. It is required to determine:

a—The concentration distribution of solute on the plates after an amount of eluent has passed through the plates such that $u_1 = 8$.

b—The shape of the elution curve.

c—The value of u_1 corresponding to maximum effluent concentration.

(a) From Plate 1 to Plate 6, the concentration of solute is determined from the equation

$$R_n = \frac{y_n}{y_1^0} = \phi_{n-1}^{u_1}$$

$$R_1 = \phi_0^8 = 0{\cdot}000335, \qquad R_2 = \phi_1^8 = 0{\cdot}002684$$

$$R_3 = \phi_2^8 = 0{\cdot}010735, \qquad R_4 = \phi_3^8 = 0{\cdot}028626$$

$$R_5 = \phi_4^8 = 0{\cdot}05725, \qquad R_6 = \phi_5^8 = 0{\cdot}091604$$

On layer 2; $R_6 = 0{\cdot}091604 \times k_1/k_2$

$= 0{\cdot}183208$

From Plate 7 to Plate 10, the concentration is determined according to the equation

$$R_{n_1+n_2} = \frac{y_{n_1+n_2}}{y_1^0}$$

$$= e^{-u_2}\, a_1^{n_1}\, a_2^{n_2-1} \int^{[n_2-1]} P_{n_1}^{u^*}$$

$$u_2 = u_1 \frac{k_2}{k_1} = 4 \qquad u^* = u_1 \frac{k_1 - k_2}{k_1} = 4$$

$$a_1 = \frac{k_1}{k_1 - k_2} = 2 \qquad a_2 = \frac{k_2}{k_1 - k_2} = 1$$

$$R_7 = R_{6+1} = e^{-4} \times 2^6 \times 1^0 \int^{[0]} P_6^4$$

$$= 0{\cdot}018316 \times 64 \times 0{\cdot}214870$$

$$= 0{\cdot}25187$$

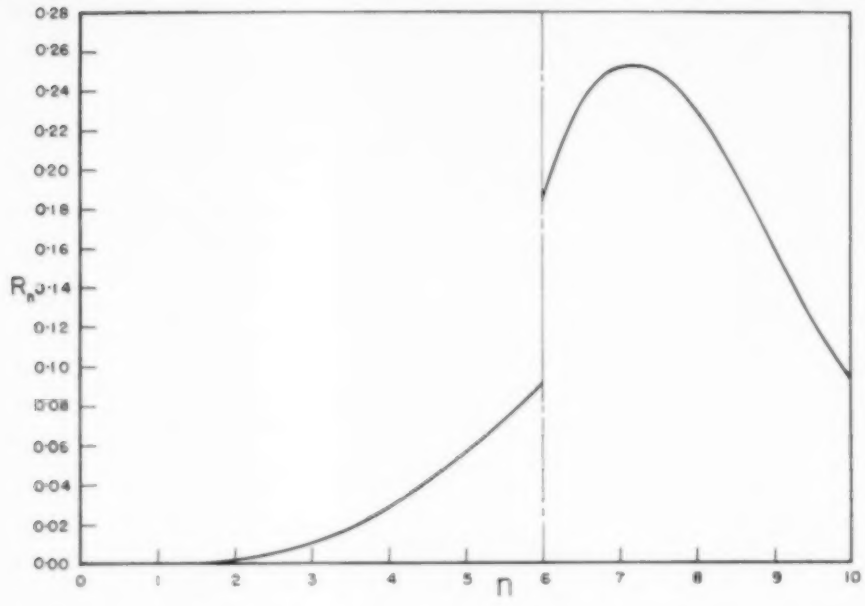

Fig. 1. Concentration distribution of solute on a two-layer non-homogeneous column during elution.

Table 2

n^*	n_2	$\int_6^{[3]} P_6^{n^*}$	e^{-n_2}	$R_{10} = e^{-n_2} a_1^{n_1} a_2^{n_2-1} \int_n^{[n_2-1]} P_n^{n^*}$
6	6	0	1	0·0000
2	2	·000423	·135335	0·0037
2·4	2·4	·001841	·090718	0·0106
3	3	·009910	·049787	0·0315
3·6	3·6	·037338	·027324	0·0652
4	4	·078464	·018316	0·0918
4·4	4·4	·151191	·012277	0·1187
5	5	·355367	·006738	0·1533
5·4	5·4	·585838	·004517	0·1693
5·8	5·8	·922417	·003028	0·1788
6	6	1·141089	·002479	0·1809
6·2	6·2	1·396320	·002029	0·1813
6·4	6·4	1·695717	·001602	0·1811
7	7	2·043016	·001360	0·1778
8	8	2·901878	$9·120 \times 10^{-4}$	0·1675
9	9	6·2670	$3·355 \times 10^{-4}$	0·1329
10	10	10·9190	$4·461 \times 10^{-5}$	0·0619
12	12	52·0634	$6·145 \times 10^{-6}$	0·0195
14	14	107·3482	$8·317 \times 10^{-7}$	0·0057
16	16	194·6699	$1·125 \times 10^{-7}$	0·0014

$$R_8 = R_{6+2} = e^{-4} \times 2^6 \times 1^1 \int_{\cdot}^{[1]} P_6^4$$
$$= 0{\cdot}018316 \times 64 \times 0{\cdot}195434$$
$$= 0{\cdot}22905$$
$$R_9 = R_{6+3} = e^{-4} \times 2^6 \times 1^2 \int_{\cdot}^{[2]} P_6^4$$
$$= 0{\cdot}018316 \times 64 \times 0{\cdot}136588$$
$$= 0{\cdot}16008$$
$$R_{10} = R_{6+4} = e^{-4} \times 2^6 \times 1^3 \int_{\cdot}^{[3]} P_6^4$$
$$= 0{\cdot}018316 \times 64 \times 0{\cdot}078464$$
$$= 0{\cdot}09238.$$

The different values of R_n are plotted vs. n in Fig. (1).

(b) In order to plot the elution curve, the values of R_{10} corresponding to different values of u are calculated from equation (9). R_{10} represents the ratio between the concentration on Plate 10 and the initial concentration on Plate 1. It represents also the ratio between the concentration of solute in the effluent and the concentration of solute in a solution in equilibrium with Plate 1 when the concentration on the plate is equal to y_1^0. One can also plot R_{10} vs. u. The curve will be the same as R_{10} vs. u except that the ordinates will be multiplied by the constant value k_2.

Values of R_{10} for different values of u^* were calculated according to equation (9) and are tabulated in Table 2. Fig. (2) is a plot of R_{10} vs. u^*. $\int_{\cdot}^{[3]} P_6^{u^*}$ is equal to $\sum^{[3]} P_6^{u^*}$ and its values were obtained from Table 1.

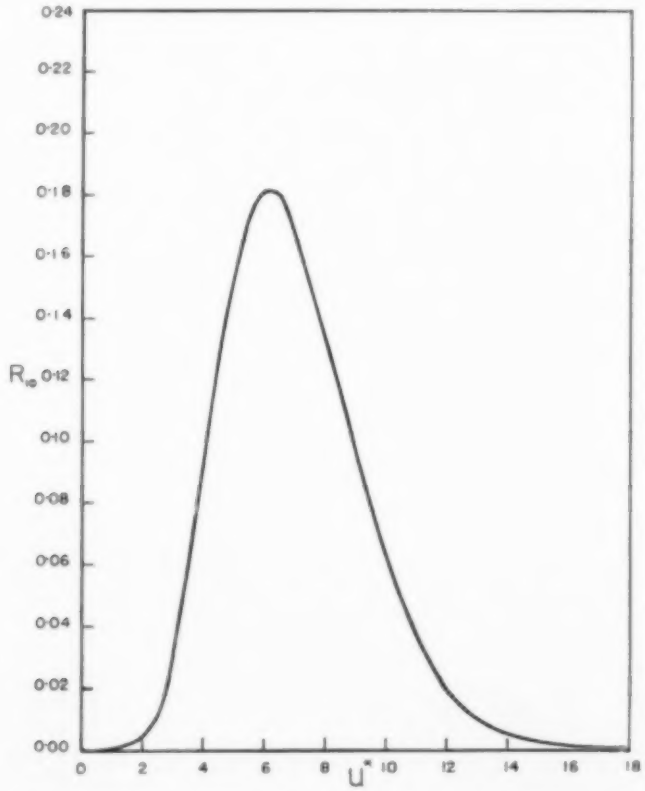

FIG. 2. Elution curve for a two-layer non-homogeneous column.

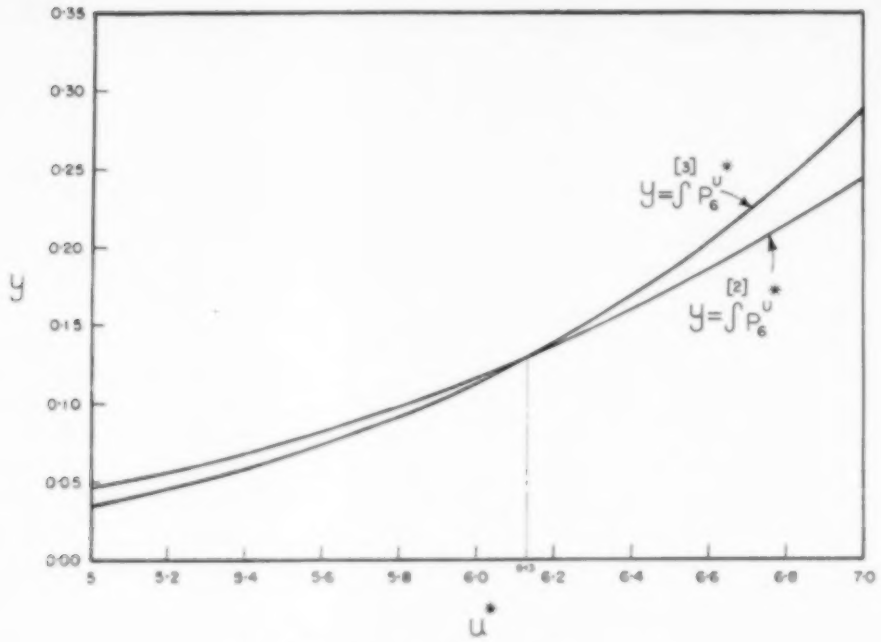

FIG. 3. Graphical solution of the equation:

$$\int^{[2]} P_6^{u^*} = \int^{[3]} P_6^{u^*}$$

For all the points $a_1 = 2$, $a_2 = 1$, $n_1 = 6$, $n_2 = 4$ and $u_2 = u^* \dfrac{k_2}{k_1 - k_2} = u^*$.

(*c*) *Maximum concentration.* In order to find u^*_{max}, one differentiates R_{10} with respect to u^* and equates to zero.

$$R_{10} = \exp(-u_2) \times 2^6 \times 1^3 \int^{[3]} P_6^{u^*}$$

$$= 64 \exp(-u_2) \int^{[3]} P_6^{u^*}$$

since

$$u_2 = \frac{k_2}{k_1 - k_2} u^* = u^*$$

$$\therefore R_{10} = 64 \exp(-u^*) \int^{[3]} P_6^{u^*}$$

$$\frac{dR_{10}}{du^*} =$$

$$64 \exp(-u^*) \int^{[2]} P_6^{u^*} - 64 \exp(-u^*) \int^{[3]} P_6^{u^*}$$

and for maximum R_{10}

$$\frac{dR_{10}}{du^*} = 0$$

Table 3

u^*	5	5·4	5·8	6·0	6·2	6·4	6·6	7
$\int^{[2]} P_6^{u^*}$	·466799	·696709	·999213	1·181089	1·385140	1·612611	1·864793	2·447522
$\int^{[3]} P_6^{u^*}$	·355367	·585838	·922417	1·141089	1·396320	1·695717	2·043016	2·901878

Therefore

$$\int_{[2]} P_6^{u^*} = \int_{[3]} P_6^{u^*}$$

Plotting

$$y \equiv \int_{[2]} P_6^{u^*} \text{ vs. } u^* \text{ and } y \equiv \int_{[3]} P_6^{u^*} \text{ vs. } u^*$$

The two curves intersect at $u^* = u^*_{max}$. In Fig. (3), u^*_{max} is found to be equal to 6·13.

Table 3 lists the values of $\int_{[2]}^{u^*} P^6$ and $\int_{[3]} P_6^{u^*}$ for different values of u^*. These values were obtained from Table 1 and were used in preparing Fig. 3.

Notation

$a_1 = \dfrac{k_1}{k_1 - k_2}$

$a_2 = \dfrac{k_2}{k_1 - k_2}$

c, a = constants

k = adsorption or exchange coefficient for the homogeneous column

k_n = adsorption or exchange coefficient at plate n for the non-homogeneous column

$k_g^n = k_1 \times k_2 \times k_3 \cdots k_n$
= geometrical mean raised to the nth power

$k_{nr} = \prod_{s \neq r}^{n} (k_s - k_r)$

N = total number of plates in column

$P_n^u = \sum_{r=n}^{\infty} \phi_r^u$

$R_n = y_n / y_0$

$R_n^0 = y_n^0 / y_0$

$\overline{R}_n = k_n y_n / \overline{y}_0$

$\overline{R}_n = k_n y_n / y_0$

S = total weight of adsorbent in the column

$u = kx$

$u^* = (k_1 - k_2)\, x = u_1 - u_2$

w = weight of eluent or solvent that has passed through any plate in the column

$x = wN/S$

y_n = concentration of solute on plate n, g solute/g adsorbent during elution

$\overline{y}_n$ = concentration of solute in eluent in equilibrium with plate n during elution

y_n^0 = concentration of solute on plate n at the beginning of the elution process

y_0 = concentration of solute on adsorbent if in equilibrium with solvent containing the solute at a concentration $\overline{y}_0$

$\overline{y}_0$ = concentration of solute in solvent before entering Plate 1

$\phi_n^u = e^{-u} u^n / n!$ = Poisson exponential function

References

[1] Said A. S. *Amer. Inst. Chem. Engrs. J.* 1956 **2** 477.

[2] Said A. S. Some properties of the Poisson distribution. *Amer. Inst. Chem. Engrs. J.* In press.

[3] Bateman H. *Proc. Camb. Phil. Soc.* 1910 **15** 423.

Chemical Engineering Science, 1958, Vol. 9, pp. 164 to 169. Pergamon Press Ltd.

Enthalpy-concentration diagram for the system hydrogen peroxide-water at 50 mm Hg total pressure

P. S. Murti
Department of Chemical Technology, Andhra University, Waltair, India.

(*Received* 13 *November* 1957)

Abstract—An enthalpy-concentration diagram of the binary system hydrogen peroxide–water was constructed at 50 mm Hg total pressure. Lack of information on heat capacities of the solutions at different temperatures necessitated the author assuming that the excess heat capacity of mixing remains constant in the temperature range required in this diagram. Isobaric liquid–vapour equilibrium data were also calculated at 50 mm Hg from the isothermal data of Scatchard, Kavanagh and Ticknor [1]. The results of these calculations are presented in a Figure.

Résumé—L'auteur a préparé un diagramme enthalpie concentration du système binaire eau oxygénée-eau pour une pression totale de 50 mm Hg. Un manque de données sur les capacités calorifiques des solutions à différentes température a obligé l'auteur à supposer que l'excès de capacité calorifique du mélange reste constant dans le domaine de température de ce diagramme. A partir des données isothermes de Scatchard, Kavanagh et Ticknor I, l'auteur aussi calculé à 50 mm de Hg les données isobares d'équilibre liquide-vapeur. Les résultats de ces calculs sont reproduits sur une figure.

Zusammenfassung—Für das binäre System Wasserstoffperoxyd-Wasser wurde bei einem Gesamtdruck von 50 Torr ein Enthalpie-Konzentrationsdiagramm entworfen. Fehlende Kenntnis über die Wärmekapazitäten der Lösungen bei verschiedenen Temperaturen zwang zu der Annahme dass die Überschuss-Wärmekapazität der Mischung im Temperaturbereich des Diagramms konstant blieb. Isobare Flüssigkeit-Dampf-Gleichgewichte wurden bei 50 Torr aus den Isothermenwerten von Scatchard, Kavanagh und Ticknor (1) berechnet. Die Ergebnisse dieser Rechnungen sind in einem Bild wiedergegeben.

Hydrogen peroxide finds extensive use as an oxidizing agent in the bleaching of cellulosic and wool materials, as a foaming agent in the manufacture of porous substances, as a source of free radicals to initiate polymerization processes, as a starting material for the preparation of the inorganic and organic peroxy compounds, and as a liquid propellant. Although only 47 per cent by weight of hydrogen peroxide (100 per cent) is available as oxygen for the combustion of a fuel, a substantial quantity of heat will be released when it is decomposed to water and oxygen. It can, therefore, be used as a monopropellant in which it is decomposed under pressure to yield a gaseous mixture of oxygen and superheated steam, or as a bipropellant in which the hydrogen peroxide is first decomposed and then the fuel, such as hydrazine, burned in the hot decomposition products.

The earlier commercial production of this chemical is by the action of acids upon inorganic peroxides such as barium peroxide. This process, however, yields low strength hydrogen peroxide (6-8 per cent by weight). Over 80 per cent of the present world production involves the manufacture, in the first place, of peroxy-disulphate by an electrochemical process followed by hydrolysis. The concentration of hydrogen peroxide obtained in the above process (nearly 36 per cent by weight) is adequate for some of the industrial applications other than propellants which require, however, a concentration of around 90 per cent. Various methods of production and purification have been clearly outlined in the monograph

brought out by the American Chemical Society [2] and these generally involve the absorption of hydrogen peroxide vapours and fractionation of the liquid at low pressures. Since hydrogen peroxide decomposes at hight emperatures, the processes are usually carried out at 40-60 mm Hg total pressure [3].

The author found a great need for the enthalpy-concentration diagram for the hydrogen peroxide–water system to base the design of the absorbers and the fractionators in the above process on a more fundamental and accurate basis. The application of these Merkel charts has been shown to the design of fractionators by PONCHON [4] and SAVARIT [5] and to the design of single and multiple effect evaporators by HIRSCH [6]. McCABE [7] reviewed the use of such a chart for sodium hydroxide-water system in heat balance equations. BOSNJAKOVIC [8] has given a complete development of its use and applied to heat exchange processes and chemical processes. Although, the importance of using such a chart in solving a problem on a binary solution involving the first law of thermodynamics is very well known, not very many charts are available for some of the industrially important systems to the designers. This is primarily due to the lack of availability of the data on physical properties such as heat capacities of the mixtures at various temperatures and heats of mixing.

In the following pages, a detailed account of the method used in preparing the Merkel chart is presented.

A. Liquid–Vapour Equilibrium at 50 mm Hg.

SCATCHARD, KAVANAGH and TICKNOR [1] have recently reported isothermal phase equilibrium data, over wide temperature and composition ranges, obtained in a recirculation still. The data are believed to be the most accurate available to the author. Because of the uncertainity in the composition of the vapour, SCATCHARD *et al.*, relied on the total pressure measurements and expressed total pressure in terms of vapour pressure, composition and chemical potential of the components as :—

$$P_T = P_w x_w \exp\left(\frac{1}{RT}\left[\mu_w^E - (\beta_{ww} - V_{ww})(P_T - P_w)\right]\right) + P_h x_h \exp\left(\frac{1}{RT}\left[\mu_h^E - (\beta_{hh} - V_{hh})(P_T - P_h)\right]\right) \quad (1)$$

where

$$\mu_w^E = (1 - x_w)^2 \left[B_0 + B_1(1 - 4x_w) + B_2(1 - 2x_w)(1 - 6x_w)\right] \quad (2a)$$

and

$$\mu_h = x_h^2 \left[B_0 + B_1(3 - 4x_w) + B_2(1 - 2x_w)(5 - 6x_w)\right] \quad (2b)$$

Substituting equations (2) into (1) and fitting the isothermal data to equation (1), the authors evaluated the constants as :—

$$B_0 = -752 + 0{\cdot}97\ t^\circ\text{C}. \quad (3)$$
$$B_1 = 85$$
$$B_2 = 13$$

Remembering that

$$\mu^E = RT \ln \gamma \quad (4)$$

the activity coefficients were expressed as

$$\ln \gamma_w = \frac{(1 - x_w)^2}{RT}\left[-1017 + 0{\cdot}97\ T + 85(1 - 4x_w) + 13(1 - 2x_w)(1 - 6x_w)\right] \quad (5a)$$

and

$$\ln \gamma_h = \frac{x_w^2}{RT}\left[-1017 + 0{\cdot}97\ T + 85(3 - 4x_w) + 13(1 - 2x_w)(5 - 6x_w)\right] \quad (5b)$$

At even values of hydrogen peroxide composition, the bubble point temperature at 50 mm Hg was found out by trial and error procedure bearing in mind that :—

$$P_T = 50 = \gamma_w P_w x_w + \gamma_h P_h x_h \quad (6)$$

The vapour pressures for hydrogen peroxide were obtained through the equation of SCATCHARD *et al.* :—

$$\log P_h = 44{\cdot}5760 - 4025{\cdot}3/T - 12{\cdot}996 \log T + 0{\cdot}0046055\, T \quad (7)$$

and for water, the equation of KEYES [9] was employed. The calculated phase equilibrium data are presented in Table 1 together with dew point temperatures read from a large scale plot of $t - x - y$.

Table 1. *Calculated values of liquid–vapour equilibrium at* 50 mm Hg *total pressure*

Mole fraction liquid	*Hydrogen peroxide vapour*	*Bubble point* (°C)	*Dew point* (°C)
0·000	0·000	38·11	38·11
0·100	0·0041	40·3	54·8
0·200	0·0123	43·2	60·8
0·300	0·0280	46·7	65·2
0·400	0·0575	50·8	68·5
0·500	0·1071	55·5	71·3
0·600	0·1900	60·3	74·0
0·700	0·3100	65·6	76·3
0·800	0·4824	70·7	78·0
0·900	0·7125	76·5	79·4
1·000	1·000	80·42	80·42

B. Enthalpy Data in the Liquid Region

The reference temperature is taken as 0°C at which the enthalpies of the pure components, as liquids, are taken to be equal to zero. Integral heats of solution data were reported by GIGUIERE and MORISSETTE [10] at 26·9°C. However, data at 25°C were calculated by SCHUMB, SATTERFIELD and WENTWORTH [2] using the excess heat capacity data and the equation (8) :—

$$(\Delta H_s)_{T1} = (\Delta H_s)_{T2} + \Delta C_{Pm}\,(T_2 - T_1) \quad (8)$$

where $(\Delta H_s)_{T1}$, $(\Delta H_s)_{T2}$ are the molal integral heats of solution, cal/g mole of H_2O_2 at temperture T_1 and T_2 respectively and ΔC_{Pm} is the difference between the heat capacities of the components of the solution and the solution itself per mole of hydrogen peroxide contained. The excess heat capacity data were listed in the A.C.S. monograph [2] and were assumed independent of temperature; this assumption was shown to hold good by the authors by a comparison of the data on heat of dilution to infinite dilution at 14°, 20° with those reported by other investigators [11-14], and with those calculated from phase equilibrium measurement of SCATCHARD *et al.* at 56°C.

Heat capacity data for liquid hydrogen peroxide at different temperatures were not available in the literature. The data, therefore, were predicted from the ideal vapour heat capacities as outlined by HOUGEN and WATSON [15]. It has been found that the reduced temperature, even at the highest bubble point temperature, is less than 0·55 and hence it was assumed that $C_{P(L)} - C^{*}_{P(V)} =$ constant and this constant was evaluated using the liquid heat capacity at 25°C. The calculated heat capacities were found to follow a linear variation with temperature and the following equation was fitted to the data by the method of least squares :—

$$C'_{PL} = 0{\cdot}6220 + 0{\cdot}000235\, t°\text{C. cal/g °C}$$

The enthalpy of a liquid mixture at any composition, x'_h is then given by :—

$$(H'_L)_{t,x'_h} = x'_h \int_0^t (0{\cdot}6220 + 0{\cdot}000235\, t)\, dt + x'_w (H'_{H_2O})\, t + x'_h\, (\Delta H'_s)_t \quad (9)$$

The enthalpy of liquid water H'_{H_2O} at any specified temperature is obtained through interpolation of the tables of KEENAN and KEYES [16]. The integral heats of solution $(\Delta H'_s)_t$ were calculated using the experimental data at 26·9°C, and equation (8) and then reducing to a basis of one pound of hydrogen peroxide. The points on the saturated liquid curve were similarly determined using the data given in Table 1 and calculating the enthalpies of the liquid mixtures by the method outlined above.

C. Enthalpy Data at Dew Point Temperatures and in Superheated Vapour Region

The terminal points on the saturated vapour curve are located by adding the latent heat of vaporization of the pure components to the values of the enthalpy at the two ends of the saturated

liquid curve. The other points on the saturated vapour curve were located by the intersection of the isotherm and the corresponding concentration of a point on the dew point – composition curve, the data of which are presented in Table 1. The heats of vaporization of hydrogen peroxide were obtained by using the equation (10) [2] which was derived from the vapour pressure equation and the application of Clapeyron equation :—

$$\Delta H_v = 18412 + 0{\cdot}021066\ T^2 - 25{\cdot}817\ T \quad (10)$$

The data for water were taken from the tables presented by KEENAN and KEYES [16].

The enthalpies of the pure superheated vapours were obtained by using the following equation :—

$$H'_v = H'_{sv} + \frac{1}{\text{Mol. wt.}} \int_{T_s}^{t} C^{\circ}_{P(v)}\, dT \qquad (11)$$

where

H'_v = enthalpy of the superheated vapour at a temperature t °C, C.H.U/lb.

H'_{sv} = enthalpy of the saturated vapour at t_s °C, C.H.U/lb.

$C^{\circ}_{p(v)}$ = ideal heat capacity of the vapour, cal/g mole °K.

Mol. wt. = Molecular weight

The ideal heat capacity data were taken from reference [2] and are given below.

Hydrogen peroxide

$$C^{\circ}_{P(v)} = 8{\cdot}514 + (0{\cdot}948)\ 10^{-2}\ T - (0{\cdot}3)\ 10^{-5}\ T^2 \qquad (T \text{ in } {}^{\circ}K)$$

Water

$$C^{\circ}_{P(v)} = 7{\cdot}256 + (0{\cdot}2298)\ 10^{-3}\ T + (0{\cdot}0283)\ 10^{-5}\ T^2\ (T \text{ in } K) \quad (12)$$

Table 2. Calculated values of enthalpies in liquid region : reference enthalpies are zero for liquid hydrogen peroxide and water at 0°C

	Liquid enthalpies (C.H.U./lb.)						
x'/(t°C)	0	10	20	25	30	40	*At bubble point*
0·000	0	10·40	20·02	24·99	30·56	------	38·09 (38·11°C.)*
0·100	− 1·87	7·91	17·02	21·69	26·92	---	35·09 (39· 2°C.)
0·200	− 3·90	5·38	14·10	18·50	23·46	31·96	32·62 (40·75°C.)
0·300	− 5·88	2·97	11·29	15·55	20·24	28·42	30·78 (42·75°C.)
0·400	− 7·53	0·91	9·04	12·97	17·43	25·31	29·63 (45·25°C.)
0·500	− 8·72	− 0·66	7·24	10·96	15·19	22·80	29·51 (48· 5°C.)
0·600	− 9·03	− 1·43	6·24	9·65	13·77	21·11	30·67 (52· 6°C.)
0·700	− 8·64	− 1·30	6·10	9·43	13·21	20·30	33·36 (58·0 °C.)
0·800	− 7·02	− 0·064	7·11	10·21	13·79	20·55	38·24 (64· 5°C.)
0·900	− 4·10	2·489	9·42	12·33	15·79	22·32	43·65 (72· 1°C.)
1·000	0	6·23	12·91	15·62	18·77	25·07	50·57 (80·42°C.)

*Bubble point temperatures are given in parentheses.

Substituting these equations into (11) and integrating one can get the enthalpies in the vapour region. It was assumed that the heats of solution of vapours were equal to zero, and that the enthalpy of the vapours change very little with pressure, particularly at low pressures. By these two assumptions, it is evident that the enthalpy of a mixture of vapours is a linear function of the weight fraction of hydrogen peroxide. Hence, the isotherms in the vapour region can be located by drawing straight lines through those points on the two pure components.

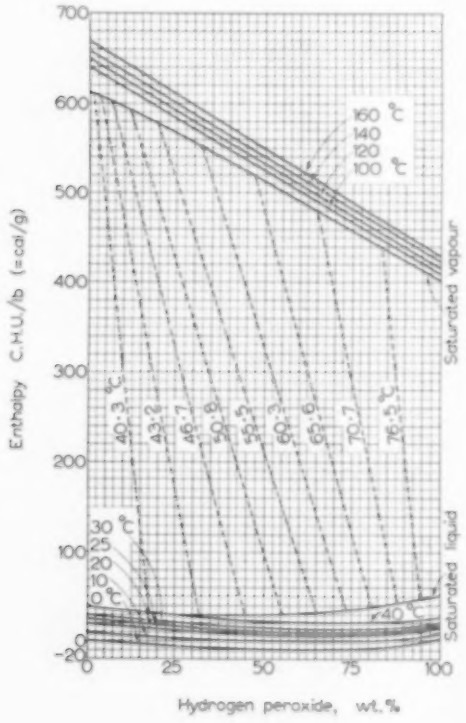

Fig. 1

All the calculated values of the enthalpies are presented in Tables 2 and 3 at even weight fractions of hydrogen peroxide, and the accompanying Figure indicates the Merkel diagram for this system. The phase equilibrium compositions are also shown as dotted lines and the inscribed figures indicate the bubble point temperatures at 50 mm Hg total pressure, read from a large scale plot of $t - x' - y'$.

Table 3. Enthalpy data of the vapour in the saturated and superheated region: reference enthalpies are zero for liquid hydrogen peroxide and water at 0°C

Saturated Region		*Superheated Region*		
x'	*Enthalpy* (C.H.U./lb)	*Temp.* (°C)	H_2O_2	H_2O
0	614	100	407·5	642
0·1	596	120	414·4	651
0·2	576	140	421·4	660
0·3	554	160	428·4	669
0·4	534			
0·5	511			
0·6	488			
0·7	466			
0·8	445			
0·9	423			
1·0	401			

Notation

B_0, B_1, B_2 = constants in the equation.
C_{pL} = heat capacity of the saturated liquid, cal/g mole °C.
C'_{pL} = heat capacity of the liquid, cal/g °C.
C'_{pv} = heat capacity of the vapour in the ideal gaseous state, cal/g mole °K.
ΔC_{pm} = excess heat capacity of the mixture per mole of hydrogen peroxide, cal/g mole °C.
H_L, H'_L = enthalpy of the liquid, C.H.U./ lb mole and C.H.U./lb respectively.
H_v, H'_v = enthalpy of the vapour, C.H.U./lb mole and C.H.U./lb respectively.
$\Delta H_s, \Delta H'_s$ = integral heat of solution, C.H.U./lb mole H_2O_2 and C.H.U./lb H_2O_2 respectively.
P_h, P_w = vapour pressure in mm Hg of hydrogen peroxide and water respectively.
P_T = total pressure in mm Hg.
R = gas constant 1·987 cal/g mole °K.
t = temperature °C.
T = temperature °K.
v = molal volume of the liquid, cm^3/g mole.
x, x' = mole fraction and weight fraction of hydrogen peroxide respectively.
μ^E = excess chemical potential, cal/g mole.
γ = activity coefficient.
β = second Virial coefficient cm^3/g mole.

Subscripts h, w refer to hydrogen peroxide and water respectively. A prime indicates either weight fraction or per pound of the substance.

Enthalpy-concentration diagram for the system hydrogen peroxide-water at 50 mm Hg total pressure

References

[1] Scatchard G., Kavanagh G. M. and Ticknor L. B. *J. Amer. Chem. Soc.*, (1952) **74** 3715.

[2] Schumb W. C., Satterfield C. N. and Wentworth R. L. *Hydrogen Peroxide*, American Chemical Society Monograph Series, Reinhold, New York, 1955.

[3] Kirk R. E. and Othmer D. F. *Encyclopedia of Chemical Technology* **7** p. 734. Interscience Encyclopedia Inc., New York, 1951.

[4] Ponchon M. *Tech. moderne* 1921 **13** 20, 25.

[5] Savarit R. *Chemie and Industrie*, Special number May 1923 737.

[6] Hirsch H. *Verdampfen, Kondensieren, und Kuhlen* 7th Ed. Springer, Berlin, 1931.

[7] McCabe W. L. *Trans. Amer. Inst. Chem. Engrs.* 1935 **31** 129

[8] Bosnjakovic F. *Technische Thermodynamik, I and II.* T. Steinkopf, Leipzig, 1935.

[9] Keyes, F. G. *J. Chem. Phys.* 1947 **22** 15 602.

[10] Giguiere P. A. and Morissette B. G. *Can. J. Chem.* 1955 **33** 804.

[11] Forcrand R. de *Compt. rend.* 1900 **130** 1620.

[12] Roth W. A., Gran R. and Meichsner A. *Z. Anorg. Chem.* 1930 **193** 161.

[13] Pike H. H. M. and Green H. Cited in reference 2.

[14] Kubaschewski O. and Weber W. *Z. Elektrochem.* 1950 **54** 200.

[15] Hougen O. A. and Watson K. M. *Chemical Process Principles, Part II.* Wiley, New York 1948.

[16] Keenan J. H. and Keyes F. G. *Thermodynamic Properties of Steam.* Wiley, New York, 1936.

Chemical Engineering Science, 1958, Vol. 9, pp. 170 to 175. Pergamon Press Ltd.

Flooding rates in packed liquid extraction towers

M. Raja Rao and C. Venkata Rao
Department of Chemical Technology, Andhra University, Waltair, Southern India

(*Received* 1 *November* 1957)

Abstract—As incidental to our main studies on mass transfer, flooding rate data have been obtained in a packed liquid–liquid extraction tower with no solute transfer, with $\frac{3}{8}$ in. Raschig rings, $\frac{1}{2}$ in. copper rings and 6 mm glass beads as the different packing materials, using water as the continuous phase and each of the following solvents, toluene, Pegasol, kerosene and methyl *iso*butyl ketone, which do not preferentially wet the packing, respectively as the dispersed phase. Visual observations, aided by photographic studies supplemented the measurements of the flooding velocities. The flow rates at the flooding point have been satisfactorily fitted on the square root plot as a preliminary correlation, and have been well correlated by the method of Dell and Pratt. It was observed that flooding rates decreased with decreasing size of the packing for any given system, and that higher flooding rates are favoured by high density difference and low interfacial tension of the liquid systems.

Résumé—A l'occasion de leurs principales études sur le transfert massique, les auteurs ont obtenu des résultats expérimentaux sur l'engorgement produit dans une colonne à garnissage pour l'extraction liquide-liquide, sans transfert de soluté. Les garnissages suivants ont été utilisés: anneaux Raschig de 0·95 cm, anneaux de cuivre de 0·64 cm et billes de verre de 6 mm. La phase continue était de l'eau, alors que la phase dispersée contenait un des solvants suivants: toluène, Pegasol, kerosène, méthyléthylcétone, qui ne mouillent pas préférentiellement le matériau de remplissage. Les mesures de vitesses d'engorgement ont été réalisées de manière visuelle ainsi que par des études photographiques.

Une corrélation préliminaire a permis aux auteurs de reproduire d'une manière satisfaisante les débits à l'engorgement par la méthode des racines carrées. L'utilisation de la méthode de Dell et Pratt a permis de corréler les résultats avec succès. Les auteurs ont observé que les vitesses d'engorgement diminuent avec les dimensions du garnissage pour tout système, et que les grandes vitesses d'engorgement sont favorisées par une grande différence de densité et une faible tension interfaciale des systèmes liquides.

Zusammenfassung—Im Zuge unserer Untersuchungen über den Stoffaustausch wurden Flutungsgeschwindigkeiten in einer Füllkörpersäule zur Flüssig-Flüssig-Extraktion ohne Übertragung von Gelöstem ermittelt. Als Packungsmaterial dienten Raschigringe von 9·5 mm, Kupferringe von 6·4 mm und Glasperlen von 6 mm. Die geschlossene Phase war Wasser und die disperse Phase waren folgende Lösungsmittel, Toluol, Pegasol, Kerosen und Methyl-*Iso*butyl-Keton, welche das Packungsmaterial vorzugsweise nicht benetzten. Visuelle Beobachtungen, unterstützt durch photographische Aufnahmen, ergänzten die Messungen der Flutungsgeschwindigkeiten. Der Mengenstrom am Flutungspunkt wurde befriedigend durch eine quadratische Beziehung in vorläufiger Form wiedergegeben und konnte gut nach der Methode von Dell und Pratt dargestellt werden. Es wurde festgestellt, dass die Flutungsgeschwindigkeiten abfielen mit fallender Packungsgrösse für ein gegebenes System und dass höhere Flutungsgeschwindigkeiten begünstigt werden durch hohe Dichtedifferenz und niedrige Grenzflächenspannung der flüssigen Systeme.

Introduction

Much of the early work on flooding rates in packed liquid–liquid columns was done incidentally to other investigations, and in this category came the reports of Rushton [1], Appel and Elgin [2], Sherwood *et al.* [3], and Row *et al.* [4]. Blanding and Elgin [5] described their investigations of the design and operation of spray and packed columns, pointing out the importance of the proper design of the entrance sections and distributor.

During recent years, flooding rates have been

studied in packed liquid extraction towers by several investigators [6-11], and of these special mention should be made of DELL and PRATT, [9] who have made a rather extensive study of flooding rates in columns of 3 in. and 6 in. inside dia., using a wide variety of liquid systems and packings. The above authors correlated their data by means of a theoretical equation :—

$$\left[1 + 0{\cdot}835\left(\frac{\rho_D}{\rho_C}\right)^{1/4}\left(\frac{U_D}{U_C}\right)^{1/2}\right] = C\left[\left(\frac{U_C^2 a}{g\,\epsilon^3}\right)\left(\frac{\rho_C}{\Delta_\rho}\right)\gamma^{1/4}\right]^n$$

The value of n was found to be $-1/4$. The constant C has slightly different values for each type of packing used, and the values recommended for design are 0·68, 0·80, and 0·88 for Raschig rings, Lessing rings and Berl saddles respectively. Each of the flooding correlations so far developed for packed liquid–liquid columns is applicable over a particular range of the different operating variables, and as pointed by TREYBAL [12], it is necessary to exercise due caution in utilizing any of the flooding correlations to cases where the packing sizes, system properties and also column sizes are outside the range for which they are applicable.

APPARATUS

The extraction equipment consisted essentially of an extraction tower and the necessary accessories to maintain a steady flow of the two liquid phases. The design of the packed column was based on the recommendations of BLANDING and ELGIN [5], and the apparatus used has been fully described elsewhere [13,14]. To facilitate visual observation of the column in operation, the column proper was constructed of Pyrex glass tubing, 1·88 in. inside dia., and two column lengths of 60 and 34 in. respectively were used in the experimental work. A dispersed phase distributor with 21 × $\frac{5}{32}$ in. nozzles was used in the flooding rate studies.

MATERIALS

Of the dispersed solvents, kerosene and methyl *iso*butyl ketone were supplied by the Burmah-Shell Oil Co., Pegasol by the Standard Vacuum Oil Co., and toluene by the Bengal Chemical and Pharmaceutical Works, Calcutta. The physical properties of these solvents are recorded in Table 1. Tap water of negligible acidity, drawn

Table 1. (*a*) *Properties of packing materials*

Packing	*Material*	*Average size of units*			*No. of units per* ft.^{3}	a $\frac{\text{ft.}^2}{\text{ft.}^3}$	ϵ	
		O.D. (in.)	*I.D.* (in.)	*Length* (in.)			*Measured*	*Calculated*
$\frac{3}{4}$ in. Raschig rings	Porcelain	0·375	0·273	0·384	28,680	178·1	0·610	0·667
$\frac{1}{2}$ in. Copper rings	Copper	0·250	0·175	0·250	81,060	215·4	0·635	0·692
6 mm Glass beads	Glass	6 mm dia. sphere			163,000	198·0	0·381	0·396

(*b*) *Properties of solvents at* 30°C

Solvent	*Density at* 30°C (g/cm^3)	*Viscosity in c.p.*	*Interfacial tension* (dyn/cm)
Kerosene	0·778	1·08	39
Pegasol	0·785	0·854	29
Toluene	0·859	0·556	26
Methyl *iso*butyl ketone	0·800	0·520	10

from the Andhra University mains supply was used in the experimental work.

Three types of packing materials were used : (1) $\frac{3}{8}$ in. non-porous and unglazed porcelain Raschig rings, manufactured and supplied by the Maurice A. Knight Co. of Akron, (2) $\frac{1}{4}$ in. copper rings, and (3) 6 mm glass beads. The column was filled with water, and the packing material dropped in from the top, a few pieces at a time, slowly and at random to the desired height. The packing was not shaken or tamped. The properties of the packing materials are listed in Table 1.

With each of the three different packing materials, the liquid systems studied were : 1. toluene–water, 2. Pegasol–water, 3. kerosene–water, and 4. methyl *iso*butyl ketone–water, using water as the continuous phase and the organic solvent as the dispersed phase.

Procedure

Each of the liquid phases was first saturated with the other, as this is particularly necessary when the solvent and water have appreciable mutual solubility, as in the case of water and methyl *iso*butyl ketone in the present investigation. The continuous water phase was first admitted into the column and then set at the desired flow rate. The dispersed solvent phase was then slowly introduced, and its flow rate was gradually increased in 5 to 10 steps until the flooding point, as indicated by the first appearance of a thin layer of the dispersed phase underneath the packing support, was reached. In a few runs, when the dispersed phase rate was high, the procedure was reversed by first establishing the rate of the dispersed phase and then gradually increasing the continuous phase rate up to the flooding point. The flooding results obtained by the two methods agreed quite well.

In all the runs extra care was taken to maintain the liquid-liquid interface in the upper end section at the same level, and during each run, the flow rates were not only checked, but also the exact rates of the solvent and water phases were obtained by timing the exit streams for a known interval of time and measuring their volumes.

Column Behaviour

A good number of photographs were taken of the column during operation with a view to interpreting the flooding data in terms of drop size, holdup and coalescence of the dispersed phase. In general, it was observed with each of the packings and liquid systems used that the streams of the dispersed phase droplets worked their way up the column, deforming and following a torturous path while passing up through the interstices of the packing. With increased flow rate of the dispersed phase its holdup was markedly increased, and the drops became very closely packed up in the column. As the flooding rate was closely approached the drops were observed to coalesce, forming slugs which gradually tended to travel down the column. The flooding rate was taken at the first appearance of a thin layer of the dispersed phase below the packing support. As compared with $\frac{3}{8}$ in. Raschig rings, the column was rather densely packed with $\frac{1}{4}$ in. rings, and more particularly with 6 mm beads. With the latter packing the drops showed a greater tendency to coalescence, and for any liquid system the flooding rates were lower than those for ring packings.

It was observed that smaller and finer drops were formed with solvents like methyl *iso*butyl ketone, and comparatively larger drops, showing increased tendency to coalesce, with kerosene and Pegasol. No attempt was made to determine either pressure drop or holdup at the flooding point.

Results and Correlation

Altogether over 50 runs have been taken on flooding rates with the different liquid systems and packings, and the data are presented in Table 2. Maximum flooding rates were obtained with $\frac{3}{8}$ in. Raschig rings with the methyl *iso*butyl ketone–water system, and the least with kerosene–water and Pegasol–water systems. The larger drops, and their increased tendency to coalesce observed with the last two systems, as compared with the relatively smaller drops of the ketone–water system, may perhaps be due to the fact that the interfacial tension (σ) of the ketone–water system is only 10 dyn/cm, which is much

Table 2. Experimental flooding data : 1·88 in. i.d. column, 21 × $\frac{5}{32}$ in. nozzle distributor. Continuous phase : water. Dispersed phase : solvent

Series No.	*Run No.*	*System*	*Packing Material*	U_C (ft/hr)	U_D (ft/hr)
I	1	M.I.B.K.–water	$\frac{3}{8}$ in. Raschig rings	66·0	49·0
	2	,,	,,	47·9	64·9
	3	,,	,,	25·9	103·4
	4	,,	,,	84·2	27·5
	5	,,	,,	11·6	143·0
	6	,,	,,	105·6	20·4
II	7	Kerosene–water	,,	64·9	38·5
	8	,,	,,	98·5	12·7
	9	,,	,,	42·9	64·4
	10	,,	,,	79·8	31·4
	11	,,	,,	18·2	115·5
	12	,,	,,	30·3	88·2
III	13	Toluene–water	,,	17·6	44·6
	14	,,	,,	23·7	27·0
	15	,,	,,	29·7	17·1
	16	,,	,,	35·2	13·8
	17	,,	,,	59·4	9·4
IV	18	Toluene–water	$\frac{1}{4}$ in. Copper rings	26·5	46·3
	19	,,	,,	32·5	43·0
	20	,,	,,	19·3	56·2
	21	,,	,,	11·0	76·0
	22	,,	,,	44·6	30·3
	23	,,	,,	49·6	26·5
	24	,,	,,	54·0	22·6
V	25	Kerosene–water	,,	23·7	21·5
	26	,,	,,	12·7	33·6
	27	,,	,,	20·3	30·9
	28	,,	,,	36·4	12·1
VI	29	Pegasol–water	,,	26·5	71·6
	30	,,	,,	49·6	46·3
	31	,,	,,	15·4	84·3
	32	,,	,,	64·5	34·2
VII	33	M.I.B.K.–water	,,	8·8	79·3
	34	,,	,,	17·4	56·2
	35	,,	,,	24·2	43·5
	36	,,	,,	40·8	28·1
VIII	37	,,	6 mm Glass beads	22·6	16·0
	38	,,	,,	14·9	19·0
	39	,,	,,	23·1	15·4
	40	,,	,,	11·0	21·5
IX	41	Kerosene–water	,,	16·5	35·3
	42	,,	,,	25·9	26·2
	43	,,	,,	12·7	38·6
X	44	Pegasol–water	,,	15·4	40·8
	45	,,	,,	26·5	29·2
	46	,,	,,	39·1	16·0
	47	,,	,,	29·8	23·1
	48	,,	,,	22·6	28·7
XI	49	Toluene–water	,,	25·9	12·7
	50	,,	,,	12·1	31·5
	51	,,	,,	16·5	25·5

smaller than those of kerosene–water ($\sigma = 39$ dyn/cm) and Pegasol–water ($\sigma = 29$ dyn/cm). In general, flooding rates decreased with decreasing size of the packing. These observations are in quite good agreement with those of the earlier investigators. The flooding rate data (Table 2) show clearly that higher flooding rates are favoured by high density difference and low interfacial tension of the system.

A general type of plot which has been utilized by previous investigators in preliminary correlation of flooding data is to plot the square root of flow rate of the dispersed phase against that of the continuous phase at flooding. On such a plot

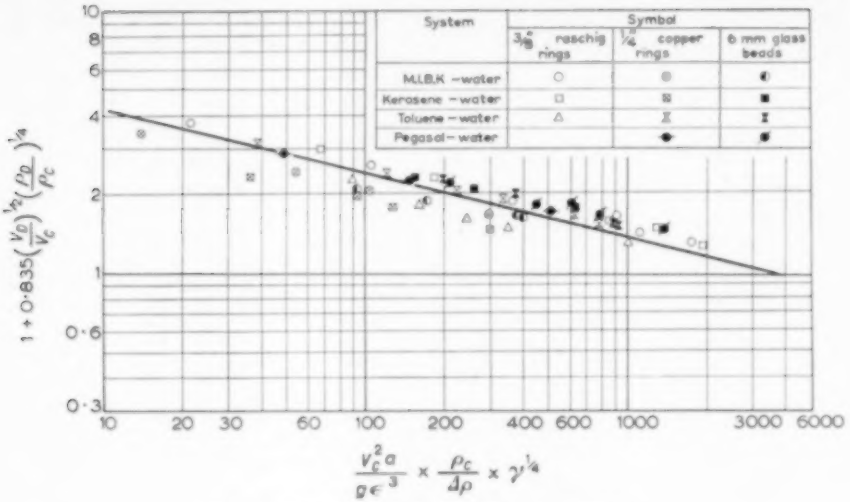

Fig. 1. Flooding correlation of Dell and Pratt.

a series of almost parallel straight lines was obtained, one for each set of conditions. The slope of all these lines was found to be close to — 1, the range being — 1·0 to — 1·1. An attempt has been made to fit the data by the well-established correlation of Dell and Pratt, and such a plot is represented in Fig. 1. The flooding data are quite satisfactorily fitted by the dimensionless equation and the computed values of the slope, n, and the constant C are found to be $-\frac{1}{4}$ and 0·66. These values are in quite good agreement with the values of $-\frac{1}{4}$ and 0·68 obtained by the above authors for Raschig rings. The excellent fit of the flooding data on Dell and Pratt's plot of correlation shows that, with the different packings used, the packing constant C in the equation is almost identical and constant at 0·66, probably because of the closer size range of the packings. In view of the excellent correlation of the flooding rate data by the method of Dell and Pratt no other correlation has been attempted.

Conclusions

Flooding rate data have been obtained in the packed extraction tower, as incidental to our main studies on mass transfer, with $\frac{3}{8}$ in. Raschig rings, $\frac{1}{4}$ in copper rings and 6 mm glass beads, using water as the continuous phase and each of the solvents toluene, Pegasol, kerosene and methyl *iso*butyl ketone which do not preferentially wet the packing, as the dispersed phase. Visual observations aided by photographic recordings of the column in operation supplemented the measurement of flooding rates. Maximum flooding rates were obtained with $\frac{3}{8}$ in. Raschig rings as packing material and methyl *iso*butyl ketone–water system, and the least rates with kerosene–water and Pegasol–water systems.

The flooding data have been fitted satisfactorily on the square root plot as a preliminary correlation, and have been well correlated by the method of Dell and Pratt with a value of $-\frac{1}{4}$ for n and 0·66 for C. It was observed that flooding velocities decreased with decreasing size of the packing for any given system, and that low interfacial tension of the system and high density difference tended to give higher flooding rates by favouring the formation of smaller drops.

Notation

a = interfacial contact area per unit tower volume ft²/ft³.
n, C = constants in Dell and Pratt's equation.
g = acceleration due to gravity.
V_C or U_C = flow rate of continuous water phase in ft³/(ft²) (hr).
V_D or U_D = flow rate of dispersed solvent phase in ft³/(ft²) (hr.)

ϵ or F = void fraction of the packing material, ft^3/ft^3.
ρ_C = density of the continuous phase in lb/ft^3.
^d_D = density of the dispersed phase in lb/ft^3.
Δ_ρ = density difference of the phases in $lb/ft.^3$
μ_C = viscosity of the continuous phase in lb/(ft) (hr).
σ or γ = interfacial tension in dyn/cm.

References

[1] Rushton J. H. *Ind. Engng. Chem.* 1937 **29** 309.
[2] Appel F. J. and Elgin J. C. *Ind. Engng. Chem.* 1937 **29** 451.
[3] Sherwood T. K., Evans J. E. and Longcor J. V. A. *Trans. Amer. Inst. Chem. Engrs.* 1939 **35** 597.
[4] Row S. B., Koffolt J. H. and Withrow J. R. *Trans. Amer. Inst. Chem. Engrs.* 1941 **37** 559.
[5] Blanding F. H. and Elgin J. C. *Trans. Amer. Inst. Chem. Engrs.* 1942 **38** 305.
[6] Breckenfeld R. R. and Wilke C. R. *Chem. Engng. Progr.* 1950 **46** 187.
[7] Ballard J. H. and Piret E. L. *Ind. Engng. Chem.* 1950 **42** 1088.
[8] Crawford J. W. and Wilke C. R. *Chem. Engng. Progr.* 1951 **47** 423.
[9] Dell F. R. and Pratt H. R. C. *Trans. Inst. Chem. Engrs. (Lond.)* 1951 **29** 89.
[10] Sakiadis B. C. and Johnson A. L. *Ind. Engng. Chem.* 1954 **46** 1229.
[11] Hoffing E. H. and Lockhart F. J. *Chem. Engng. Progr.* 1954 **50** 94.
[12] Treybal R. E. *Ind. Engng. Chem.* 1955 **47** 539.
[13] Rao M. Raja, D.Sc. Thesis, Andhra University (India), 1956.
[14] Rao M. Raja and Rao C. Venkata, Communicated to *Chem. Engng. Sci.* October 1957.

Chemical Engineering Science, 1958, Vol. 9, pp. 176 to 181. Pergamon Press Ltd.

The graphical determination of changes in the gas phase due to simultaneous heat and mass transfer

G. H. P. Bras
Air Products Incorporated, Allentown, Pa., U.S.A.

(*Received* 1 *August* 1957; *in revised form* 28 *March* 1958)

Abstract—A new graphical method is presented for the design of simultaneous heat and mass transfer equipment, handling non-saturated gas-vapour mixtures.

The condition of the non-saturated gas-vapour mixture is followed from point to point in a semi-logarithmic plot of the partial pressure of the non-diffusing gas component against the temperature. For this purpose, the following equation has been derived,

$$-\left(\frac{d\log p_g}{dt}\right)_g = \frac{\Delta \log p_g}{\Delta t} \cdot \left(\frac{Pr}{Sc}\right)^{2/3} \cdot \left(\frac{e^e - 1}{e\, e^e}\right) \cdot \left(\frac{j_m}{j_h}\right)$$

The application of this equation is shown for a simplified cooler-condenser example, in which the right hand side bracket groups of the equation were taken equal to unity.

Résumé—L'auteur présente une nouvelle méthode graphique pour le calcul d'un appareillage de transfert simultané de masse et de chaleur, opérant sur des mélanges non saturés gaz-vapeur.

L'état du mélange non saturé gaz-vapeur est suivi point par point sur un graphique semi-logarithmique de la pression partielle du composant gazeux non-diffusant, par rapport à la temperaturé. Dans ce but l'auteur a posé l'équation suivante :

$$-\left(\frac{d\log p_g}{dt}\right)_g = \frac{\Delta \log p_g}{\Delta t} \cdot -\left(\frac{Pr}{Sc}\right)^{2/3} \cdot \left(\frac{e^e - 1}{e\, e^e}\right) \cdot \left(\frac{j_m}{j_h}\right)$$

Il montre l'application de cette équation pour un exemple de condenseur simplifié, pour lequel les groupes entre parenthèses de la 2ème partie de l'équation sont pris égaux à 1.

Zusammenfassung—Für die Berechnung von Apparaten mit gleichzeitiger Wärme- und Stoffübertragung wird eine neue graphische Methode mitgeteilt, die nicht-gesättigte Gas-Dampf-Gemische behandelt.

Die Bedingung des nicht-gesättigten Gas-Damp-Gemisches wird punktweise in einem halblogarithmischen Diagramm verfolgt, in dem der Teildruck der nicht diffundierenden Gaskomponente über der Temperatur aufgetragen ist. Für diesen Zweck ist folgende Gleichung abgeleitet worden:

$$-\left(\frac{d\log p_g}{dt}\right)_g = \frac{\Delta \log p_g}{\Delta t} \cdot -\left(\frac{Pr}{Sc}\right)^{2/3} \cdot \left(\frac{e^e - 1}{e\, e^e}\right) \cdot \left(\frac{j_m}{j_h}\right)$$

Die Anwendung dieser Gleichung wird für ein vereinfachtes Beispiel eines Kühler-Kondensators gezeigt, in welchem die in Klammern stehenden Ausdrücke auf der rechten Seite der Gleichung gleich eins gesetzt werden.

Introduction

Recently, the author [1] proposed to use a diagram of the logarithm of the non–diffusing gas against the temperature for the determination of the gas–liquid interface conditions in the design of cooler condensers. The graphical design method was later improved [2], and it was also shown that the method is suitable for the calculation of equipment in which gas and liquid are in direc contact, e.g. gas saturators, gas coolers, water heaters, dryers, etc.

The use of a diagram of the above type enables the elimination of all trial and error calculations in the determination of the gas liquid interface conditions.

When a non-saturated gas–vapour mixture is

subjected to simultaneous heat- and mass-transfer, it will usually be necessary to follow the condition of the mixture from step to step. This may be done by using the equation proposed by COLBURN [3],

$$\left(\frac{dp}{dt}\right)_g = \frac{\Delta p}{\Delta t} \cdot \frac{(P - p_v)}{p_{gf}} \cdot \left(\frac{Pr}{Sc}\right)^{2/3} \cdot \left(\frac{\epsilon' - 1}{\epsilon \epsilon'}\right) \quad (1)$$

Equation (1) can be derived from the equations for the condensation of binary vapour mixtures, given by COLBURN and DREW [4]. Another derivation of an equation of this type was given by the author [5]. In the same article, equation (1) was used as the basis for a graphical design procedure for cooler condensers. The application of equation (1) for the design of a direct contact cooler for hot gases was published later [6].

These design calculations were carried out by a graphical point to point procedure in a diagram of partial vapour pressure against temperature.

Thus, in the general case of a non-saturated gas-vapour mixture, subjected to simultaneous heat and mass transfer, the design computations would involve the following two steps:

(*a*) The graphical determination of the interface conditions in a diagram of log p_g against t.

(*b*) The graphical step by step determination of the condition of the gas vapour mixture in a diagram of p against t.

Consequently, two different diagrams would be required,

In order to avoid this complicated procedure, the following method was developed, which allows to carry out both operations in the same diagram, namely log p_g vs. t.

DIFFERENTIAL EQUATION

The rate of heat and mass transfer can be written, respectively,

$$h_g \, \Delta t \, dA = - G_0 \, s \, dt_g \quad (2)$$

and,

$$k_g' \left\{ \ln (P - p_i) - \ln (P - p_v) \right\} dA = - G_0 \, d H_v \quad (3)$$

From equations (2) and (3) follows,

$$\frac{\Delta \ln p_g}{\Delta t} \cdot \frac{k_g' \, s}{h_g} = \frac{d H_v}{dt_g} \quad (4)$$

The ratio of the gas side mass, and heat transfer coefficients, k_g'/h_g may be derived from any of the correlations available in the literature. Here, the correlation proposed by CHILTON and COLBURN [7] will be used, or,

$$\frac{k_g'}{h_g} = \frac{M_v}{c \, M_m} \cdot \left(\frac{Pr}{Sc}\right)^{2/3} \cdot \frac{j_m}{j_h} \quad (5)$$

In case of packed towers, somewhat different correlations of heat and mass transfer are usually preferred.

The humid heat capacity, s, is equal to,

$$s = c \, (1 + H) \quad (6)$$

The average molecular weight, M_m can be expressed by,

$$M_m = \frac{(P - p_v) \, M_g + p_v \, M_v}{P} \quad (7)$$

The humidity, H, is given by the equation,

$$H = \frac{p_v \, M_v}{(P - p_v) \, M_g} \quad (8)$$

Thus,

$$1 + H = \frac{(P - p_v) \, M_g + p_v \, M_v}{(P - p_v) \, M_g} \quad (9)$$

From equations (7) and (9) follows,

$$M_m = \frac{(1 + H) \, (P - p_v) \, M_g}{P} \quad (10)$$

When equations (5) and (6) are substituted in equation (4), equation (11) is obtained,

$$\frac{\Delta \ln p_g}{\Delta t} \cdot \frac{(1 + H) \, M_v}{M_m} \cdot \left(\frac{Pr}{Sc}\right)^{2/3} \cdot \frac{j_m}{j_h} = \frac{dH_v}{dt_g} \quad (11)$$

Substitution of equation (10) in equation (11) delivers

$$\frac{\Delta \ln p_g}{\Delta t} \cdot \frac{M_v}{M_g} \cdot \frac{P}{(P - p_v)} \cdot \left(\frac{Pr}{Sc}\right)^{2/3} \cdot \frac{j_m}{j_h} = \frac{dH_v}{dt_g} \quad (12)$$

Differentiation of equation (8) gives the relation,

$$dH = \frac{P M_v}{(P - p_v)^2 \, M_g} \cdot dp \quad (13)$$

Substitution of equation (13) in equation (12), gives after rearranging,

$$\frac{dp_v}{(P - p_v)\,dt_g} = \frac{\Delta \ln p_g}{\Delta t} \cdot \left(\frac{Pr}{Sc}\right)^{2/3} \cdot \frac{j_m}{j_h} \qquad (14)$$

Equation (14) can now be written,

$$-\frac{d \ln p_{gv}}{dt_g} = \frac{\Delta \ln p_g}{\Delta t} \cdot \left(\frac{Pr}{Sc}\right)^{2/3} \cdot \frac{j_m}{j_h} \qquad (15)$$

If the correction for the sensible heat transferred by the diffusing vapours is taken into account, the rate of sensible heat transfer at the gas side of the gas film can be expressed by an equation, recently derived by the author [6], or,

$$-G_0\, s dt_g = h_g\, \Delta t \cdot \frac{\epsilon\, e^\epsilon}{(e^\epsilon - 1)} \cdot dA \qquad (16)$$

Introduction of the correction factor in the above derivation will give the relation,

$$-\frac{d \ln p_{gv}}{dt_g} = \frac{\Delta \ln p_g}{\Delta t} \cdot \left(\frac{Pr}{Sc}\right)^{2/3} \cdot \frac{j_m}{j_h} \cdot \left(\frac{e^\epsilon - 1}{\epsilon\, e^\epsilon}\right) \qquad (17)$$

In this equation, $\epsilon = -k_g\, \Delta p\, c_{pv}/h_g$ is equal to the ratio of the heat transfer coefficient for the sensible heat transferred by the diffusing vapours and the sensible heat transfer coefficient, h_g. Before the numerical value of ϵ can be calculated, the interface conditions must first be determined. The determination of the interface conditions, when making allowance for the sensible heat transferred by the diffusing vapours, was discussed in some more detail in a previous publication, to which reference may be made [2]. Once the interface conditions have been established, the correction factor, $(e^\epsilon - 1)/(\epsilon\, e^\epsilon)$, can be calculated, and equation (17) can be used in a straightforward manner and no further trial and error work is involved. It should be borne in mind, that the correction factor for the sensible heat of the diffusing vapours, $(e^\epsilon - 1)/(\epsilon\, e^\epsilon)$, has been theoretically derived, but needs more experimental verification.

Graphical Procedure

For the point to point calculation of the relation between the gas temperature, t_g, and the water temperature, t_w, reference will be made to Fig. 1.

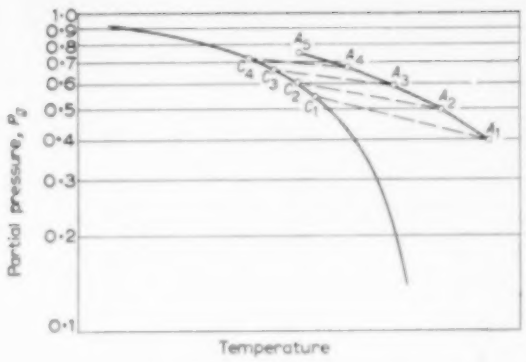

Fig. 1. Graphical Determination of Change in Gas Phase.

The curved line represents the partial pressure of the saturated non-diffusing gas against the temperature in a semi-logarithmic diagram. Point A_1 represents the known condition of the inlet gas–vapour mixture, $p_g = p_{gv1}$, and $t = t_{g1}$. Point C_1 represents the interface conditions, $p_g = p_{gi1}$, and $t = t_{i1}$. A method for the graphical determination of the interface conditions has been described elsewhere [1, 2].

The slope of the straight line $A_1\,C_1$ will now be equal to $-\Delta \log p_g/\Delta t$. Application of equation (15) will further enable the calculation of $d \log p_{gv}/dt_g$. Another straight line with a slope equal to $d \log p_{gv}/dt_g$ is drawn through point A_1, see Fig. 1. The direction of this line will indicate the initial trend in the change of the non-saturated gas vapour mixture, in respect to the logarithm of the partial pressure of the non-diffusing gas and the temperature. Although this trend is strictly valid for point A_1 only, the line may be followed over a relatively short distance, e.g., to point A_2. The co-ordinates of point A_2, $p_g = p_{gv2}$, and $t_g = t_{g2}$, can now be read from the diagram. Then, the temperature and the partial vapour pressure at point A_2 are known, and the enthalpy of the gas mixture can be calculated. The difference in enthalpy between the points A_1 and A_2 is equal to the total heat transferred.

In case of direct contact operations, all this heat is exchanged with the liquid. In case of cooler condensers, some of the heat will be in the condensate. This amount can usually be neglected, especially if the latent heat of the vapour is

relatively large. Thus, the change in the liquid temperature t_l, can be calculated from the enthalpy change, by application of an equation of the type, $L\, c_l\, dt_l = G_0\, di_g$, after integration.

After calculation of the liquid temperature, t_{l2}, in this way, the interface conditions for point A_2 are again obtained graphically. The procedure is repeated step by step until the outlet of the apparatus is reached. The typical curved line for the condition of a non-saturated gas-vapour mixture in a cooler condenser is shown in Fig. 1, by the curve $A_1 - A_5$.

Sometimes, the gas may still be non-saturated when leaving the apparatus. Then, the exact partial vapour pressure and temperature of the exit gas will not be known until the above step by step procedure has been completed.

The enthalpy of the exit gas vapour mixture will be equal to the enthalpy originally assumed for the calculation of the ratio L/G_0. However, the temperature and partial vapour pressure of the gas vapour mixture may be different from the conditions originally assumed. Obviously, a trial and error procedure for the entire design calculations would be required to let the gas leave at the temperature originally fixed. In most cases it may prove more practical to design the equipment for a certain gas exit enthalpy, rather than for exact gas exit temperature and partial vapour pressure, in order to avoid this complication.

In direct contact equipment, the liquid flow rate, L, may vary between inlet and outlet due to condensation or evaporation. Usually, it will be accurate enough for engineering design purposes, to use an average value of the liquid flow rate, L. When the variations in the liquid flow rate are relatively large, the value of L can be calculated from point to point from the variation in the gas humidity.

Example

The application of the new design method for non-saturated gas-vapour mixtures will be illustrated by the following example: An air–water vapour mixture enters a tubular cooler condenser at 382°F, and 1 atm total pressure. The partial water vapour pressure is equal to 0·8 atm. The air–water vapour mixture leaves the cooler condenser saturated at 86°F. Cooling water enters at 80°F and leaves at 120°F, and flows in countercurrent with the air–water vapour mixture. For the present purpose, the following assumptions are made:

$h_0 = 200$ B.t.u/hr ft² °F
h_g (at gas inlet) $= 25$ B.t.u/hr ft² °F
$\lambda = 978$ B.t.u/lb
$Pr/Sc = 1{\cdot}0$
Specific heat: air, average $= 0{\cdot}245$ B.t.u/lb. °F
air, 382 °F $= 0{\cdot}25$ B.t.u/lb °F
water vapour, average $= 0{\cdot}47$ B.t.u/lb °F
water vapour, 382 °F $= 0{\cdot}48$ B.t.u/lb °F

First, the ratio L/G_0 is calculated as follows: Humidity of entering air–water vapour mixture,

$$H_v = (0{\cdot}8 \times 18) / (0{\cdot}2 \times 29) = 2{\cdot}483 \text{ lb/lb.}$$

Enthalpy of entering air–water vapour mixture,

$$i = 0{\cdot}245 \times 350 + 2{\cdot}483\,(1071{\cdot}0 + 0{\cdot}47 \times 350) = 3153{\cdot}5 \text{ B.t.u/lb of dry air.}$$

Enthalpy of leaving air–water vapour mixture, saturated at 86°F,

$$i = 42{\cdot}7 \text{ B.t.u/lb of dry air.}$$

Total heat transferred, $3153{\cdot}5 - 42{\cdot}7 = 3110{\cdot}8$ B.t.u/lb of dry air.

Ratio $L/G_0 = 3110{\cdot}8/40 = 77{\cdot}77$.

Next, the interface conditions are determined by the graphical method given recently by the author [2]. Reference is made to this publication for all details.

$R = h_0/h_g = 200/25 = 8{\cdot}0$
$C_m = (0{\cdot}8 \times 0{\cdot}48 \times 18) + (0{\cdot}2 \times 0{\cdot}25 \times 29) = 8{\cdot}36$ B.t.u/lb mole. °F
$F = (L_i/C_m) \cdot (Pr/Sc)^{2/3} = 18 \times 978/8{\cdot}36 = 2106$ °F
$t_B = (8{\cdot}0 \times 120 + 382)/9{\cdot}0 = 149{\cdot}1$ °F $= (R\,t_w + t_g)/(R+1)$

In Fig. 2, the curved line represents the saturation line in a semi-logarithmic plot of p_g against t. Point B_1 has the co-ordinates $t_B = 149{\cdot}1$ °F and $p_g = 0{\cdot}2$ atm. A straight line with a slope equal to $(R+1)/2{\cdot}303\,F = 9{\cdot}0/(2{\cdot}303 \times 2106) = 0{\cdot}001856$, is drawn through point B_1. This line intersects the

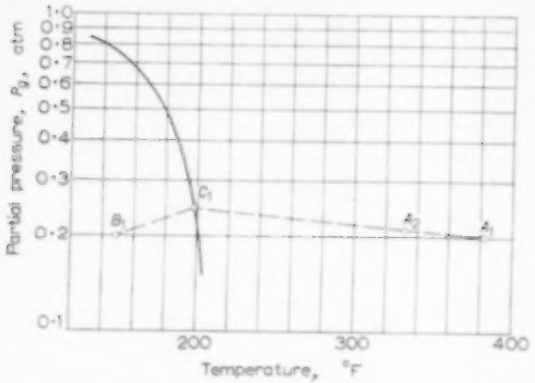

Fig. 2. Graphical Procedure Applied to Example.

saturation curve in point C_1, representing the interface conditions at the gas inlet. The co-ordinates of point C_1 are read from the diagram, or, $p_{gi} = 0{\cdot}2455$ atm, and $t_i = 198{\cdot}2$ °F. Thus the heat flux at this point is equal to $h_0 (t_i - t_w) = 200 \times 78{\cdot}2 = 15{,}640$ B.t.u/hr ft².

Point A_1 represents the condition of the non-saturated air at the inlet of the cooler condenser. The known co-ordinates of point A_1 are, $p_g = 0{\cdot}2$ atm, and $t_g = 382$°F. When a straight line is drawn through the points A_1 and C_1 the slope of this line will be equal to $-\Delta \log p_g/\Delta t = -0{\cdot}000484$. From equation (17) follows, for $(Pr/Sc)^{2/3} = 1{\cdot}0$, $(e^e - 1)/(\epsilon\, e^e) = 1{\cdot}0$, and $j_m/j_h = 1{\cdot}0$, $d \log p_{gc}/dt_g = -0{\cdot}000484$. Thus, the line $A_1 C_1$ may be followed over a relatively short distance, until point A_2.

In this particular case, the two lines representing $\Delta \log p_g/\Delta t$, and $d \log p_{gc}/dt$, respectively, have the same slope in Fig. 2. In general, the slopes of the two lines through point A_1 will be different, see Fig. 1. When the slope of the two lines is different, it will be obvious that point A_2 is located on the line for $d \log p_{gc}/dt$.

The co-ordinates of point A_2 are read from the diagram, or $p_g = 0{\cdot}2124$ atm, and $t_g = 332$°F. Therefore at point A_2, $p_v = 0{\cdot}7876$ atm, $H = (0{\cdot}7876 \times 18)/(0{\cdot}2124 \times 29) = 2{\cdot}30$ lb/lb, and the enthalpy is $i = 0{\cdot}245 \times 300 + 2{\cdot}30\,(1071 + 0{\cdot}47 \times 300) = 2861{\cdot}6$ B.t.u/lb of dry air. Heat transferred in the first increment is then $Q_1 = 3153{\cdot}5 - 2861{\cdot}6 = 291{\cdot}9$ B.t.u/lb of dry air.

Neglecting the heat of the condensate, the temperature of the cooling water at point A_2 is calculated from $L\,(120 - t_w) = G_0 \times 291{\cdot}9$. For $L/G_0 = 77{\cdot}77$, follows $t_w = 116{\cdot}3$ °F.

For the design of the cooler condenser, the above calculation is repeated for various points. When necessary, new values for the heat and mass transfer coefficients may be calculated at intermediate points. After calculation of the heat flux at various intermediate points, the condenser tube area is obtained by graphical integration of the equation,

$$A = \int d\,A = \int \frac{d\,Q}{h_0\,(t_i - t_l)}$$

The graphical integration is carried out by plotting the reciprocal heat flux, $1/h_0\,(t_i - t_l)$, against the total heat transferred, Q. The area under the integration curve so obtained, is equal to the area A.

The design calculations for direct contact equipment are carried out along the same general lines.

Notation

A = surface area, ft²
c, c_{pv} = specific heat at constant pressure of gas–vapour mixture and vapour, respectively, B.t.u/lb °F
c_l = specific heat of liquid, B.t.u/lb °F
C_m = specific heat at constant pressure of gas–vapour mixture, B.t.u/lb mole °F
D = diffusion coefficient, ft²/hr
G = mass velocity of gas–vapour mixture, lb/hr ft²
G_0 = flow rate of vapour free gas, lb/hr
H = humidity, lb/lb of vapour-free gas
h_0 = combined heat transfer coefficient for cooling water, tube wall, scale, and condensate, B.t.u/hr ft² °F. In case of direct contact, between gas and liquid, h_0 reduces to h_l, the liquid side heat transfer coefficient, B.t.u/hr ft² °F
h_g = gas side heat transfer coefficient, B.t.u/hr ft² °F
j_h, j_m = heat and mass transfer factor, respectively, dimensionless
k = thermal conductivity of gas–vapour mixture, B.t.u/hr ft °F
k_g = gas side mass transfer coefficient, lb/hr ft² atm
$k_g' = k_g\, p_{gf}$, lb/hr ft²
L = liquid flow rate, lb/hr
L_v, L_i = latent heat of evaporation, respectively at main body of gas–vapour mixture, and at gas–liquid interface, B.t.u/lb mole

M_v, M_m = molecular weight of vapour and of gas–vapour mixture, respectively, lb/lb mole
P = total pressure, atm
Pr = Prandtl number, $c\,\mu/k$, dimensionless
p_v, p_i = partial vapour pressure in the gas–vapour mixture, and at the gas–liquid interface, respectively, atm
$\Delta p = p_v - p_i$, atm
$\Delta \ln p_g = \ln p_{gi} - \ln p_{gv}$
p_{gi}, p_{gv} = partial pressure of non-diffusing gas component, respectively, at interface and in main body of the gas–vapour mixture, atm
p_{gs} = partial pressure of the saturated non-diffusing gas component, atm
p_{gf} = logarithmic mean partial pressure of non-diffusing gas, atm
Q = total heat transferred, B.t.u/hr
$R = h_\theta/h_g$, dimensionless
Sc = Schmidt number, $\mu/\rho D$, dimensionless
t = temperature, °F
t_R = reference temperature, °F
t_g, t_i, t_l = temperature of gas mixture, of gas–liquid interface, and of liquid, respectively, °F
$\Delta t = t_g - t_i$, °F
$\epsilon = -k_g\,\Delta p\,c_{pv}/h_g$, dimensionless
λ = latent heat of evaporation, B.t.u/lb
ρ = density of gas–vapour mixture, lb/ft^3
μ = viscosity of gas–vapour mixture, lb/hr ft

References

[1] Bras G. H. P. *Chem. Engng. Sci.* 1957 **6** 277.

[2] Bras G. H. P. *Chem. Proc. Engng.* 1957 **38** 427.

[3] Colburn A. P. *Proc. Inst. Mech. Engrs.* 1951 **164** 448.

[4] Colburn A. P. and Drew T. B. *Trans. Amer. Inst. Chem. Engrs.* 1937 **33** 197.

[5] Bras G. H. P. *Chem. Engng.* 1953 **60** No. 4 223 ; No. 5 238.

[6] Bras G. H. P. *Chem. Engng* 1954 **61** No. 12 191 ; 1955 **62**, No. 1 195.

[7] Chilton T. H. and Colburn A. P. *Ind. Engng. Chem.* 1934 **26** 1183.

Zur Berechnung des Volumens adsorbierter Schichten

Das Volumen einer adsorbierten Schicht wird meist nach der Formel $V_a = F\,\Delta$ berechnet, wobei F die Oberfläche des adsorbierenden Körpers und Δ die Dicke der adsorbierten Schicht darstellt. Diese Formel gilt jedoch nur, solange die Dicke Δ klein gegenüber dem Krümmungsradius der betreffenden Oberfläche ist. In Abb. 1 stelle beispielsweise der schraffierte Teil den Querschnitt eines

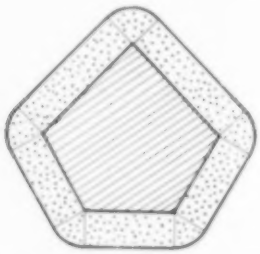

Abb.1. Adsorbierte Schicht an einem Körper mit polygonförmigem Querschnitt.

stäbchenförmigen Körpers dar, um den sich eine adsorbierte Schicht gelagert hat. Wie man sich leicht überlegt, ist der durch Punkte dargestellte Querschnitt dieser Schicht nicht gleich $U\,\Delta$ (U = Länge der Umfangslinie) sondern gleich $U\,\Delta + \Delta^2\,\pi$. Zu den fünf den Seiten entsprechenden Rechtecken treten nämlich noch die fünf Kreissektoren hinzu, die zusammen eine volle Kreisfläche ergeben. Ist L die Länge des Stäbchens, und wird das Volumen der an den Enden absorbierten Schicht vernachlässigt, so beträgt das am zylindrischen Teil absorbierte Volumen:

$$V_a = L\,(U\,\Delta + \Delta^2\,\pi) = F\,\Delta + L\,\Delta^2\,\pi > F\,\Delta.$$

Wie steht es nun aber, wenn wir die Wirkung der Enden nicht mehr vernachlässigen dürfen, d.h. wenn wir zum allgemeinen dreidimensionalen Problem übergehen? Glücklicherweise haben auch diesen Fall die Mathematiker bereits vorausgedacht. Von Steiner wurde nämlich ein Satz über den "äusseren Parallelkörper" von "Eikörpern" abgeleitet [1] und vergl. dazu z.B. [2], nach dem sich das Volumen der adsorbierten Schicht darstellen lässt durch:

$$V_a = F\,\Delta + M\,\Delta^2 + (4/3)\,\pi\,\Delta^3$$

Als Eikörper wird dabei ein Körper bezeichnet, der durch Ebenen oder konvexe Flächen begrenzt ist, also nirgends eingebuchtet ist und nirgends einspringende Ecken aufweist. Der Ausdruck M wird als das "Integral der mittleren Krümmung" bezeichnet. Für M ergeben sich für die Kugel (Radius R), den Zylinder (Höhe h) und für das Oktaeder (R = Radius der umschriebenen Kugel) beispielsweise die Werte $4\,\pi\,R = 12{,}56\,R$ bzw. $\pi^2\,R + \pi\,h$, bzw. $10{,}45\,.\,R$. Werte für zahlreiche andere Körper finden sich in den Tabellen auf S. 36/37 im Buch von Hadwiger. Natürlich lässt sich die Formel nur dann anwenden, wenn der Abstand der einzelnen Körper so gross ist, dass sich die an ihnen absorbierten Schichten nicht überdecken.

Eidg. Technische Hochschule Zürich P. Grassmann

Literatur

[1] Steiner, J., Ueber parallele Flächen. *Mber. preuss. Akad. Wiss.* S. 114-118 1840; oder *gesammelte Werke* Bd. 2 S. 77/91. Reiner, Berlin 1882.

[2] Hadwiger H., *Altes und Neues über konvexe Korper*, S. 31. Birkhäuser Verl. 1955.

Book Reviews

E. A. Guggenheim : **Thermodynamics.** (3rd Ed.) North Holland Publishing Co., 1957. xxii + 476 pp.

Unlike the second edition, which was substantially the same text as the first, the third edition of Guggenheim's valuable book has recently been published with two extensive modifications.

The more important of the two is a rearrangement of the material on solutions and mixtures. In the original text, systems of two components were discussed in a separate chapter from the chapter in which systems containing more than two were considered, and this resulted in a good deal of repetition. This has been avoided in the present edition which contains a new chapter on " mixtures " where all components are treated on the same basis.

As a result of this change the number of chapters in the book would have been less by one, but for the second major alteration, which is an entirely new chapter on " Onsager's Reciprocal Relations." Here the author gives an outline of what has become known as the thermodynamics of irreversible processes, or the thermodynamics of the steady state. This chapter occupies only 10 pages, with a result that the applications described are rather limited and do not include non-isothermal systems.

Two other new features of the book are an "Introduction on Notation" and the use of Stille's values (1955) of the physical constants in place of those of Birge (1941). The most interesting change here is the value of the ice point which is quoted : 273·15°K in place of 273·16°K.

K. G. Denbigh

H. Hausen : **Handbuch der Kältetechnik.** Vol. 8, The Liquefaction and Separation of Gas Mixtures (In German).

The industrial application of low temperatures has developed during the past 50 years ; and particularly during the past 20 years the development has been very rapid. Throughout most of this period Hausen has been in intimate contact with the subject, to which he has made many notable contributions. Thus the new textbook devoted to the low temperature industry, and forming part of the massive series on refrigeration edited by Rudolf Plank, speaks with authority and from rich experience.

The book is divided into two parts, the first and larger part dealing with the theory of gas liquefaction and separation, the second part chiefly with technical aspects of low temperature processes.

The first 50 pages are devoted to a review of the laws of thermodynamics and the properties of real gases. Equal space is then given to the theory of gas liquefaction ; all the common liquefaction cycles are discussed, including the new Philips gas expansion machine. The thermodynamics of gas separation and then treated, firstly by outlining the laws governing the behaviour of mixtures, and secondly by describing the properties of a rectification column and its associated design methods.

Air separation is dealt with at length, all the common industrial cycles being reviewed. Tonnage oxygen plant features largely but not to the exclusion of plant for the production of high purity gases and the recovery of the rare gases. The separation of all other industrial gas mixtures is dismissed in 15 pages. The first section of the book concludes with the theory of heat exchangers and regenerators, subjects in which the author has done much pioneering work.

The second part of the book includes very useful sections dealing with the practical design or selection of equipment for all the major components of a low temperature plant. Much useful detail is given in a field which has not previously been treated to any extent in a textbook. Some cost data are also provided. A short section is devoted to the physical properties of fluids at low temperatures, and the book concludes with a review of the applications of the products of low temperature plant.

Two criticisms may be made of the work. On the one hand, in attempting to be completely comprehensive the author has included material, particularly at the beginning and end of the book, which could without great loss have been omitted, whilst treating some of the centre sections too briefly. On the other hand the author is biased strongly in the selection of material by his close association with the Linde Company, and this has resulted in a disproportionate concentration on air separation as compared to other technical gas mixtures. However, in view of the amount of useful and well ordered information contained within this volume it is likely to become a standard work of reference in low temperature technology.

G. G. Haselden

Chemical Engineering Practice. Vol. 3: Solid Systems. Edited by H. W. Cremer and Trefor Davies. Butterworths Scientific Publications, London, 1957. vi + 534 pp., 95s.

This journal is concerned exclusively with the application of the sciences to chemical engineering problems. No doubt most of its readers, when not actually absorbed in its pages, have some contact with the rough-and-tumble side of the profession, in which it is more important to make something work than to know why it does so. Nevertheless, we may suspect that they tend to be drawn from the " Egghead " wing of the profession, and as such they are likely, paradoxically, to find the volume

under review more stimulating than its two predecessors. Volume 3 really gets down to brass tacks ; here we are in the world of practical engineers at last. The volume is full of machines – for crushing, grinding, classifying, mixing and so on – which are the product of experience, intuition and remarkable ingenuity. Science seems to have had very little to do with the development of most of them ; in fact, far from having led the field, it has not even caught up in most cases, judging from the very meagre shreds of "theory" attached to many of the topics. It is true that the theoretical development has gone further than might be supposed from reading some of the sections – that on cyclones, for instance. In general, however, the techniques described pose a large number of unsolved and interesting problems, which should serve to stimulate the theoretician. In many cases the general principles involved are clear, but there is no quantitative theory which can be used for that accurate prediction of performance which forms the basis of good design. For instance, although a number of tentative approaches have been made to the theory of mixtures and mixing, they have probably had no influence at all on the methods of specifying the design and size of a mixer for a given job – methods which are about as scientific as winetasting. Dr. H. Heywood, in his interesting article on the Principles of Crushing and Grinding, gives an idea of the way in which a scientific attack can be opened on an intractable problem.

In general, however, the theoretical treatment is perfunctory, and the book consists mainly of descriptions of machines, their applications and mode of action, and is copiously illustrated, with diagrammatic drawings which are (for the most part) simple enough to expose the mode of action clearly. The topics covered are crushing, grinding and pulverising ; size analysis, screening, grading, classifying and sedimentation ; the mixing storage and handling of solids ; and the cleaning of gases. I believe the volume will be a useful preliminary reference book for those in industry who are unfamiliar with these fields, and who want to know the general types of equipment which are available. However this may be, it cannot be too highly recommended as wholesome reading for the more academic chemical engineer. Apart from its intrinsic interest, it drives home the fact that inventiveness is at least as important as scientific analysis in chemical engineering.

P. V. Danckwerts

Modern Chemistry for the Engineer and Scientist. Edited by G. Ross Robertson.

This book consists of 19 chapters each by different authors. The chapters are, without exception, of high technical and scientific interest, but the differences in style and objective are marked. The title and preface of the book suggest that the text might form a suitable introduction for the non-chemical scientist or engineer to modern chemistry. This is only true in the sense that such a reader would discover some of the topics which make up the subject but this could be achieved in perhaps one quarter of the present text, much of which is taken up with specific examples rather than concepts. In this respect the book is probably better suited to the applied chemist, chemical engineer or even the specialist chemist.

It is not possible to classify the chapters unequivocally in terms of objectives, but those on thermodynamics, contact catalysis, photochemistry, rubber elasticity, metal creep, clay minerals and organic reaction mechanisms are largely devoted to reviews of fundamentals. The last of these is exceptional in demanding specialised knowledge and vocabulary in the reader. All are accompanied by good references and bibliographies.

A second group of chapters is devoted to measurement techniques including isotopic tracer methods, column chromatography, and methods for the study of fast reaction kinetics. These chapters are uniformly interesting and well presented although that on chromatography relates almost entirely to specialised branches of organic chemistry.

A third group of chapters provides reviews of the production and properties of silicones and carbon fluorine compounds, the petroleum chemical and food technology industries and of chemical relationships with the earth. These reviews accord well with the professed objectives of the book each giving a well rounded and informative account of its topic. That on petroleum chemicals is exceptionally good : one regrets the paucity of its list of references.

The last four chapters of the book are devoted to biochemical and biomolecular topics, the biochemistry of insecticides, chemistry and physiological action in the living organism, and the structural chemistry of proteins. They will tax the scientific vocabulary of the average chemical engineer without direct reward, although the survey of synthesis in the living organism gives a most useful background and a proper sense of modesty.

In summary the text is worth-while reading and probably a worth-while purchase for the chemical engineer with a chemical bent. Most of the chapters repay several readings.

N. L. Franklin

M. Benedict and T. Pigford : **Nuclear Chemical Engineering.** McGraw-Hill, London, 1957. xiv + 597 pp., 71s. 6d.

This book is intended for the student although it includes a number of graphs and tables and comprehensive bibliography which are a useful source of reference. It presents with extreme clarity an account of some of the process aspects of nuclear engineering. Chapters on isotope separation and one on properties of irradiated fuel is particularly notable.

After a chapter of introduction and one on nuclear reactions, there is a detailed account of fuel cycles and irradiation schemes. The algebraic manipulation of this

section conceals the practical uncertainties in effective neutron cross-sections and reactor performance. Much of the discussion is based on reactivity arguments, their relevance to chemical engineering is not clear. Subsequent chapters on uranium production and on special nuclear materials are impaired by the absence of information on fabrication techniques, fuel element fabrication being dismissed in nine lines. This makes it impossible to define adequately the properties, other than nuclear purity, which are being sought in the production techniques.

An adequate chapter on solvent extraction is followed by an excellent discussion of irradiated fuel properties which defines the requirements of irradiated fuel processing and which gives an indication of the theoretical basis for solvent extraction processing. The subsequent discussion on irradiated fuel processing is disappointing to the specialist. There is no discussion of effluent disposal problems, and plant design concepts, plant control, process equipment, plant inspection and decontamination escape comment. Even criticality control in enriched uranium or plutonium receives only passing mention. The chapter provides a simple and clear discussion of the flowsheets of a number of solvent processes but excludes most of the more detailed information declassified since the 1955 Geneva Conference.

The last third of the book is devoted to isotope separation. The treatment is related periodically to the more familiar concepts of distillation theory, an advantage to the chemical engineer. Classification precludes any discussion of gaseous diffusion equipment technology, and transient behaviour of cascades is not treated: within these limitations the treatment of the principles of isotope separation is excellent.

The book can be recommended to the student and specialist alike. The latter will regret that classification and timing have prevented the authors from treating a number of topics which would have benefited from the clear analysis and style which they apply in this book.

N. L. Franklin

Chemical Reaction Engineering. Edited by K. Rietema. Pergamon Press, London, 1957. 200 pp., 80s.

This book is a collection of fourteen papers, mostly in English, presented at an international symposium held in Holland in 1957.

Chemical reaction engineering, which has as its ultimate aim the successful design of commercial reactors from first principles, is still in its infancy. Important in this field is not only the study of fluid mechanics, heat and mass transfer, and chemical reaction kinetics, but also the interrelation of these subjects. The problems involved are complex and as yet little progress has been made towards their solution.

The symposium has been divided into five parts — introductory papers, transport phenomena in heterogeneous reactions, non-uniform concentration distributions, reactor efficiency and stability, and reactor development. Of necessity, much of the material is in the nature of a review, but some interesting new work is also presented.

This volume will undoubtedly prove valuable to all interested in this field.

G. A. Ratcliff

SELECTION OF CURRENT SOVIET PAPERS OF INTEREST TO CHEMICAL ENGINEERS*

A. I. Baranova : Partial pressures of sulphuric acid vapour and of water above solutions of sulphuric acid. *Zh. prikl. Khim.* 1958 **31** 167-177.

I. G. Plit : Scrubbing process of absorption of CO_2 by potash solution. *Zh. prikl. Khim.* 1958 **31** 186-191.

S. N. Ganz and M. A. Lokshin : Intensification of purification of coke-oven gas from H_2S in high-speed rotary absorbers. *Zh. prikl. Khim.* 1958 **31** 191-197.

V. I. Atroshchenko and V. M. Kaut : Kinetics of absorption of oxides of nitrogen in concentrated nitric acid. *Zh. prikl. Khim.* 1958 **31** 352-360.

S. N. Ganz : Absorption of oxides of nitrogen by aluminosilicate sorbents. *Zh. prikl. Khim.* 1958 **31** 360-368.

G. G. Devyatikh, A. D. Zorin and N. I. Nikolaev : Investigation of separation of isotopes of carbon and oxygen by distillation of carbon monoxide, methane and molecular oxygen. *Zh. prikl. Khim.* 1958 **31** 368-375.

V. V. Kafarov and S. A. Zhukovskaya : Investigation of main characteristics of operation of jet extractors and comparative performance of extractors. *Zh. prikl. Khim.* 1958 **31** 376-380.

M. E. Pozin and B. A. Kopylev : Influence of gas velocity on mass transfer in bubbling and foam regimes of absorption *Zh. prikl. Khim.* 1958 **31** 387-393.

F. F. Krivonos : Solubility of chlorine in benzine. *Zh. prikl. Khim.* 1958 **31** 500-504.

V. N. Kozlov and B. I. Smolenski : Distribution of acetic acid between two co-existent phases : aqueous and non-aqueous. *Zh. prikl. Khim.* 1958 **31** 508-512.

Ya Tsiborovski and A. Tseletski : Some data on desorption of liquids in a fluidised bed. *Zh. prikl. Khim.* 1958 **31** 518-525.

Fu Tszyui-fu : Approximate calculation of batch rectification columns. *Zh. prikl. Khim.* 1958 **31** 525-532.

L. A. Mocharova and M. Kh. Kishinevski : On kinetic relations in absorption by bubbling method. *Zh. prikl. Khim.* 1958 **31** 533-542.

I. P. Mukhlenov and E. Ya Tarat : On hydraulic resistance of sieves. *Zh. prikl. Khim.* 1958 **31** 542-549.

R. A. Melikyan : On hydraulic regimes existing in sieve type and bubble-cap type equipment. *Zh. prikl. Khim.* 1958 **31** 550-558.

V. V. Kafarov and Yu. I. Ditnerski : Minimum equivalent height of packing in absorption, rectification and extraction packed columns. *Zh. prikl. Khim.* 1958 **31** 631-633.

A. R. Brun-Tsekhovoi : Feeding control of granular materials by injection of a stream of gas. *Zh. prikl. Khim.* 1958 **31** 634-635.

V. V. Kafarov : On calculation of processes of mass transfer. *Zh. prikl. Khim.* 1958 **31** 706-711.

A. P. Nikolaev : Mass transfer during distillation in wetted-wall columns. *Zh. prikl. Khim.* 1958 **31** 711-718.

M. E. Pozin, B. A. Kopilev and N. A. Petrova : Absorption of H_2S by arsenic-soda solution in a foam apparatus. *Zh. prikl. Khim.* 1958 **31** 849-859.

G. L. Antipenko, E. S. Beletskaya and A. G. Krilova : Variation of density of pure nitric acid with temperature. *Zh. prikl. Khim.* 1958 **31** 859-863.

V. N. Kozlov and B. I. Smolenski : Process of recovery of acetic acid from its aqueous solution by extraction method. *Zh. prikl. Khim.* 1958 **31** 924-931.

G. M. Skurikhina and V. I. Yurev : Study of exchange and adsorption properties of monocarboxylcellulose. *Zh. prikl. Khim.* 1958 **31** 931-937.

V. A. Malyusov, N. A. Malofeev and N. M. Zhavoronkov : Investigation of the process of distillation in a molecular still of centrifugal type. *Khim. Prom.* 1958 **31** 31-36.

E. N. Eremin : Experiments on manufacture of acetylene by electrocracking of natural methane. *Khim. Prom.* 1958 73-80.

N. I. Gelperin : Mechanical lifting of liquids by vapours in evaporators. *Khim. Prom.* 1958 96-101.

*Translations or photostats of the article can be supplied on request by the Pergamon Institute (a non-profit making foundation) at a nominal charge.

K. E. Novinkova and A. G. Natradze : Graphical method of calculation of binary azeotropic mixtures. *Khim. Prom.* 1958 102-105.

G. V. Samsonov and S. Ya Plotkin : Metalo-ceramic materials for the chemical industry. *Khim. Prom.* 1958 106-110.

A. A. Polushkin : Combined method of drying of chemical products. *Khim. Prom.* 1958 111-113.

V. A. Zarinski and Ya M. Kots : Electrochemical characteristics of ion-exchange membranes. *Khim. Prom.* 1958 115-116.

A. E. Kalaus, M. G. Lapuk and T. D. Vikulova : Tube reactor for continuous polymerisation in emulsion state. *Khim. Prom.* 1958 133-138.

M. G. Slinko : Influence of heat and mass transfer processes on reaction rate in oxidation of ethylene. *Khim. Prom.* 1958 138-146.

V. I. Klassen and R. Z. Erenburg : On application of controlling reagents in flotation of native sulphur ores. *Khim. Prom.* 1958 152-155.

A. G. Kasatkin, Yu I. Ditnerski and S. U. Umarov : On calculation of perforated plate columns without downcomers. *Khim. Prom.* 1958 166-173.

A. A. Komarovski and V. V. Streltsov : On calculation of optimum operating range of batch filters. *Khim. Prom.* 1958 173-176.

M. M. Zaitsev and F. I. Murashkevich : On influence of position of liquid feed on hydraulic resistance and performance of a turbulent gas washer. *Khim. Prom.* 1958 178-183.

P. P. Budnikov : New constructional materials. *Khim. Nauka i Prom.* 1958 **3** 2-7.

L. A. Nikolaev and A. A. Askadski : Influence of ultrasonics on catalytic processes. *Khim. Nauka i Prom.* 1958 **3** 131-132.

V. V. Kafarov and T. A. Malinovskaya : Investigation of influence of cake structure on rate of industrial filtration. *Khim. Nauka i Prom.* 1958 **3** 133-134.

M. A. Planovskaya : Methods of manufacture of finely dispersed dyestuffs in the aniline-dye industry. *Khim. Nauka i Prom.* 1958 **3** 249-256.

S. I. Shapiro : Mechanisation of the process of drying in the aniline-dye industry. *Khim Nauka i Prom.* 1958 **3** 256-262.

I. V. Krotov : Application of radioactive isotopes in investigation of processes of corrosion and passivity of metals. *Uspekhi Khim.* 1958 **27** 643-667.

D. O. Zykov : Rectification of multicomponent mixtures—method of calculation. *Izv. Akad. Nauk SSSR, Otd. tekh. Nauk* 1958 100-106.

L. V. Radushkevich : Investigation of capillary condensation of vapours in highly dispersed systems. 2. Estimation of some approximate calculations of capillary condensed volumes. *Izv. Akad. Nauk SSSR, Otd. Khim. Nauk*, 1958 285-289. 3. Capillary condensation in cells consisting of two contacting spheres of unequal radii. *ibid.*, 1958 403-410.

A. V. Kiselev and E. V. Khrapova : Adsorption of nitrogen vapours on graphitised carbon black and charcoals. *Izv. Akad. Nauk SSSR, Otd. Khim. Nauk*, 1958 389-402.

M. M. Dubinin and E. G. Zhukovskaya : Study of adsorption properties of carbon adsorbents. 2. Study of adsorption properties of active charcoals by benzine vapours and nitrogen. *Izv. Akad. Nauk SSSR, Otd. Khim. Nauk.* 1958 535-544.

A. M. Chikin and A. M. Markevich : Determination of thermal conductivities of gases and gaseous mixtures. *Zh. fiz. Khim.* 1958 **32** 116-120.

I. E. Ampilogov, A. N. Kharin and I. S. Kurochkina : Study of longitudinal mixing in the flow of solutions through a non-sorbing bed. *Zh. fiz. Khim.* 1958 **32** 141-145.

M. M. Shelechnik : Temperature distribution in a reaction column for processes in the region of diffusionkinetics *Zh. fiz. Khim.* 1958 **32** 152-156.

S. D. Gromakov : Methods of calculation of properties of quinary systems from data on binary systems. *Zh. fiz. Khim.* 1958 **32** 232-257.

L. V. Radushkevich : Theory of deposition of particles from a gas stream on an isolated cylinder. *Zh. fiz. Khim.* 1958 **32** 282-290.

V. I. Kuzmich and I. Z. Fisher : On the theory of separation of a gaseous mixture under high pressures. *Zh. fiz. Khim.* 1958 **32** 291-297.

A. N. Kharin and I. E. Ampilogov : Comparative evaluation of the part played by kinetic factors in the dynamics of adsorption of acetic and butyric acids from their aqueous solution in a charcoal bed. *Zh. fiz. Khim.* 1958 **32** 341-348.

G. M. Panchenkov, B. I. Gorshkov and M. V. Kuklanova : Effect of the addition of organic solvents on ion exchange equilibrium. I. Effect of alcohols on the equilibrium of alkaline ion exchange on "sulpho" resins. *Zh. fiz. Khim.* 1958 **32** 361-367. II. Effect of acetone on ion-exchange equilibrium of alkiline metals on "sulpho" resins. *ibid.* 1958 **32** 616-619.

M. Kh. Karapetyans : Heats of vapourisation of some substances. *Zh. fiz. Khim.* 1958 **32** 554-568.

V. P. Shestopalov : Boundary diffusion layer in a diffuser. *Zh. fiz. Khim.* 1958 **32** 585-591.

Yu B. Ivanov and V. G. Levich : Convective diffusion in a binary liquid system in the critical region. *Zh. fiz. Khim.* 1958 **32** 592-597.

S. E. Bressler : Theory of chromatographic separation of isotopes. *Zh. fiz. Khim.* 1958 **32** 628-634.

A. A. Isivikyan and A. A. Kiselev : Heat of adsorption of benzine vapours on silica gel. *Zh. fiz. Khim.* 1958 **32** 679-680.

A. K. Burshtein, A. G. Pshenichnikov and N. A. Shumilova : Apparatus for determination of pore size distribution. *Zh. fiz. Khim.* 1958 **32** 697-698.

L. P. Filippov : Application of dimensional analysis to the description of properties of liquids. V. Crystallisation temperature. *Zh. fiz. Khim.* 1958 **32** 760-761. VI. Temperature dependence of saturated vapour pressure. *ibid.* 1958 **32** 986-990.

A. A. K. Abraham : On the oscillating cylinder viscometer for elastic liquids. *Zh. fiz. Khim.* 1958 **32** 914.

G. M. Panchenkov and T. S. Maksareva : An optical micromethod for determination of diffusivities of liquids. *Zh. fiz. Khim.* 1958 **32** 922-929.

V. A. Marinin : Temperature dependence of diffusivities of methyl alcohol and sugar in glycerol-water mixtures. *Zh. fiz. Khim.* 1958 **32** 1068-1073.

L. F. Vereshchagin, A. A. Semerchan and F. M. Filler : On the velocity break in a water jet. *Zh. tech. fiz.* 1958 **28** 433-435.

V. M. Borishanski and S. S. Kutateladze : Heat transfer and hydraulic resistance during flow of liquid metals in circular tubes. *Zh. tekh. fiz.* 1958 **28** 836-847.

S. S. Kutateladze : Heat transfer during flow of liquid metals in a tube and on a plate. *Zh. tekh. fiz.* 1958 **28** 848-854.

A. A. Tanaev : Influence of gravity on the motion in a laminar boundary layer during longitudinal flow of gas along a plate. *Zh. tekh. fiz.* 1958 **28** 862-871.

N. N. Tunitski, G. G. Devyatikh, P. S. Petrov and B. Z. Torkin : Separation of carbon isotopes by thermal diffusion of carbon monoxide. *Zh. tekh. fiz.* 1958 **28** 881-885.

G. D. Rabinovich : On the calculation of heat exchangers. *Zh. tekh. fiz.* 1958 **28** 1077-1083.

A. P. Zhdanov and V. N. Kuzmin : Preparation of suspensions with spherical particles. *Zh. tekh. fiz.* 1958 **28** 1118-1120.

A. A. Voskresensky : Adsorption of NH_3 on graphitised carbon black. *Dokl. Akad. Nauk SSSR*, 1958 **119** 724-726.

N. V. Kalashnikov and V. I. Chernikin : Study of heat transfer between vibrating heaters and viscous liquids. *Dokl. Akad. Nauk SSSR.* 1958 **119** 735-736.

I. N. Plaksin and E. M. Chaplygina : Influence of oxygen and nitrogen on the separation of titanium and zirconium minerals by flotation. *Dokl. Akad. Nauk SSSR.* 1958 **119** 756-758.

E. A. Anifomova, V. A. Glembotski, I. N. Plaksin and A. S. Shcheveleva : Influence of structural features and surface properties on froth-flotation extraction of poorly floatable lead minerals. *Dokl. Akad. Nauk SSSR.* 1958 **119** 961-963.

L. Guan-Tsun and V. A. Malyusov : Calculation of the wetted-wall rectification process. *Dokl. Akad. Nauk SSSR.* 1958 **120** 151-154.

I. N. Plaksin and V. I. Tyurnikova : Unhomogeneity of reagent distribution in sulphide flotation. *Dokl. Akad. Nauk SSSR.* 1958 **120** 155-158.

A. A. Tager, M. V. Tsilipotkina and A. I. Suvorova : Determination of specific area and pore volume in solid polymeric sorbents. *Dokl. Akad. Nauk SSSR.* 1958 **120** 570-572.